Copyright

by

Yul Young Park

2011

The Dissertation Committee for Yul Young Park Certifies that this is the approved version of the following dissertation:

Persistent and Transient Na^+ Currents in Hippocampal CA1 Pyramidal Neurons

Committee:

Daniel Johnston, Supervisor

Chandrajit L. Bajaj

Adela Ben-Yakar

Andrew Dunn

Harel Shouval

Persistent and Transient Na^+ Currents in Hippocampal CA1 Pyramidal Neurons

by

Yul Young Park, B.S.; M.S.E.

Dissertation

Presented to the Faculty of the Graduate School of

The University of Texas at Austin

in Partial Fulfillment

of the Requirements

for the Degree of

Doctor of Philosophy

The University of Texas at Austin

August, 2011

Dedication

Dedicated to my parents, wife and sons.

Acknowledgements

This work would not be possible without the unfailing support of my advisor, Dr. Daniel Johnston. His amazing patience and generosity enabled me to get through the academic and personal obstacles during my training period and kept me going this far. Whenever problems occurred to me, he always became my side and waited until I could handle the problems properly and reach out for me whenever I needed his help. I deeply appreciate all his considerate care and commitment. I also would like to thank my dissertation committee members: Dr. Chandrajit Bajaj, Dr. Adela Ben-Yakar, Dr. Andrew Dunn, and Dr. Harel Shouval. I think I am very fortunate to have such a supportive committee members. Whenever I asked for their help, they gave their hands without hesitation. I am also eager to express my special thankfulness to Dr. Richard Gray. All his teaching, technical assistance, encouragement, and especially joke shaped my skill, knowledge, and life in electrophysiology, and helped me finish this dissertation. I also thank Dr. Adron Harris for his help to my alcohol experiment and Dr. Richard Aldrich for his interest and helpful comments on my research.

I must acknowledge past and present Johnston lab members, and give thanks to them for invaluable help. Dr. Rishikesh Narayanan and I enjoyed spending nighttime for experiments together while sharing slices and experimental materials. I am still missing those times. Dr. J. Amiel Rosenkranz taught me nucleated patch clamp technique, and Dr. Xixi Chen helped me out coding data acquisition and analysis program. Dr. Raymond Chitwood taught me current-clamp technique and offered me a teaching assistantship to his class. The discussions with Dr. Kevin Dougherty made my understanding and design of the voltage-clamp experiment better. Dr. Darrin Brager generously created and

provided epilepsy model rats for my experiment, and Dr. Nikolai Dembrow helped me perform histology and immunohistochemstry. Dr. Payne Cheng taught me transgenic mice husbandry. I also thank Drs. Brian Kalmbach, Laurea Diaz, Cliff Rumsey, Stephanie Carlson, Seena Mathew for their supports and valuable suggestions to my research. Also, I am indebted to other graduate students in Johnston lab: Chung Sub Kim, Ann Clemens, Sachin Vaidya, Brandy Routh, Andrea Dickson, and thank them for their encouragement and help. I would like to extend my thankfulness further to Gayathri Ranganathan, Chang Hoon Lee, and Krystal Phu for their various helps that made my graduate life brighter and more enjoyable. Thanks to AKPC people for their prayers and supports and to Korean friends in Austin for cheering me up.

Finally, but most importantly, I would like to thank my family: my parents, brother, sister, my wife and sons. They excused and supported me when I could not spend time with them for many occasions due to my hectic research. Their ceaseless prayer, support, and love were the most powerful momentum that made me persistent in my journey. Especially, the presence of my wife, Eunha Kim, and three sons, Johan, Bohan, Juhan held my feet firm on the ground when I was stumbling. All that I achieved, if any, can find their meaning only when they are together with me. I thank and love you so much!

Persistent and Transient Na^+ Currents in Hippocampal CA1 Pyramidal Neurons

Publication No._____

Yul Young Park, Ph. D.

The University of Texas at Austin, 2011

Supervisor: Daniel Johnston

The biophysical properties and distribution of voltage gated ion channels shape the spatio-temporal pattern of synaptic inputs and determine the input-output properties of the neuron. Of the various voltage-gated ion channels, persistent Na^+ current (I_{NaP}) is of interest because of its activation near rest, slow inactivation kinetics, and consequent effects on excitability. Overshadowed by transient Na^+ current (I_{NaT}) of large amplitude and fast inactivation, various quantitative characterizations of I_{NaP} have yet to provide a clear understanding of their role in neuronal excitability. We addressed this question using quantitative electrophysiology to compare somatic I_{NaP} and I_{NaT} in 4–7 week old Sprague-Dawley rat hippocampal CA1 pyramidal neurons. I_{NaP} was evoked with 0.4 mV/ms ramp voltage commands and I_{NaT} with step commands in hippocampal neurons from *in vitro* brain slices utilizing nucleated patch-clamp recording. I_{NaP} was found to have a density of 1.4 ± 0.7 pA/pF in the soma. Compared to I_{NaT}, it has a much smaller amplitude (2.38% of I_{NaT}) and distinct voltage dependence of activation (16.7 mV lower half maximal activation voltage and 41.3% smaller slope factor than those of I_{NaT}). The

quantitative measurement of I_{NaT} gave the activation time constant (τ_m) of 22.2 ± 2.3 μs at 40 mV. Hexanol, which has anesthetic effects, was shown to preferentially block I_{NaP} compared to I_{NaT} with a significant voltage threshold elevation (4.6 ± 0.7 mV) and delayed 1st spike latency (221 ± 54.6 ms) suggesting reduced neuronal excitability. The number of spikes evoked by either given step current injections or α-EPSP integration was also significantly decreased. The differential blocking of I_{NaP} by halothane, a popularly used volatile anesthetic, further supports the critical role of I_{NaP} in setting voltage threshold. Taken together, the presence of I_{NaP} in the soma demonstrates an intrinsic mechanism utilized by hippocampal CA1 pyramidal neurons to regulate axonal spike initiation through different biophysical properties of the Na^+ channel. Furthermore, I_{NaP} becomes an interesting target of intrinsic plasticity because of its profound effect on the input-output function of the neuron.

Table of Contents

List of Figures

Chapter 1 Background and Introduction

1.1 LEARNING AND MEMORY

Information garnered from our daily life such as knowledge, language, events, and skills constitutes indiosyncrasies of an individual's character. 'How' and 'Where' the information is stored is therefore a daunting question, because every aspect of the individual as a biological information processing system spanning from molecular to cellular, system and behavioural level is convolved in complicated ways. Answering those questions should explicate not only the local phenomena restricted to a certain level, but also clarify the inter-correlated global effects of the localized phenomena throughout all the levels of the system.

One sussecssful and still influential attempt was made by Hebb in 1949. He intended to explain human behaviour by bridging the gap between neurophysiology and psychology. He postulated that persistent and correlated activity of two neurons could bring about an association so that one neuron can more efficiently excite the other neuron through the growth process or metabolic change of one or both cells (Hebb 1949). Although the absence of the crucial neurological and anatomical information at that time made him mostly rely on speculations, his hypothesis was supported by a plethora of experimental and theoretical findings much later and became a fundamental idea of cellular models of learning and memory known as Hebbian theories or Hebbian plasticities.

Long-term potentiation (LTP), a long lasting enhanced synaptic efficacy in response to appropriate synaptic stimulation, is one of the most successful experimental findings supporting Hebb's hypothesis (Bear 2003, Bliss & Collingridge 1993, Bliss &

Lomo 1973). High frequency presynaptic stimulation or pairing presynaptic stimulation to postsynaptic depolarization makes N-methyl-D-aspartate receptor (NMDA-R) activated by presynaptic neurotransmitter release and unblocking of Mg^{2+} ion from the receptor. The Ca^{2+} ions through NMDA-Rs trigger a cascade of intracellular signaling pathways causing the modification of synaptic strength between pre- and post-synaptic neurons. With different types of synaptic stimulation, the synaptic efficacy could be reduced to the opposite direction of LTP causing long-term depression (LTD) of the synapse. Synaptic plasticity, the bi-directional change of synaptic efficacy (strengthening or weakening), thus suggested that information is stored in the $\sim 10^4$ synaptic contacts of neurons to other neurons from a total of $\sim 10^{11}$ of neurons following Hebb's hypothesis.

However, in Hebbian plasticity the network is eventually destabilized by the saturation of synaptic efficacy because a synapse already potentiated (or depressed) has a higher probability of experiencing further potentiation (or depression) due to the previous enhanced synaptic efficacy. Repetitive potentiation (or depression) eventually saturates the ability of the neuron into either of two extreme modes: high firing rates or no firing. This positive feedback makes the system unstable and keeps it away from an appropriate working range. Thus, such extreme network activities need to be monitored and regulated in a homeostatic manner in order to maintain proper operation of the neuron. One of the regulatory processes to maintain stability of neuronal activity is a 'synaptic scaling' mechanism that scales the strength of all the synaptic inputs to a neuron up or down depending on the activity of the neuron (Turrigiano 2008, Turrigiano & Nelson 2000). For example, the global pharmacological suppression (or enhancement) of the activity of a cultured cortical neuron causes the concomitant increase (or decrease in the α-amino-3-hydroxy-5-methyl-4-isoxazole propionic acid (AMPA) mediated glutamatergic synaptic strength onto the neuron, which returns the activity of the neuron to the original firing

rate (Turrigiano et al 1998). Scaling total synaptic strength while preserving the relative strength among synapses therefore provides a way to make LTP/LTD of a specific synapse intact and achieves the stability of the global neuronal activity at the same time.

Another regulatory processe is intrinsic plasticity, which is a persistent change in neuronal excitability mediated by the regulation of voltage-gated ion channels in an activity-dependent manner. Given the synaptic stimulations, voltage gated-ion channels on the neuron shape the integration of the inputs and determine the action potential generation as a final output of the neuron. If the neuronal excitability is regulated in the opposite direction to the concomitant synaptic plasticity by voltage-gated ion channels, intrinsic plasticity can provide a negative feedback to the system counterbalancing the positive feedback of Hebbian plasticity. Previous studies reported such a regulation of voltage-gated ion channels accompanying synaptic plasticity (Brager & Johnston 2007, Fan et al 2005, Frick et al 2004, Narayanan & Johnston 2007). This intrinsic plasticity could provide not only a homeostatic mechanism of network stability, but also alternative information storage other than synapses in the brain during learning tasks (Nolan et al 2004, Zhang & Linden 2003). Knowledge of the biophysical properties, distribution, modulation, and plasticity of voltage-gated ion channels, as well as ligand-gated ion channels, is crucial to elucidate how the brain processes and stores information while learning.

1.2 HIPPOCAMPUS IN LEARNING AND MEMORY

The hippocampus is a paired structure that is halved on each side of the brain. It is located under the medial temporal lobe of the mammalian brain and named after its sea-horse like shape. The cell bodies and processes of the neurons in the hippcampus are organized in a highly laminated fashion providing an advantage for neuroanatomical and

electrophysiological studies. The hippocampus can be further sub-divided into CA1, CA2, and CA3 fields depending on the cell size and input connections, and it constitutes the *hippocampal formation* together with other brain regions such as the dendate gyrus, subiculum, pre- and para- subiculum, and entorhinal cortex. The excitatory signal tranversing through the hippocampal formation is largely unidirectional. As a simplified description, the multimodal sensory signals from cortical areas enter into the entorhinal cortex. The layer II cells of the entorhinal cortex transmit the inputs to the dentate gyrus and the hipocampal CA3 region via a pathway called the *perforant path*. Then, the mossy fibers from the granule cells in the dentate gyrus project to the CA3 region. The pyramidal neurons in CA3, in turn, project to both other CA3 neurons and CA1 neurons through the pathways called the *associational connections* and the *Schaffer collaterals*, respectively. Upon receiving the input from CA3, the CA1 pyramidal neurons process and transmit the signal to the subiculum and the deep layer of the entorhinal cortex. The cells in the subiculum also project to the deep layer of the entorhinal cortex, and the entorhinal cortex finally sends the transformed inputs back to the cortex where the signals originate (Figure 1.1). The unidirectional progression of the excitatory pathway that starts from the entorhinal cortex, dentate gyrus, hippocampus, and back to entorhinal cortex forms a *trisynaptic circiut* (Anderson et al 1971). In addition to the trisynaptic circuit, there is a direct projection from the entorhinal cortex neurons in layer III to the distal dendrite of CA1 neurons through the *temporoammonic pathway* (Witter et al 1989).

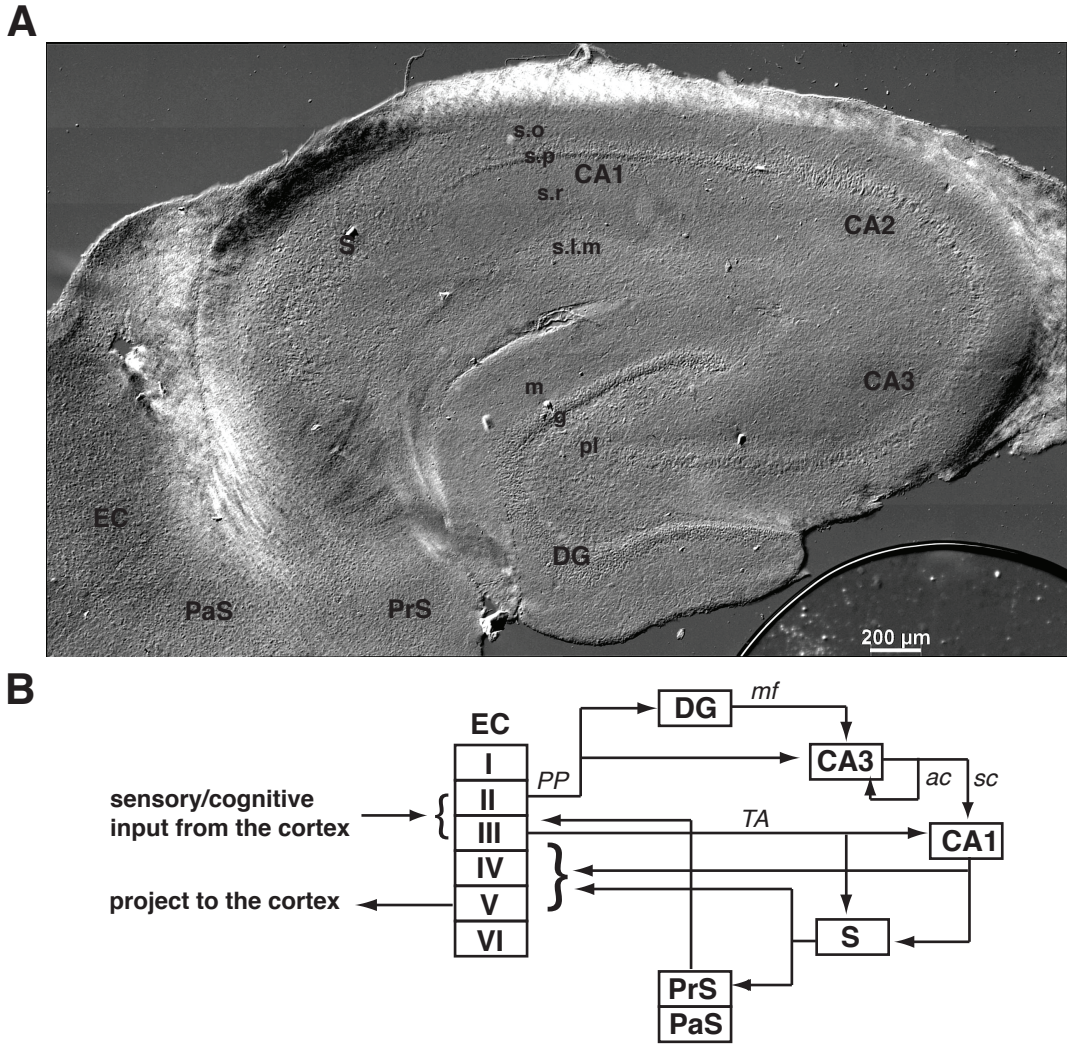

Figure 1.1: Structure and circuitry of the hippocampal formation
A: Differential interference contrast (DIC) microscope image of cryostat resectioned transverse hippocampal slice (50 μm thickness) illustrates major components of the hippocampal formation. Abbreviations: CA3, CA2, CA1 fields of the hippocampus; DG, dentate gyrus; S, subiculum; PrS, presubiculum; PaS, parasubiculum; EC, entorhinal cortex. All hippocampal fields consist of 5 layers: the alveus, stratum oriens (s.o), stratum pyramidale (s.p), stratum radiatum (s.r), and stratum lacunosum-moleculare (s.l.m). The dentate gyrus has 3 layers: the molecular layer (m), the granule cell layer, and the polymorphic cell layer (pl). **B**: Schematic diagram illustrates the excitatory pathways in the hippocampal formation. For the detail of circuitry, see text. Abbreviations: PP, perforant pathway; TA, temporal ammonic pathway; mf, mossy fiber; ac, associational connectionc; sc, Schaffer collaterals. [Figure 1.1A was made by the author and the diagram in B was adapted from Witter et al. (Witter et al 1989)]

Several surgical cases have revealed an important role of the hippocampus in learning and memory function (Scoville & Milner 1957). A patient, Henry Molaison, known as H.M., had bilateral medial temporal-lobe excisions that removed both hippocampi and the surrounding area due to intractable epilepsy. Although there was no impairment in his personality, general intelligence, perception, abstract thinking, or reasoning ability, he was unable to create long-term memories about new facts and events subsequent to the surgery, which is an example of anterograde amnesia associated with the hippocampus. Other studies of human dementia originated from the damage to this area by surgical resections or Alzheimer's disease (AD) confirmed the critical role of the hippocampus in learning and memory (Hyman et al 1984, Hyman et al 1986, Squire & Zola-Morgan 1991, Zola-Morgan et al 1982). Interestingly, a case study reported that the ischemic damage restricted to the CA1 field of the hippocampus was sufficient to cause similar anterograde amnesia without any significant cognitive impairment (Zola-Morgan et al 1986). Taken together, these findings provide grounds to choose the hippocampus, more specifically the CA1 subfield, as a model system for learning and memory study. Again, in this context, it is of no surprise that the first LTP experiment was conducted in the hippocampal region and a plethora of consequent research to elucidate the relationship between memory and LTP in this area followed.

1.3 CA1 PRYMIDAL NEURONS IN THE HIPPOCAMPUS

The hippocampal CA1 pyramidal neuron is one of the best prototype neurons for the study of information processing in the nervous system. A substantial amount of synaptic and intrinsic plasticity research has been done on this neuron. A hippocampal CA1 pyramidal neuron has an elaborate dendritic morphology and receives about 30,000

excitatory and 1,700 inhibitory synaptic inputs (Megías et al 2001). The excitatory synaptic input mostly impinges on dendritic spines, a protrusion of the postsynaptic membrane where an excitatory synapse is formed with the presynaptic axonal terminal, while most inhibitory synapses target to the perisomatic and proximal dendrite of non-spine area. The release of neurotransmitter from the presynaptic terminal of the pyramidal neurons generates the excitatory post-synaptic potentials (EPSPs) via post-synaptic glutamatergic receptors such as NMDA, AMPA, and kainate acid receptors. The EPSPs spread along the dendrite and suffer from the filtering effects of the dendrite: slowing kinetics and decrease in amplitude. The attenuated EPSPs from the distal synaptic input, however, can be partly compensated by ncreasing density of AMPA receptor at distal dendrite (Magee & Cook 2000).

The EPSPs traveling along the dendrite are also shaped and integrated by a myriad of voltage-gated ion channels (VGICs) that reside on the membrane of CA1 pyramidal neurons and regulate the final neuronal output and intrinsic excitability in a complex manner. In the postsynaptic dendritic region, VGICs shape and transmit the incoming EPSPs to the soma while compensating for the dendritic filtering effect. The VGICs in the peri-somatic region integrate the transmitted incoming signals that break the inward-outward current balance and elicit an action potential or spike. The VGICs in the axon transfer the generated spike to the presynaptic terminals for the neurotransmitter release onto the next neuron in the pathway. The action potential generated in the axonal region also propagates backward to the dendrite. The backpropagating action potentials (bAPs) suffer from gradual decrease in amplitude depending on the distance from soma and the activity of the neuron and the VGICs along the dendrite modulate the amplitude of bAPs (Colbert et al 1997, Hoffman et al 1997, Jaffe et al 1992, Spruston et al 1995, Stuart & Sakmann 1994). The intrusion of bAPs into the dendrite as a rapid feedback

signal was shown crucial to the Hebbian synaptic plasticity (Johnston et al 2003, Magee & Johnston 1997). Thus, the VGICs along the dendrite are involved in the association of the retrograde bAPs with anterograde EPSP signals in a complicated manner.

The molecular diversity of voltage gated-ion channels is enormous. For example, it has been known that at least 4 Na^+, 36 K^+, 8 Ca^{2+} and 4 hyperpolarization-activated cyclic nucleotide gated (HCN) channel genes are expressed in mammalian central nervous system (Vacher et al 2008), and part of them are expressed in the CA1 pyramidal neurons in the hippocampus. Thus, there are largely 4 classes of voltage-gated membrane currents based on the type of ion conducting through the transmembrane ion channel pores of a CA1 pyramidal neuron: Na^+, K^+, Ca^{2+}, and non-specific cation currents. Each ionic conductance can be further classified into heterogeneous subtypes by their current-voltage relationships and activation/inactivation. Since the ionic conductances mediated by ion channel types and their distributions on a neuron regulate the electrophysiological behavior and functional significance, characterizing the voltage-gated ion channels of pyramidal neurons in the CA1 region is a fundamental and crucial step for the study of intrinsic excitability and plasticity, and consequently, learning and memory.

1.4 VOLTAGE-GATED ION CHANNELS IN CA1 PYRAMIDAL NEURONS

Voltage-dependent Na^+ channels in CA1 pyramidal neurons have been shown to have a relatively uniform distribution across the axo-somato-dendritic axis by cell-attached recording. Both early transient and late occurring channel activities were recorded with the same single channel conductance of ~15 pS (Colbert & Johnston 1996, Magee & Johnston 1995a). There is, however, heterogeneity in Na^+ channels. Although

the density of Na^+ conductance is distributed relatively uniform in neurons, dendritic Na^+ channel is known to experience substantial amount of activity-dependent slow inactivation (or slow recovery from inactivation) compared to the somatic Na^+ channel (Colbert et al 1997, Jung et al 1997) suggesting that they could have different biophysical properties. Na^+ channel slow inactivation in the apical dendrite causes severe amplitude attenuation of backpropagating action potentials generated by repetitive somatic firing. This condition seems an unfavorable situation for Hebbian plasticity due to the limited bAPs as the associative signals for LTP induction (Magee & Johnston 1997, Spruston et al 1995). However, the uniform Na^+ distribution along the dendrite supports dendritic spike generation and suggests an alternative way to provide increased postsynaptic calcium influx for synaptic potentiation (Golding et al 2002, Jaffe et al 1992). Dendritic Na^+ channels activated by subthreshold EPSPs also can affect dendritic information processing such as EPSP and bAP boosting and the non-linear summation of bAPs and distal synaptic inputs (Magee & Johnston 1995b, Stuart & Häusser 2001, Stuart & Sakmann 1994). The altered somatic Na^+ channel properties can regulate intrinsic excitability. Xu and colleagues have found that increased neuronal excitability is attributed to the hyperpolarizing shift of the somatic Na^+ channel activation curve and that it shared the same signaling pathway with LTP induction, which, however, seems against the homeostatic regulation of neuronal excitability (Xu et al 2005). On the other hand, the uniform functional expression of Na^+ conductance is inconsistent with the non-uniformly high Na^+ channel density in axonal area, especially shown by a quantitative electron microscopy (EM) immunogold method (Lorincz & Nusser 2010). This discrepancy is an interesting topic for research and raises an important basic neuroscience question: how is an action potential initiated in the axonal initial segment area (Johnston 2010).

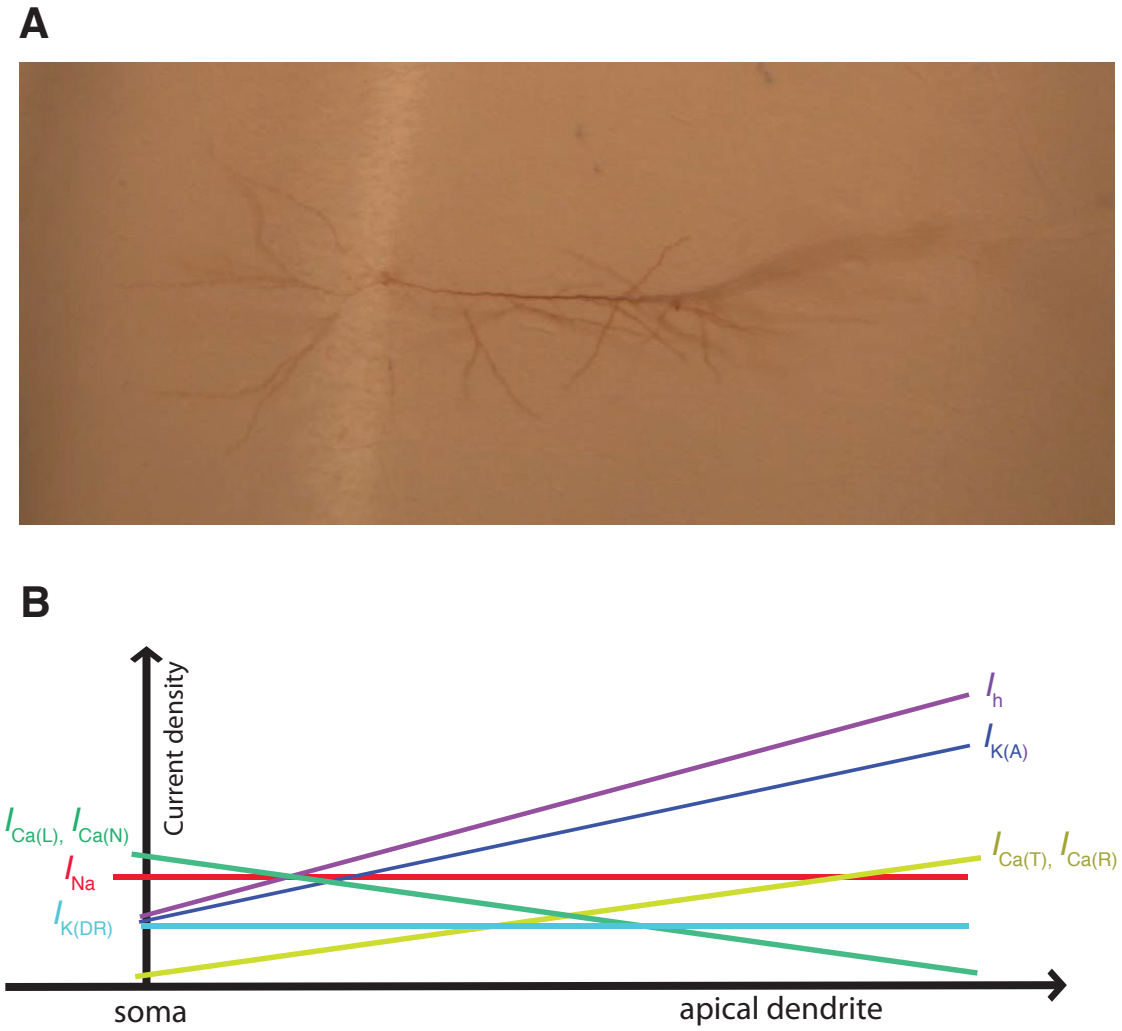

Figure 1.2: Voltage-dependent ionic conductance in CA1 pyramidal neuron
A: Morphology of a CA1 pyramidal neuron. Neurobiotin stained CA1 pyramdial neuron shows elaborate dendritic arbors. The slices were fixed with 4% paraformaldehyde (PFA) and processed using avidin-HRP system activated by diaminobenzidine (DAB, Vector Labs), then visualized with compound microscope (Diaplan, Leitz). **B**: distribution of voltage-gated ionic conductance along the dendrite of CA1 pyramidal neuron. Na^+, Ca^{2+}, K^+, HCN current density were shown along the apical dendrite. For a detailed explanation about each conductance, see text. [The stained neuron was made by the author, and the bottom graph is rough summary from several studies (Hoffman et al 1997, Magee 1998, Magee & Johnston 1995a)]

Voltage dependent Ca^{2+} channels in the CA1 pyramidal neuron also show relatively constant current density although the subtypes of Ca^{2+} channels are distributed to different degrees within the soma and dendritic region of the cell (Magee & Johnston 1995a). Most of the subtypes of Ca^{2+} channels were found in CA1 pyramidal neurons: low voltage activated (LVA) fast inactivating T-type Ca^{2+} channel of ~10 pS single channel conductance, high voltage activated (HVA) R-, N-, P/Q- type Ca^{2+} channel with moderate conductance of ~17 pS, and HVA non-inactivating L-type Ca^{2+} channels with large conductance of ~27 pS. The CA1 dendrite has a high density of T- and R- type Ca^{2+} channels while a lower density of N- and L- type Ca^{2+} channels expressed in the dendrite. The CA1 somata have the reverse distribution of those channels with some P/Q-channel expressed at the soma (Magee & Johnston 1995a). This location dependent expression of multiple subtypes of Ca^{2+} channels with different voltage-dependent properties can affect synaptic integration and plasticity. The dendritic T-type channel can be activated by subthreshold EPSPs and induce localized Ca^{2+} influx at distal dendrites while a single or train of bAP can make more widespread Ca^{2+} influx to the perisomatic region of the neuron through L-, P/Q-, R-, N- type Ca^{2+} channels (Christie et al 1995, Magee et al 1995, Magee & Johnston 1995a). Dendritic Ca^{2+} channel also supports dendritic Ca^{2+} spike generation that mediates somatic burst firing (Golding et al 1999).

The K^+ channels in CA1 pyramidal neurons under cell-attached recording also revealed 5 different K^+ conductances: delayed rectifier K^+ channel with a single channel conductance of ~ 19 pS, M-type K^+ channel of ~ 11 pS, D-type K^+ channel of ~18 pS, A-type K^+ channel of ~ 6 pS, and G protein-coupled inwardly-rectifying K^+ (GIRK) channel of ~33 pS (Chen & Johnston 2004, Chen & Johnston 2005, Hoffman et al 1997). The sustained delayed rectifier K^+ current with a uniform distribution from the soma to the dendrite has an inactivation time constant of ~1.6 second at +50 mV and contributes to

the most of the macroscopic sustained K^+ currents. The density of non-inactivating M-type K^+ current is too low to contribute to this (Chen & Johnston 2004). The delayed rectifier K^+ current facilitates the repolarization of the bAP at a depolarized potential (Chen & Johnston 2006), and can maintain the membrane stability by compensating the down-regulation of A-type K^+ current (Colbert & Pan 1999). On the other hand, the fast inactivating A-type current shows about a five-fold increase in the current amplitude along the dendrite (Hoffman et al 1997). This linear increase in A-type K^+ current amplitude dampens the amplitude of bAP along the dendrite and provides an answer why the amplitude of bAP progressively declines in amplitude along the dendrite even though there is a uniform dendritic distribution of Na^+ and Ca^{2+} conductances. Since the bAP provides a postsynaptic depolarization for the NMDA-receptor opening and Ca^{2+} influx into the postsynaptic neuron as an associative feedback signal for LTP induction (Magee & Johnston 1997), the amplified bAP amplitude through A-type current modulation such as by the activation of protein kinase A (PKA), protein kinase C (PKC), and mitogen-activated protein kinase (MAPK) or gene deletion enhances synaptic plasticity induction (Chen et al 2006, Hoffman & Johnston 1998, Watanabe et al 2002, Yuan et al 2002). Furthermore, Ca^{2+} imaging at the specific synapse where the LTP occurs revealed the increased bAP amplitude via the hyperpolarizing shift of inactivation curve of local A-type channels and demonstrated both the change in synaptic efficacy and local dendritic excitability (Frick et al 2004). Slowly inactivating D-type current has been proposed to provide the higher threshold for Ca^{2+} spike generation at the soma (Golding et al 1999). The G protein-coupled inwardly-rectifying K^+ channel provides an inhibitory modulation through the hyperpolarization of the membrane potential (Chen & Johnston 2005).

Hyperpolarization-activated non-specific cation current (I_h) has been shown to have an increasing density along the dendrite over six-fold (Magee 1998). Because of the

increasing density along the dendrite, both A-type and I_h conductances reduce dendritic excitability, but in a different way. While A-type K^+ current suppresses the spike generation and reduces the amplitude of bAPs, I_h current dampens the synaptic integration at subthreshold voltage ranges. Since I_h is active at resting membrane potential, it can affect the passive properties of the neuron such as a decrease in input resistance and membrane time constant, which is crucial to the temporal summation of EPSPs (Magee 1998). When the EPSPs travel down from the dendrite to the soma, the passive cable filtering effect of the dendrite decreases their amplitude and slows the kinetics depending on the distance from the soma. However, it has been found that when the EPSPs from different locations of the dendrite arrive at the soma, they are indistinguishable (Magee 1999, Magee 2000, Magee & Cook 2000). This is because the distance-dependent attenuation of EPSP amplitude is compensated by the gradual increase in AMPA receptor density along the dendrite (Andrasfalvy & Magee 2001) and the increasing density of I_h along the dendrite counterbalances the slowed kinetics of the EPSPs (Magee 1999). I_h also normalizes neuronal firing after the LTP induction in homeostatic manner. The increase in localized synaptic strength after LTP increases the propensity of an action potential generation by the potentiated EPSPs. However, the global intrinsic excitability is reduced by the increase in I_h current that occurs through the synaptic signaling pathway triggered by LTP induction protocol. This intrinsic plasticity of I_h thus can achieve the balance between enhanced local dendritic excitability and reduced global neuronal excitability and provide a homeostatic mechanism of network stability (Fan et al 2005). Furthermore, I_h density can be changed in the opposite direction by LTD induction providing a mechanism of bidirectional change in intrinsic excitability (Brager & Johnston 2007). On the other hand, the non-uniform distribution of I_h along the dendrite determines the activity- and location- dependent intrinsic oscillatory response of

the neuron that mediates a characteristic 3–10 Hz theta frequency membrane potential oscillations in the hippocampus (Narayanan & Johnston 2007, Narayanan & Johnston 2008).

1.5 STRUCTURE AND FUNCTION OF Na^+ CHANNEL

The voltage-gated sodium channel is a main source of inward current in neurons and plays an important role in generation and back-propagation of action potentials, initiation of dendritic spikes, and integration of synaptic inputs. A functional Na^+ channel is composed of four α-subunit homomers as a single protein and associated with one or more auxiliary β subunits. The α-subunit of voltage-dependent Na^+ channel is encoded by 10 genes ($Na_V1.1$ –1.9 and Na_X). Among them, $Na_V1.1$–1.3 and $Na_V1.6$ are expressed in the mammalian central nervous system. Since $Na_V1.3$ is transiently expressed in a certain developmental period such as embryonic and neonatal age, the Na^+ currents in the brain are mainly constituted by the $Na_V1.1$, $Na_V1.2$ and $Na_V1.6$ isoforms (Vacher et al 2008). The α-subunit of Na^+ channel can be associated with four auxiliary β subunits (β1–4) and is about 260 kDa size transmembrane protein with 4 interconnected homologous domains (I–IV). Each domain consists of 6 helical transmembrane segments (S1–S6), of which the S4 segment has positively charged residues at every 3rd position and serves as the voltage sensor. Upon depolarization of the membrane potential, these residues move across the membrane and activate the channel. With prolonged depolarization, the intracellular loop linking domain III and IV, acting as an inactivation gate, blocks the channel pore and inactivates the channel. Extracellular membrane re-entrant loops between S5 and S6 of each domain and the inner pore lined by S5 and S6

segments selectively filter and permeate Na^+ ions into the cytoplasmic side (Catterall et al 2005, Vacher et al 2008).

Three functionally different macroscopic Na^+ currents are expressed by $Na_V1.1$, $Na_V1.2$, and $Na_V1.6$ isoforms in the CNS neuron: a transient fast inactivating current (I_{NaT}), resurgent current (I_{NaR}), and persistent, slowly or non-inactivating current (I_{NaP}). The transient Na^+ current (I_{NaT}) is activated rapidly and inactivates within a few milliseconds. For instance, it was reported that I_{NaT} in hippocampal neurons can be activated with the activation time constant (τ_m) of 0.16 ms and inactivation time constant (τ_h) of 0.84 ms at -20 mV at room temperature (Martina & Jonas 1997), but see Fig. 3.3 in Chapter 3 for recent measurements. Activation is half maximal at -23.9 mV and the voltage-dependence of activation changes in e-fold (i.e. 2.72 fold) with membrane voltage change of 11.8 mV (Martina & Jonas 1997). The fast inactivation is mediated through the blocking of the opened channel by the cytoplasmic domain III – IV linker, more specifically, three hydrophobic isoleucine-phenylalanine-methionine (IFM) residues (Patton et al 1992, Stühmer et al 1989, Vassilev et al 1989). The rapid onset of activation and inactivation and its large amplitude make I_{NaT} suitable for the generation of action potentials.

The resurgent current (I_{NaR}) is an unusual time- and voltage-dependent Na^+ current evoked by an action potential-like voltage command that mimics the strong depolarization and subsequent repolarization of the spike. For instance, the repolarization to -40 mV following +30 mV depolarization evokes transient TTX-sensitive inward current of several hundred pA (Raman & Bean 1997). It may be generated by rapid recovery from inactivated channels through open states overcoming the 'refractory period' that is inevitable in conventional fast inactivation of Na^+ channel. I_{NaR} seems to be mediated by an endogenous open channel blocking particle other than the III-IV linker of

the Na^+ channel. The blocking particle seems to bind to the channel in the open state and prevent the channel from undergoing fast inactivation. This blocking particle could exit during membrane repolarization generating I_{NaR}. The possible locations of the blocking particle are $Na_V1.6$ pore-forming α-subunits and cytoplasmic tail of the β4 Na^+ channel subunit (Grieco et al 2005, Raman & Bean 1997). Since I_{NaR} provides further depolarization right after the repolarization, it could underlie high frequency firing and all-or-none burst firing of the neuron.

Persistent, slowly or non-inactivating Na^+ current (I_{NaP}) is a small Na^+ conductance activated at subthreshold voltage ranges where most of neuronal computations occur. As its name indicates, I_{NaP} inactivates slowly or does not inactivate up to several seconds depending on the voltage command applied. The mechanism underlying this slow- or non-inactivation of Na^+ channel is not known. I_{NaP} has 0.5 – 5 % of amplitude of I_{NaT} and 10–30 mV lower half maximal activation voltage than that of I_{NaT} (Bean 2007, Crill 1996). Due to its slowly- or non-inactivating characteristics and activation at resting membrane potential, I_{NaP} can have a significance impact on the neuronal excitability by regulating spike initiation, repetitive firing, amplifying dendritic depolarization, and producing afterdepolarizations and plateau potentials. The question about the role of I_{NaP} in those physiological functions forms the basic of this dissertation.

1.6 PERSISTENT SODIUM CURRENT(I_{NaP}) AND NEURONAL EXCITABILITY

In heart muscle, persistent inward Na^+ current is activated during the upstroke of cardiac action potential and plays an important role in setting the action potential duration that is critical to rhythmic beating of the heart (Attwell et al 1979, Dudel et al 1967). In contrast, I_{NaP} in the central nervous system was first described by Hotson and colleagues

as an ionic conductance that is responsible for the increase in membrane resistance in a voltage range subthreshold to neuronal firing and is sensitive to tetrodotoxin (TTX) in hippocampal CA1 neurons (Hotson et al 1979). Llinás and Sugimori reported a slow local depolarization before spikes and prolonged plateau potential outlasting the stimulus in their intracellular recording of the Purkinje cell, and attributed those observations to the non-inactivating Na^+ conductance (Llinás & Sugimori 1980). Later, a series of studies in various preparations showed that non-inactivating inward current could be blocked by extracellular TTX, intracellular QX-314, or substitution of $[Na^+]_{out}$ ions by choline or Tris, and that it was activated at lower voltages than the transient Na^+ current (I_{NaT}) by ~10 mV (Brown et al 1994, Connors et al 1982, French et al 1990, Stafstrom et al 1982, Stafstrom et al 1984). I_{NaP} has been found throughout the central nervous system in regions such as the neocortex, hippocampus, thalamus, entorhinal cortex, and cerebellum (Crill 1996, Taylor 1993). One of Na^+ channel isoforms, $Na_V1.6$, has been considered as a possible molecular substrate for I_{NaP} due to its slow inactivation kinetics (Raman et al 1997, Rush et al 2005, Smith et al 1998).

It remains controversial whether I_{NaP} originates from a distinct subset of sodium channels or a separate gating mode of the same channel. Data supporting I_{NaP} resulting from a separate channel include directly recorded non-inactivating channels (Magistretti & Alonso 1999, Masukawa et al 1991). The lower activation voltage of I_{NaP} than I_{NaT} by about 10 mV (French et al 1990) and a differential distribution of a non-inactivating subtype $Na_V1.6$ of sodium channel (Waxman 2000, Waxman 2006) could be counted as indirect, but not conclusive, evidence. On the other hand, there are data that supports the idea that I_{NaP} results from a modified or alternate gating mode of the "normal" I_{NaT} sodium channel. The late openings or long-duration bursts of opening of the channels in the patch were recorded and their summation was interpreted as a sustained inward current

showing more than one gating mode of Na^+ channel (Alzheimer et al 1993b). The Na^+ channels that open late or in burst mode show the same single channel conductance and reverse potential as the Na^+ channel that makes only early transient opening (Patlak & Ortiz 1985, Patlak et al 1986). The slow inactivation of I_{NaP} just as I_{NaT} further provided a support for modal gating hypothesis (Fleidervish & Gutnick 1996).

In spite of the controversy concerning its mechanism, there is a consensus that I_{NaP} can play an important functional role in information processing of the neuron. Although the amplitude of I_{NaP} is small, I_{NaP} can have an influence on neuronal firing behavior because it is activated at subthreshold voltage range where the input resistance is high and most of other voltage gated channels are not activated (Crill 1996). For example, rhythmic firing and self-sustained depolarization toward spike threshold resulting from I_{NaP} were observed in the neocortical neurons (Stafstrom et al 1982). Protein kinase C (PKC) phosphorylated Na^+ channels up-regulated I_{NaP} resulting in spike threshold reduction (Astman et al 1998). Prepotentials, which are local regenerative depolarizations at subthreshold voltages preceding the somatic spike, are sensitive to TTX, but not Cd^{2+} nor Ni^{2+} indicating the role of I_{NaP} in their generation (Hu & Hvalby 1992, Macvicar 1985). Similarly, the amplification of dendritc and/or somatic synaptic integration was explained by the presence of subthreshold Na^+ conductance (I_{NaP}) in neurons because the inward current was activated at depolarized potentials and blocked by TTX (González-Burgos & Barrionuevo 2001, Schwindt & Crill 1995, Stuart & Sakmann 1995). Furthermore, the amplification of the backpropagating action potential observed at distal dendrites could be attributed to the activation of I_{NaP} due to its sensitivity to TTX (Stuart & Häusser 2001). The involvement of I_{NaP} in pacemaking activity, subthreshold oscillations, afterhyperpolarizations (AHPs), afterdepolarizations (ADPs), and plateau potential also have been reported (Alonso & Llinás 1989, Beurrier et al 2000, Bevan &

Wilson 1999, Do & Bean 2003, Hoehn et al 1993, Hu et al 2002, Llinás & Sugimori 1980, Vervaeke et al 2006, Yue et al 2005).

The modulation of I_{NaP} in physiological and pathophysiological conditions, therefore, can have a significant influence on neuronal function. A fast posttranslational modification of Na^+ channel through phosphorylation can often drive a short-term modification of I_{NaP} (Astman et al 1998). The rapid modulation of Na^+ channel can occur through phosphorylation of second messenger dependent protein kinases such as cyclic adenosine monophosphate (cAMP)-dependent protein kinase A (PKA), diacylglycerol (DAG)-dependent protein kinase C (PKC), and mitogen-activated protein kinase (MAPK) (Cantrell & Catterall 2001, Numann et al 1991, Smith & Goldin 1997, Wittmack et al 2005). For instance, although PKA activation does not modulate I_{NaP} effectively (Maurice et al 2001), the modulation of I_{NaP} by PKC signaling pathways such as PKC mediated doparminergic or muscarinic modulation of I_{NaP} was observed (Astman et al 1998, Gorelova & Yang 2000, Mittmann & Alzheimer 1998, Rosenkranz & Johnston 2007). PKC is known to phosphorylates Na^+ channel on serines 554, 573, 576, and 1506 (Cantrell et al 2002, Numann et al 1991, West et al 1991). Also, it has been known that prolonged sodium channel inactivation on the dendrite decreased the amplitude of bAPs in an activity-dependent manner and the recovery from slow inactivation was enhanced by PKC phosphorylation of Na^+ channel (Colbert & Johnston 1998, Colbert et al 1997, Jung et al 1997). Other signaling pathways known to modulate I_{NaP} are the nitric-oxide pathway and direct G-protein interactions (Hammarström & Gage 1999, Ma et al 1997). The long term changes of Na^+ channel density and composition of $Na_V1.6$ isoform were observed in pathological conditions of neurons such as de-myelination, neuroma, axonal transaction, and sensory input deprivation and resulted in increased neuronal excitability through up-regulation of I_{NaP} (Aizenman et al 2002,

Waxman 2000, Waxman 2006). The increase in osmolarity resulting form the salt loading condition could up-regulate the expression of $Na_V1.6$ channel and consequent I_{NaP} density (Tanaka et al 1999).

1.7 General Methodology

In spite of many interesting biophysical and physiological features stated above, I_{NaP} is one of the most unexplored ion currents in neurons due to the difficulties in using quantitative biophysical techniques, such as voltage-clamp, in neurons with a complex morphology. Neurons have a complex 3-dimensional structure. The combination of passive electrical properties and active ionic currents determines a particular neuron's electrotonic structure. When a voltage clamp is applied to a neuron with complex morphology, there will be ionic current across the membrane and intracellular current flow along the axial direction. The membrane potential can be held constant only in the vicinity of the electrode, and the rest of the neuron will show a gradually attenuated membrane potential resulting in non-constant membrane potential in space, so called 'space clamp problem' (Johnston & Wu 1995, Williams & Mitchell 2008). Because it is difficult to obtain an adequate space clamp in whole cell configuration where the voltage is expected to be maintained constant throughout whole region, one can achieve a good voltage control by clamping a small membrane area using cell-attached configuration and study the behavior of a single or small number of individual ion channels in the patch. However, because I_{NaP} takes up only <5% of transient Na^+ current, a channel showing persistent activity would be detected in very low probability in the small size of patch in cell attached patch recordings. To increase the probability of measuring I_{NaP} with a reasonable quality of voltage clamp, we mainly utilized a nucleated patch recording, a

technique that obtains a spherical shape of large size of perisomatic membrane patch along with the support of the nucleus pulled (Martina & Jonas 1997). Channel blockers and choice of voltage command protocols in the nucleated patch recording can be used to increase the quality of the voltage clamp and obtain useful data.

Chapter 2 Materials and Methods

Slice preparation and typical conditions

Transverse hippocampus brain slices were prepared from 4-6 week-old male Sprague Dawley rats following a protocol that was approved by the University of Texas at Austin Institutional Animal Care and Use Committee (IACUC). The animals were anesthetized with an injection of a mixture of ketamine (91 mg/ml) and xylazine (9.1 mg/ml) intraperitoneally. Anesthetized rats were purfused intracardially with ice-cold dissection buffer containing (in mM) 2.5 KCl, 1.25 NaH_2PO_4, 25 $NaHCO_3$, 0.5 $CaCl_2$, 7 $MgCl_2$, 7 dextrose, 210 sucrose, 1.3 ascorbic acid, and 3 sodium pyruvate (all drugs were from Sigma, St. Louis, MO, unless specified otherwise). After perfusion, the animal was decapitated, the brain was quickly removed and 350 μm thick slices were made with a Vibratome (Vibratome Series 1000; Vibratome, St. Louis, MO). The brain slices were incubated in continuously oxygenated (95% O_2 and 5% CO_2) external solution including (in mM) 125 NaCl, 2.5 KCl, 1.25 NaH_2PO_4, 25 $NaHCO_3$, 2 $CaCl_2$, 2 $MgCl_2$, 10 dextrose, 1.3 ascorbic acid, and 3 sodium pyruvate. They were incubated about 15 minutes at 35–37°C and then moved to room temperature (24°C) for at least 50 minutes before they were transferred to the recording chamber and the experiment begun. All recordings were performed in the recording chamber that was continuously perfused with artificial cerebrospinal fluid (ACSF) containing (in mM) 125 NaCl, 3 KCl, 25 $NaHCO_3$, 2 $NiCl_2$, 1 $MgCl_2$, 10 dextrose, 1.3 ascorbic acid, and 3 Na^+ pyruvate, and aerated with 95% O_2/5% CO_2. CA1 pyramidal neurons were visualized with a Zeiss Axioskop (Carl Zeiss Microimaging, Thornwood, NJ) equipped with infrared differential interference contrast

(IR-DIC) optics and a 60x water-immersion objective (Olympus, Center Valley, PA). Pyramidal neurons with long apical dendrites were selected for the recording. Borosilicate glass electrodes of 2.0 mm OD and 1.16 ID (Sutter Instruments, Novato, CA) were used to pull 4–6 MΩ patch electrodes using a Flaming/Brown P-97 micropipette puller (Sutter Instrument, Novato, CA). All recordings were carried out near physiological temperature (31–34 °C) and electrodes were wrapped in Parafilm (Pechiney Plastic Packaging, Chicago, IL) within about 200 μm from the tip to reduce electrode capacitance.

Whole-cell voltage-clamp recordings

Somatic whole-cell voltage clamp recordings were performed to access qualitatively the presence of persistent Na^+ current in CA1 pyramidal neurons and test the effect of drugs during the initial stages of the project. Pipette solutions included (in mM) 10 CsCl, 120 Cs-gluconate, 10 HEPES, 4 NaCl, 0.1 3,4-diaminopyridine, 4 Mg-ATP, 0.3 Na-GTP, 7 K_2-phosphocreatine and PH 7.3 adjusted by TEA-OH. A slow ramp voltage protocol of 10 mV/s velocity was applied to inactivate all the transient sodium currents leaving persistent Na^+ currents. The current signals were amplified and filtered at 1kHz using Axopatch 200B (Axon instruments; Molecular Devices, Sunnyvale, CA). Series resistance (17.0 ± 1.7 MΩ; n=7) and baseline membrane current were monitored throughout the experiment on-line without compensation. If the change in series resistance of the cell went above 30%, the experiment was discarded.

Nucleated patch voltage-clamp recordings

Nucleated patch recordings were made after a whole-cell recording was obtained by slowly withdrawing the electrode while applying negative pressure (Martina & Jonas

1997, Sather et al 1992). Nucleated patches had input resistances of 2–10 GΩ. Current signals were collected with an Axopatch 200B amplifier (Axon instruments; Molecular Devices, Sunnyvale, CA). The pipette solution included (in mM) 10 CsCl, 120 Cs-gluconate, 10 HEPES, 4 NaCl, 0.1 3,4-diaminopyridine, 4 Mg-ATP, 0.3 Na-GTP, 7 K_2-phosphocreatine and was adjusted to pH 7.3 with TEA-OH. Since there was significant amount of Ca^{2+} current by low voltage activated (LVA) and high voltage activated (HVA) Ca^{2+} channels (Magee and Johnston, 1995), 2 mM extracellular Ca^{2+} was replaced by 2 mM Ni^{2+} to block the Ca^{2+} currents. Persistent Na^+ current was elicited by a 0.4 mV/ms ramp voltage command. Persistent Na^+ current was isolated either by subtracting traces recorded in the presence of tetrodotoxin (TTX) from traces recorded in standard experimental saline (TTX subtraction; Fig. 2.1A) or by fitting a line to points more negative than -60 mV and subtracting the extrapolated line from the whole trace (linear leak subtraction; Fig. 2.1B). Currents in response to step commands were corrected for leakage currents by subtracting the scaled leak traces generated by 1/10 amplitude of voltage command from the raw traces (P/10 protocol) or by using the TTX subtraction method. For the activation conductance-voltage (G-V) curves, a series of depolarizing step voltage commands from -70 to +40 mV in steps of 10 mV for 50 ms with V_{hold}= -80 mV was applied with a 2–3 second interval (activation protocol). Conductance (G) was calculated by dividing the peak amplitude (I) for each step by the driving force: $G = I/(V - E_{Na})$. The normalized conductance was plotted against the voltage command. For the steady state inactivation curve, 500 ms pre-pulses to voltages varying from -90 mV to -10 mV in steps of 10 mV were followed by a constant 50 ms test pulse to 0 mV with V_{hold} = -90 mV (inactivation protocol) and the same P/10 protocol was used for leak subtraction. Peak amplitude of current during the test voltage command was normalized and plotted versus pre-pulse potential. Series resistance (9.2 ± 1.0 MΩ; n=17) was monitored and

compensated up to 60% using a built-in series resistance compensation circuitry in Axopatch 200B amplifier. The measured liquid junction potential of -7.5 mV were not corrected.

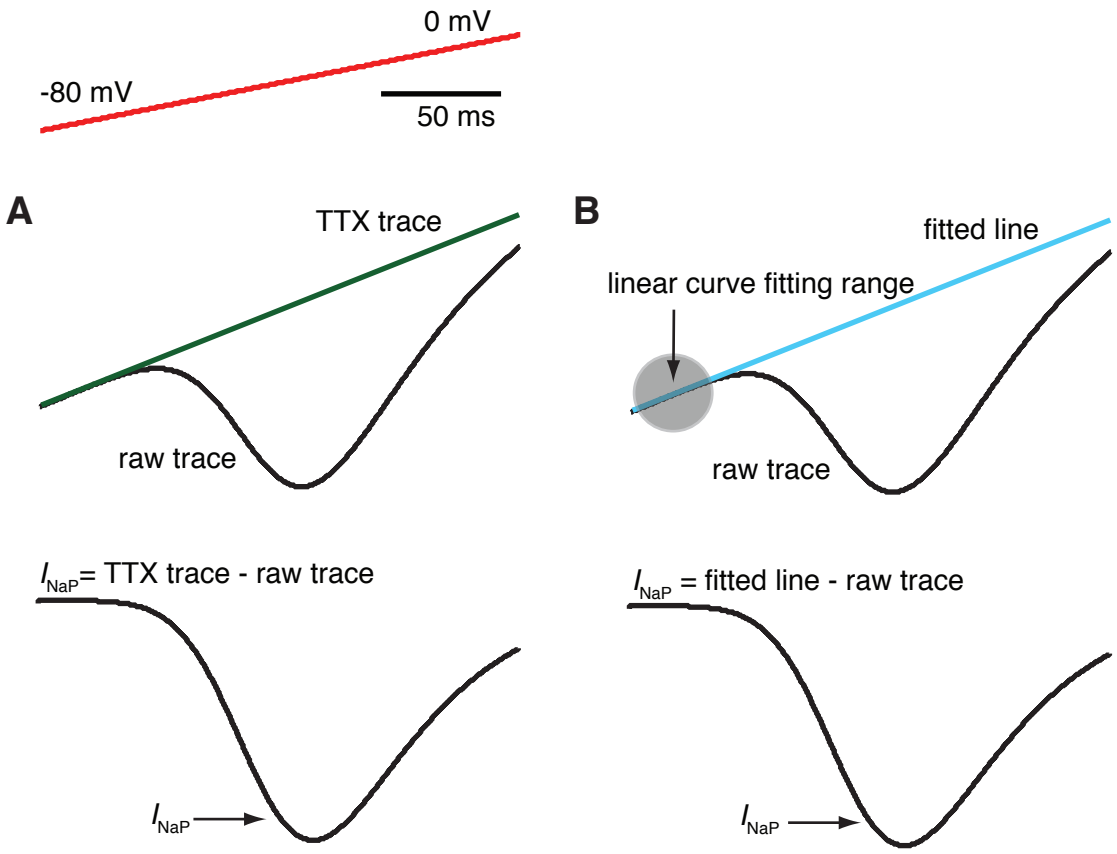

Figure 2.1: Schematic diagrams illustrating how the persistent Na^+ current was isolated by two leak current correction methods

A: Persistent Na^+ current was isolated by TTX subtraction method. For the detailed explanation, see text. **B**: Persistent Na^+ current was isolated by linear leak subtraction method. For the detailed explanation, see text. Both methods generate isolated I_{NaP}.

Whole-cell current-clamp recordings

The pipette solution included (in mM) 20 KCl, 120 K-gluconate, 10 HEPES, 4 NaCl, 4 Mg-ATP, 0.3 Na-GTP, 7 K_2-phosphocreatine with pH adjusted to 7.3 with KOH. Voltage signals were amplified and filtered at 5 kHz using a BVC-700A amplifier (Dagan, Minneapolis, MN). Access resistance and resting membrane potential were monitored throughout the experiment on-line. Access resistance was compensated with the amplifier's bridge circuit and was no more than 30 MΩ and resting membrane potential was positioned in the range of -68 to -60 mV

Drug application

0.5 μM tetrodotoxin (TTX) and 1.4 mM hexanol, putative Na^+ channel blockers, were bath applied for both whole cell voltage-clamp and current-clamp experiments. For nucleated patch recordings, 2 μM TTX, 2.8 mM hexanol, 10 μM riluzole, or 30 μM ranolazine was included in a puffer pipette that also contained (in mM) 149 NaCl, 3 KCl, 1 $MgCl_2$, 10 HEPES, 2 $NiCl_2$, 10 dextrose, 1.3 ascorbic acid, and 3 Na^+ pyruvate with pH adjusted to 7.3 with NaOH. A pair of puffer pipettes of 3–4 μm diameter was pulled and one electrode was loaded with fast green dye in order to confirm the diffusion pattern of puffing. The other electrode was loaded with the drug being used for that experiment and the patch was located in the drug diffusion region identified by the dye. Drugs were applied by a pressurized injection system (Picospritzer II, General Valve Corporation) or passive release of pressure via check valve. When it was necessary for a neuron to be isolated from the network, all AMPA, NMDA, $GABA_A$, and $GABA_B$ receptor mediated synaptic transmission was blocked respectively by CNQX (10 μM) or DNQX (20 μM), DL-AP-5 (50 μM), bicuculline (10 μM in DMSO) and pircrotoxin (10 μM in ethanol), and (2S)3-[[(1S)-1-(3,4-dichlorophenyl)ethyl] amino-2-hydroxypropyl] (phenylmethyl)-

phosphinic acid (CGP55845) (2 μM in DMSO). 1 mM riluzole stock was made by dissolving it into DMSO and diluted with puffing solution to the final concentration of 10 μM right before the experiment. The total amount of DMSO in external solution remained below 0.1%, and total amount of ethanol in the bath was maintained below 0.05%. Halothane, a volatile anesthetic agent, was dissolved into ACSF using sonication (Model 50HT, VWR, Randor, PA) and prepared about 16 mM stock solution in a gas tight condition. The halothane stock solution was backfilled into the puffing pipette, and the remaining halothane in the puffing pipette after drug application was quantified by high-performance liquid chromatography-UV (HPLC-UV) system in the protein and metabolite analysis facility in the campus. The concentration of halothane remaining in the pipette ranged 1–3 mM.

Data collection and analysis

Data acquisition, stimulus generation, and analysis were performed with an Instrutech ITC-18 DA/AD converter (HEKA Instruments, Bellmore, NY) controlled by IGOR Pro (Wavemetrics, Portland, OR) software on an Apple computer (Cupertino, CA) using locally written procedures. Data were amplified, filtered at 1–20 kHz, and digitized at 10–200 kHz, then stored on the computer for later analysis. For the measures of persistent Na^+ current in whole-cell voltage-clamp recording, peak inward current and the amount of charge influx through inward current were calculated from the measured current traces elicited by the ramp voltage protocol with the velocity of 10 mV/s. For nucleated patch recordings, I_{NaP} and I_{NaT} were quantified with activation and inactivation curves for comparison with previously published data. A Boltzman equation $f(x) = base + \frac{\max}{1 + e^{-(x - V_{1/2})/k}}$, was fitted to both activation and inactivation curves to give

$V_{1/2}$ and k values for I_{NaP} and I_{NaT}. For whole-cell current-clamp recording, a firing vs. current injection (F-I) curve was generated by counting the number of spikes evoked by step current injections from 0 to 180 pA by 30 pA increment. Currents simulated by an alpha function, $A(t/\alpha)e^{(-\alpha t)}$, were injected to mimic excitatory postsynaptic potentials (α–EPSP injection) where A is the amplitude of injected currents, t is time, and $1/\alpha$ is the time to peak. With this shape of current injection, temporal summation (α–EPSP summation) of the neuron was quantified for both sub-threshold and supra-threshold conditions by counting the number of spikes generated by α–EPSP injections at 25 Hz. Statistical tests performed were paired t-test (for 2 groups, paired data), Kruskal-Wallis test and post hoc Dunn's test (for more than 3 groups, unpaired data), and linear regression/correlation test. The markers and error bars in the plots indicate the mean value ± SEM.

Antibody staining

$Na_V1.6$, an isoform of Na^+ channel alpha subunit and putative molecular basis of persistent Na^+ current, was immuno-stained to identify its subcellular distribution in the neuron. The whole brain or recorded brain slices were fixed in 2% paraformaldehyde (PFA) in 0.1 M phosphate buffer (PB, PH=7.3) up to 2 hours at 4ºC. Then, the sample was transferred into 0.01 M phosphate buffered saline (PBS, PH=7.4) with 30% sucrose and preserved overnight. Next day, the samples were resectioned in 50 μm thinckness on a cryostat tissue slicer (Leica SM 2000R, Leica Microsystems Inc, Bannockburn, IL). After washing in PBS, the re-sectioned slices were incubated in permeablization solution (1%Triton X-100 in PBS) for 30 minute in room temperature. The slices were washed again and then incubated in blocking solution (5% normal goat serum and 0.3% Triton X-100 in PBS) at room temperature for 2 hours. Right after this, the sections were incubated

overnight at 4ºC with mouse anti-$Na_V1.6$ primary antibody (NeuroMab, Davis, CA) diluted 1:100 in the blocking solution. On following day, the slices were rinsed in PBS and incubated at room temperature for 2 hours with Alexa594-conjugated goat anti-mouse IgG secondary antibody (Invitrogen, Carlsbad, CA) diluted 1:200 in the blocking solution. Following several washes in PBS, the slices were mounted on glass slides in Fluoromount-G solution (SouthernBiotech, Birmingham, AL). The immunofluorescence signal was visualized by Axio Imager 2 microscope and AxioVision software (Carl Zeiss Microimaging, Thornwood, NJ).

Simulation of I_{NaP} current

A single compartmental model of 10 μm length and 10 μm diameter was simulated using the NEURON simulation environment (version 7.2) (Hines & Carnevale 1997). Simulations were performed with 5 μs fixed time step and at 32 ºC. The Na^+ channel model inserted into the single compartment includes the conventional Hodgkin-Huxley formulation for Na^+ channel gating (3 activation gating variables, *m*, and 1 inactivation gating variable, *h*) with one more gating variable (slow inactivation gating variable, *i*) to mimic slow inactivation of Na^+ channel (Migliore et al 1999, Migliore et al 2004). The membrane and Na^+ channel properties were: an intracellular resistivity of R_a = 150 Ωm, the specific membrane resistance of R_m = 28000 Ωcm^2, the specific membrane capacitance of C_m = 1 μF/cm^2, a membrane time constant (= $R_m \times C_m$) = 28 ms, the maximum specific Na^+ channel conductance of g_{Na} = 0.032 S/cm^2, an intracellular Na^+ concentration of $[Na^+]_{in}$ = 4 mM, an extracellular Na^+ concentration of $[Na^+]_{out}$ = 150 mM, and a membrane resting potential of V_{rest} = -65 mV. The expressions for the I_{Na} as following:

$$I_{Na} = g_{Na} \cdot m^3 \cdot h \cdot i \cdot (V_m - 93.87)$$
$$\frac{dm}{dt} = \alpha_m(1-m) - \beta_m m = (m_\infty - m)/\tau_m$$
$$\frac{dh}{dt} = \alpha_h(1-h) - \beta_h h = (h_\infty - h)/\tau_h$$
$$\frac{di}{dt} = \alpha_i(1-i) - \beta_i i = (i_\infty - i)/\tau_i$$
$$m_\infty = \alpha_m/(\alpha_m + \beta_m)$$
$$\tau_m = 0.5/(\alpha_m + \beta_m)$$
$$\alpha_m = 0.4 \cdot (V_m + 30)/(1 - e^{-(V_m+30)/7.2})$$
$$\beta_m = 0.124 \cdot (V_m + 30)/(e^{(V_m+30)/7.2} - 1)$$
$$h_\infty = 1/(1 + e^{(V_m+50)/4})$$
$$\tau_h = 0.5/(\alpha_h + \beta_h)$$
$$\alpha_h = 0.03 \cdot (V_m + 45)/(1 - e^{-(V_m+45)/1.5})$$
$$\beta_h = 0.01 \cdot (V_m + 45)/(e^{(V_m+45)/1.5} - 1)$$
$$i_\infty = (1 + 0.8 \cdot e^{(V_m+58)/2})/(1 + e^{(V_m+58)/2})$$
$$\tau_i = 3 \cdot 10^4 \cdot \beta_i/(1 + \alpha_i)$$
$$\alpha_i = e^{0.45 \cdot (V_m+60)}$$
$$\beta_i = e^{0.09 \cdot (V_m+60)}$$

where V_m is membrane potential; m, h, and i are gating variables; m_∞, h_∞, and i_∞ are steady state gating variables; τ_m, τ_h, and τ_i, are time constants; α_m, β_m, α_h, β_h, α_i, β_i are rate constants describing gating transitions.

Chapter 3 Results

3.1 Biophysical properties and mechanism of persistent Na^+ current in hippocampal CA1 neuron

3.1.1 Introduction

The biophysical properties and distribution of voltage-gated ion channels and the corresponding voltage dependent ionic conductances regulate intrinsic excitability of the neuron. The characterization of voltage-dependent ionic conductance in a macroscopic and single channel level therefore becomes a fundamental step toward understanding the electrophysiological behavior of the single neuron and network of the neurons (Johnston et al 1996, Bean 2007). Among various voltage-gated ionic conductances, I_{NaP} is one of the most unexplored ionic conductances due to several technical difficulties. It is known that I_{NaP} can only be detected as a tiny fraction (<5%) of the large amplitude of I_{NaT}, and it impose a restriction that a relatively large patch size is required to increase the probability of I_{NaP} detection. Whole-cell voltage-clamp recording therefore has been a conventional method of choice because of its large patch area. However, leaky membrane and axial current in neurons make the whole neuronal membrane unclampable at constant voltage (Johnston & Brown 1983, Johnston and Wu 1995, Williams & Mitchell 2008). To improve the poor space-clamp condition of whole-cell voltage-clamp recording on the intact neuron, dissociated neurons that have lost most of their processes can be utilized instead. Although dissociated neurons could provide better voltage control due to their balling shape, the enzymes used in the dissociation process may confound interpretation of the results. For instance, the protease added in the dissociation media could alter the

gating properties of Na^+ channel and generate unnaturally large amount of persistent Na^+ channel activity (Rudy 1978, Gonoi and Hille 1987). Furthermore, there is no pharmacological tool to seperate I_{NaP} from I_{NaT} effectively. So, to record I_{NaP} alone, one should inactivate all the transient Na^+ channels in their state and only leave persistent Na^+ channel activities by applying a slow ramp voltage command instead of a step voltage command. Considering that the ramp voltage command makes constant change in voltage with time, I_{NaP} recorded by a ramp voltage command is unable to delineate the steady state response of persistent Na^+ channels to the membrane voltage change. Moreover, depending on the velocity of the ramp voltage, there could be a large variety for the definition of the degree of 'persistence' to which the Na^+ channels are activated. Given these technical limitations, slow progress has been made on understanding I_{NaP} (Alzheimer et al 1993c, Astman et al 2006, Fleidervish & Gutnick 1996, French et al 1990, Kay et al 1998, Magistretti & Alonso 1999, Maurice et al 2001, Stafstrom et al 1985, Urbani & Belluzzi 2000).

The quantitative measurement of I_{NaP}, however, could promote further understanding of biophysical properties and functional significance of I_{Nap} on neuronal excitability. Utilizing a nucleated patch technique can minimize the space clamp issue and provide more quantitative data about I_{NaP} in *in vitro* slice experiment (Martina & Jonas 1997, Sather et al 1992). In the nucleated patch recording, a macro somatic membrane patch is excised together with the nucleus providing compromise between large patch and imperfect space-clamp. Here we have explored I_{NaP} and investigated its biophysical properties quantitatively in hippocampal CA1 pyramidal neurons by utilizing the nucleated patch clamp method. Nucleated patch clamp recordings showed two kinetically distinct components of TTX-sensitive inward current in the neurons.

3.1.2 Persistent Na^+ current is present in the perisomatic region of hippocampal neurons

With full awareness of the caveats of whole cell voltage clamp recording (Spruston and Johnston, 2008), we first tested the existence of persistent Na^+ current in hippocampal CA1 pyramidal neurons under whole cell voltage clamp because it is a quick and simple approach to explore the existence of persistent Na^+ current and can provide motivation for further efforts to quantify and characterize the ionic current in other recording configurations.

A slow ramp voltage command, which is a slowly increasing voltage with time, was shown to selectively activate I_{NaP} because I_{NaT} was inactivated (Fleidervish and Gutnick, 1996a; Fleidervish et al., 1996b; Astman et al., 2006). Thus, a slow ramp voltage command was used to record I_{NaP} traces in hippocampal CA1 pyramidal neurons. Outward potassium channels and inward calcium channels were blocked with ionic substitutions and pharmacological blockers. Cesium salts (10 mM CsCl, 120 mM Cs-gluconate), 3-4 Diaminopyridine (0.1 mM 3-4 DAP) and Tetraethylammonium hydroxide (TEA-OH) were used to block potassium channels. Nickel salt (2 mM $NiCl_2$) without external calcium was used to block calcium channels.

Initially, the optimal velocity of the voltage ramp was determined; fast ramps would predominately activate the fast, transient Na^+ current while very slow ramps might inactivate the persistent (but not totally inactivating) Na^+ current. The speed of ramp voltage command for the inactivation of transient Na^+ current but leaving persistent Na^+ current was determined by testing of several ramp speeds. Figure 3.1A shows different responses of 4 ramp slopes: 333 mV/s, 100 mV/s, 33.3 mV/s, and 10 mV/s. A slow voltage ramp with a slope smaller than 33.3 mV/s generated I_{NaP} traces stably, because I_{NaT} has undergone voltage-dependent closed-state inactivation on this time scale.

The ramp command in voltage-clamp generates an instantaneous I-V curve. Cs-rich internal solution and appropriate channel blockers with zero calcium in the external solution exclude all the other ion flow except Na^+ influx and the linear leak current can be subtracted by fitting the current trace at potentials more negative than -70 mV and subtracting the extrapolated line from the whole trace. Figure 3.1B shows an example recording: a ramp response (Fig.3.1B upper left), blocking of the ramp resonse by 0.5 μM TTX to provide estimation of I_{leak} (Fig.3.1B upper right), leak subtraction (Fig.3.1B lower left), and resulting net inward current (Fig.3.1B lower right). The inward current can be assumed to be a Na^+ current because it was blocked by 0.5 μM TTX and its slow inactivation characteristics confirm that it is a persistent current and not a fast inactivating current. After leak subtraction, the persistent Na^+ current (I_{NaP}) shows the peak amplitude of about -123 pA in this cell.

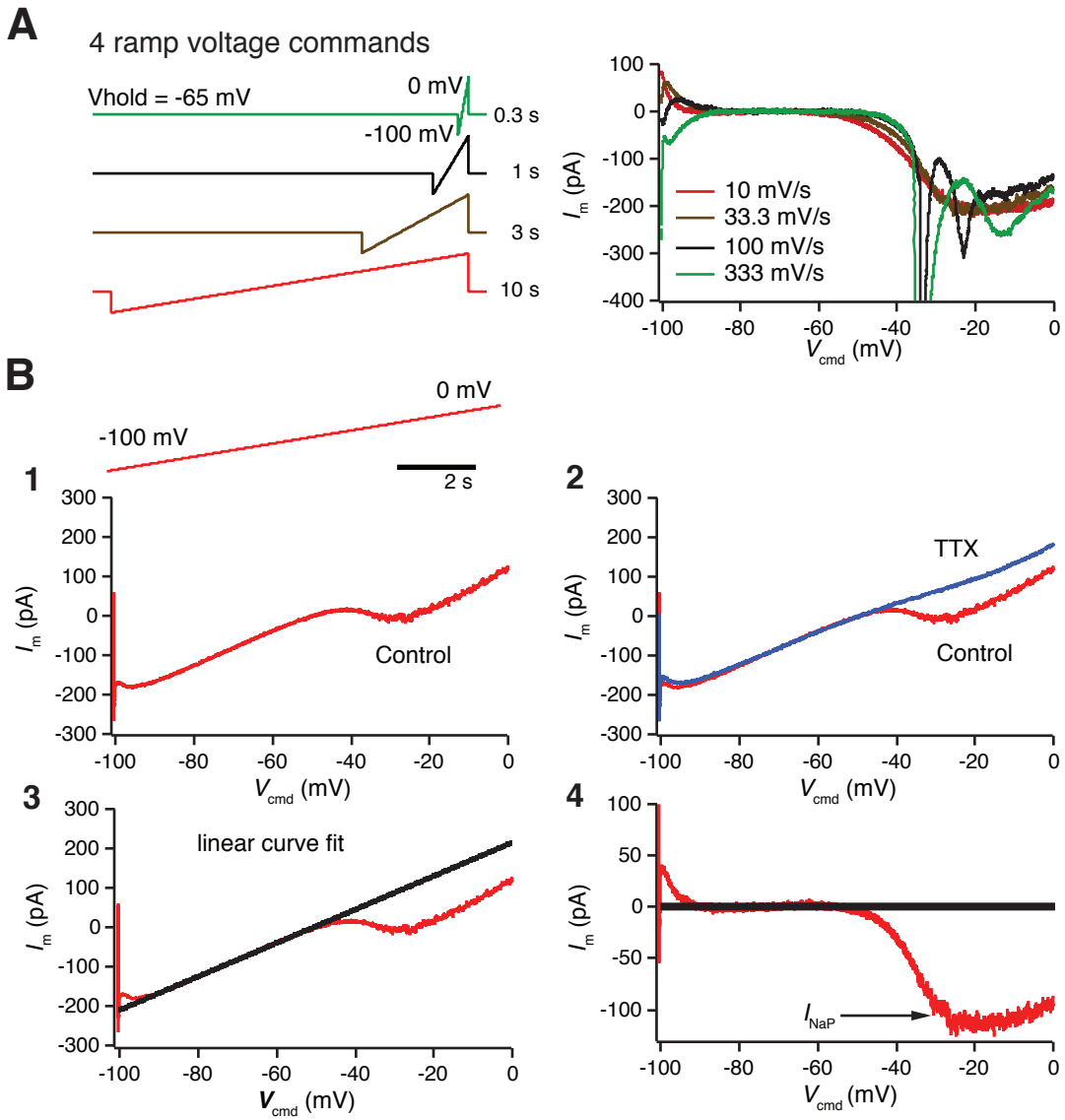

Figure 3.1: Persistent Na^+ current in whole-cell voltage-clamp recording
A: Slow voltage ramp inactivated the transient sodium current and slowly activated the persistent inward current. Slower voltage ramps with the slopes of 33.3 mV/sec and 10 mV/sec were successful in suppressing the transient sodium current and exposing the slowly inactivating persistent current. **B**: The slowly inactivating inward current was blocked by TTX. Inward persistent current evoked by 10 mV/sec ramp command (B-1) was blocked by 0.5 μM TTX (B-2). The leak current was subtracted by fitting a line along the hyperpolarized region of the recorded current around -80 to -60 mV range and subtracting it from the whole trace (B-3). After linear leak subtraction, persistent Na^+ current was shown (B-4).

3.1.3 Separation of persistent and transient Na^+ currents in hippocampal neurons

We solidified the existence of the I_{NaP} recorded in the whole-cell voltage clamp configuration by using a quantitative measurement method, nucleated patch recording (Martina & Jonas 1997, Sather et al 1992). The spherical shape and small size (~10 μm diameter) of the nucleated patch enabled us to investigate I_{NaP} with little error associated with imperfect space-clamping, and under this condition we measured both I_{NaP} and I_{NaT} to compare their properties.

In Fig. 3.2A, an exemplary nucleated patch (right) of about 10 μm diameter is illustrated that was pulled from an *in situ* neuron (left). Following the lead of others (Cummins et al 1998, Raman et al 1997), we used a slow voltage ramp command (-80 to 0 mV, 0.4 mV/ms velocity) that would allow I_{NaT} to undergo inactivation, leaving the slowly inactivating I_{NaP} (Fig. 3.2B-1). The current traces evoked by a step voltage command from resting membrane potential to -10 mV showed the reversible TTX effect and confirmed the TTX sensitive inward current in the patch (Fig. 3.2B-2). Then, we tested the existence of sustaining Na^+ current in step voltage commands by subtracting the measured current trace in presence of 2 μM TTX from the control current trace. A step voltage command from -80 mV to -20 mV applied to a nucleated patch elicited both a large transient (presumed to be I_{NaT} of -129.2 pA amplitude at the peak) and a much smaller sustained inward current (presumed to be I_{NaP} of -2.5 pA amplitude at 100 ms), both of which were blocked by TTX (Fig. 3.2C). Current in response to a subthreshold command (-70 mV) is shown for comparison and there was no identifiable inward Na^+ current (Fig. 3.2C). Thus, in nucleated patch recordings, we observed a persistent TTX-sensitive current that we tentatively identified as I_{NaP} in both ramp and step voltage command protocols.

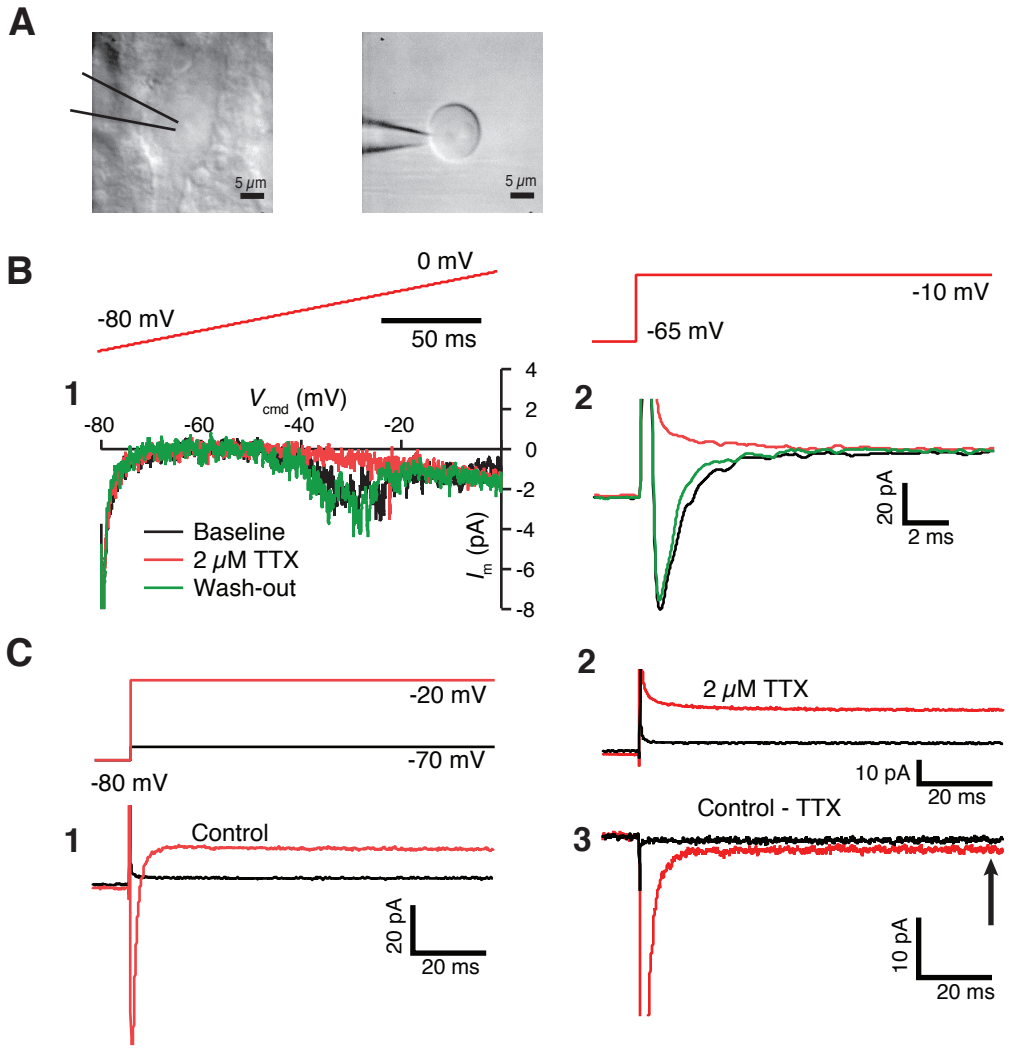

Figure 3.2: Persistent Na^+ currents in nucleated patch recording
A: Image showing a whole cell configuration (left). A nucleated patch with about 10 μm diameter was pulled from the *in situ* neuron (left). **B**: TTX-sensitive inward currents around -40 to -20 mV were elicited by 0.4 mV/ms ramp voltage command and blocked by 2 μM TTX puffing (B-1). For the comparison, the transient Na^+ current was measured by a voltage step command (B-2). **C**: 100 ms voltage step revealed a sustained inward Na^+ current. Example responses of two voltage step commands were shown where depolarization voltage steps to -20 and -70 mV (C-1). 2 μM TTX applied by puffing blocked all Na^+ currents (C-2). Subtraction of TTX traces from raw traces generates both transient and persistent Na^+ current (C-3).

Because we circumvented the space clamp problem by utilizing nucleated patch recordings, we could quantitatively characterize the activation kinetics (τ_m) of transient Na^+ current at near physiological temperature (31 – 33 ºC). With a wide bandwidth of low pass filter (20 kHz) and high sampling frequency (200 kHz), we are able to measure τ_m (22.2 ± 2.3 μs at 40 mV) (Fig. 3.3).

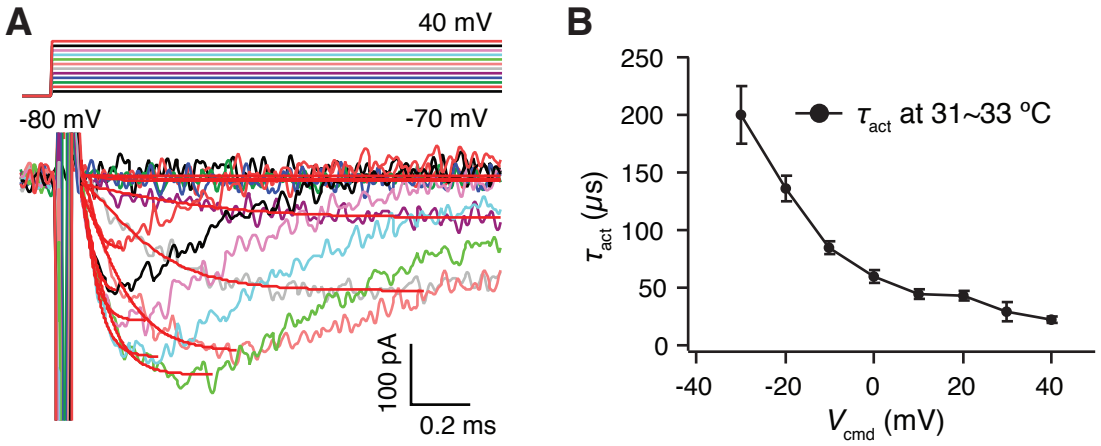

Figure 3.3: Activation time constant of Na^+ current
The onset kinetics of Na^+ current was measured at near physiological temperature (31 – 33 ºC) in high bandwidth recording (-3dB 8-pole Bessel low pass filter with 20 kHz cutoff frequency and 200 kHz sampling frequency). **A**: Exemplary Na^+ traces evoked by activation protocol (see *methods*) are shown and fitted by cubic exponential function, $f(x) = A \cdot (1 - e^{-(x-x_0)/\tau_m})^3$ to generate activation time constant, τ_m. **B**: The Na^+ current activation time constant is displayed against voltage command.

We compared this ramp-evoked Na^+ current to the transient Na^+ current at three time points to estimate the degree to which Na^+ current inactivates during the ramp command. I_{NaT} (average max amplitude -125.5 ± 28.8 pA at 0 mV; n=4) was evoked by 100-ms step commands at -70 to +40 mV from -80 mV holding potential. The mean amplitudes of I_{NaT} were calculated at three time points: peak (I_{peak}; 50 data points average around the peak), 20 ms (I_{20ms}; average from 19 to 20 ms), and 100 ms (I_{100ms}; average

from 99 to 100 ms) (Fig. 3.4A). The Na^+ current evoked by a 0.4 mV/ms ramp voltage command from -80 to 40 mV was isolated by TTX subtraction and had average peak amplitude of -6.8 ± 0.9 pA at -27.7 mV (n=4). In the same neurons, normalized IV plots of peak currents from step and slow ramp commands were compared (Fig. 3.4B-1). I_{NaP} was activated at a lower voltage range than I_{NaT} by about -27 mV. However, the I-V curve measured 20 ms after step commands (Fig. 3.4B-2) was very similar to the current in response to a slow ramp, suggesting that the Na^+ current at 20 ms reflects primarily I_{NaP} after most of I_{NaT} has been inactivated (Aldrich et al 1983). Current in response to step commands measured at 100 ms were further decreased in amplitude around -40 to -20 mV range suggesting that I_{NaP} undergoes slow inactivation (Fig. 3.4B-2).

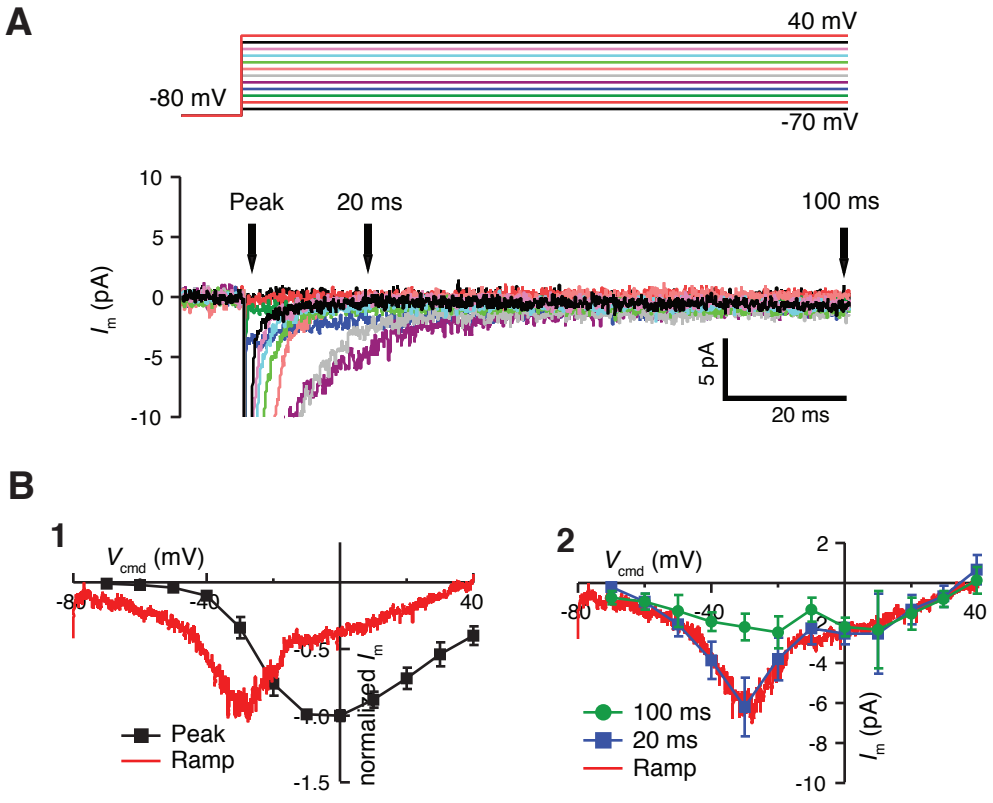

Figure 3.4: Inactivation of Na^+ current at three different time points after channel activation

A: The amplitudes of Na^+ currents isolated by TTX subtraction were measured at the peak (I_{peak}), 20 ms (I_{20ms}), and 100 ms (I_{100ms}) after the activation. **B**: Comparison among I_{Peak}, I_{20ms}, I_{100ms} and I_{ramp}. The normalized peak transient current and ramp current were displayed against voltage commands. Normalized I_{ramp} gave lower peak voltage than that of normalized I_{peak} (-28.1 mV vs -10 mV) (B-1). I_{20ms}, I_{100ms} and I_{ramp} were displayed in the same plot for direct comparison. I_{20ms} and I_{ramp} gave a remarkable match while I_{100ms} and I_{ramp} showed the mismatch between I_{100ms} and I_{ramp} around -40 to -20 mV voltage range suggesting the slow inactivation of Na^+ current in that voltage range (B-2).

3.1.4 Comparison of biophysical properties of persistent and transient Na^+ currents suggests the same origin of both currents in different gating mode

One hypothesis for the mechanism of I_{NaP} is a "window current" (Hodgkin & Huxley 1952) that is a non-inactivating current generated by overlapping of activation

and inactivation curves at narrow voltage range. To see whether a window current could explain I_{NaP}, we recorded both I_{NaP} and I_{NaT} from the same neurons (n=18) and compared I_{NaP} to the calculated "window current" from the activation and inactivation curves of I_{NaT}. Fig.3.5A shows a schematic diagram of the nucleated patch and the protocol used. Once a nucleated patch was obtained, I_{NaP} was recorded first (Fig.3.5B) and then I_{NaT} was obtained through activation and inactivation protocols (Fig.3.5C). After obtaining I_{NaT} activation traces by the activation protocol, the conductance of activation I_{NaT} (G_{NaT}) was calculated by Ohm's law, $G_{NaT} = I_{NaT} /(V_{cmd} - E_{Na})$ where E_{Na} is Na^+ reversal potential (+93.87 mV calculated from $[Na^+]_{in}$ and $[Na^+]_{out}$). The normalized G_{NaT} was displayed against V_{cmd} and fit to the peak by a single Boltzmann relation. For inactivation of I_{NaT}, the amplitudes of I_{NaT}s generated by the inactivation protocol were normalized by the maximum amplitude of I_{NaT} and displayed against prepulse potentials. The conductance of the predicted window current (G_{win}) was calculated by the product of normalized activation and inactivation condunctances. The conductance of I_{NaP} (G_{NaP}) was calculated in the same as that of G_{NaT} and the normalized G_{NaP} was displayed against V_{ramp} with a fitting to a single Boltzmann relation (Fig. 3.6A). Fig. 3.6A illustrates clear difference between G_{NaP} and G_{NaT}. G_{NaP} showed a lower $V_{1/2}$ (-37.7 vs. -21.0 mV) and smaller k (3.7 vs. 6.3 mV^{-1}) than G_{NaT}. When G_{win} was expressed as a fraction of the maximum G_{NaT}, the relative difference between G_{win} and G_{NaP} became apparent (Fig. 3.6B). The G_{NaP} peaked at 47.3 pS at -31.2 mV and declined rapidly in -30 to -15 mV range and approximated to a limiting value of much slower decrease, therefore resulting in a significant amount of G_{NaP} at depolarized potentials. On the contrary, G_{win} peaked at 6.2 pS at -42.3 mV and gradually decreased to zero. The total area of G_{win} was 16.1% of that of G_{NaP} (Fig. 3.6B).

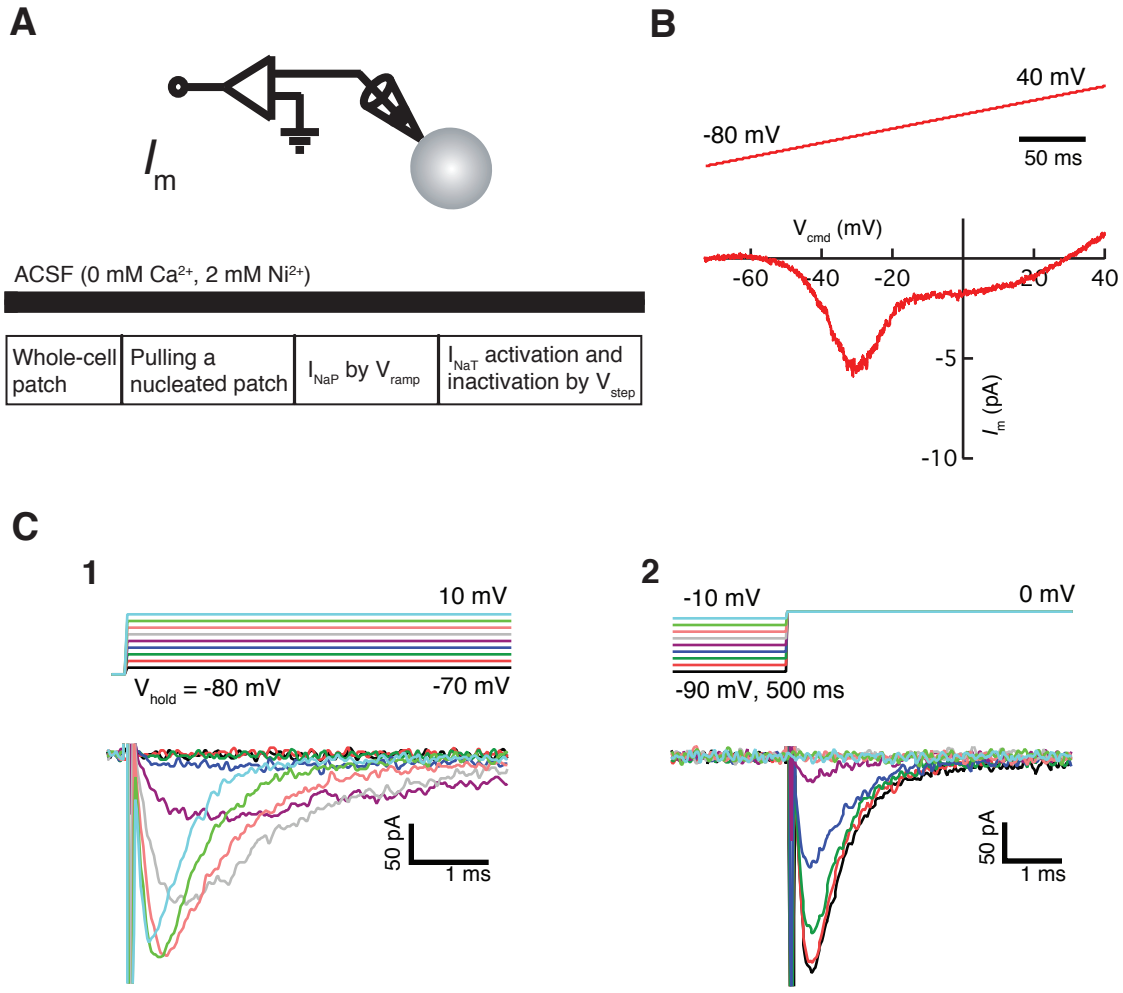

Figure 3.5: The example traces of I_{NaT} generated by activation and inactivation protocols In 18 neurons, both I_{NaP} and I_{NaT} were recorded at the same time for comparison. **A**: A schematic diagram represents the nucleated patch recording configuration. The timeline of the detail experimental protocol was illustrated in the bottom. **B**: Average of 18 recordings of I_{NaP} evoked by 0.4 mV/ms V_{ramp} showed the peak amplitude of I_{NaP} of -6.8 ± 0.5 pA at -29.8 ± 0.7 mV. I_{NaP} was isolated by linear leak subtraction of ramp current (see *methods*). **C**: The example traces of I_{NaT} generated by activation and inactivation protocols (see *methods*) are shown in (C-1) and (C-2), respectively. I_{NaT} was obtained by p/10 leak subtraction protocol (see *methods*).

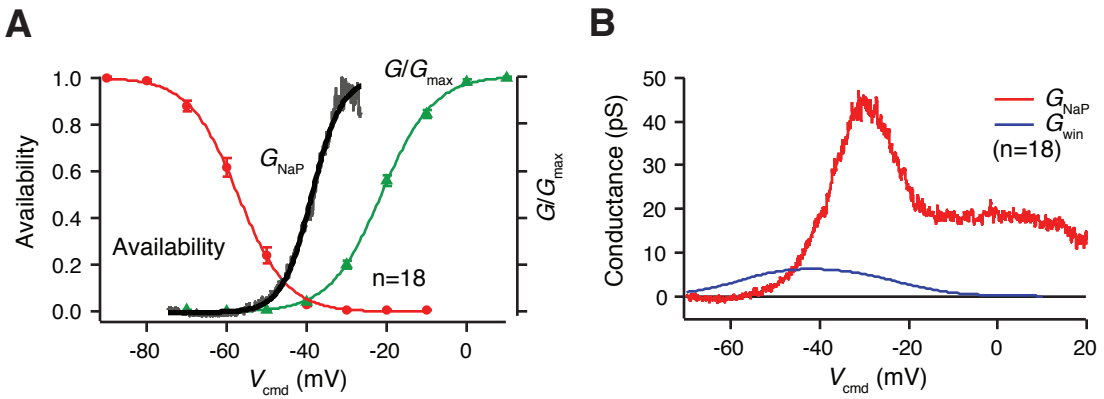

Figure 3.6: Persistent Na^+ current (I_{NaP}) is not from "window" current
A: The normalized steady state inactivation curve (availability) and activation (G/G_{max}) curves of I_{NaT}, and activation G-V curve of I_{NaP} ($G/G_{max,NaP}$) were plotted in the same figure for the comparison of voltage dependency. After being fitted to a single Boltzman function, availability curve gave -56.3 ± 1.2 mV of $V_{1/2}$ and 5.4 ± 0.1 mV^{-1} of slope factor (k). G/G_{max} gave $V_{1/2}$ = -21.0 ± 0.7 mV and k = 6.3 ± 0.1 mV^{-1}. The activation G-V curve of I_{NaP} ($G/G_{max,NaP}$) gave $V_{1/2}$ = -37.7 ± 1.0 mV and k = 3.7 ± 0.2 mV^{-1}. **B**: In the plot of both conductance of I_{NaP} and I_{win}, the difference in their amplitudes (47.3 pS at -31.2 mV vs. 6.2 pS at -42.3 mV) and peak location became more apparent. G_{win} only took the 16.1% of G_{NaP} and was mostly shown at a narrow voltage range around hyperpolarized potentials while there was significant amount of G_{NaP} at depolarized potentials.

The slow inactivation of Na^+ current as observed in Fig. 3.4B-2 was explained by using several ramp velocities (1.6, 0.8, 0.4, and 0.04 V/s). As ramp velocity decreased, the peak current also decreased (-16.1, -7.7, -4.4, and -0.7 pA, respectively) and the peak shifted to the left along the voltage axis (-22.2, -27.6, -30.7, and -32.6 mV, respectively). With a 0.04 V/s voltage command, there was almost no current other than a small limiting current at more depolarized voltage range (Fig. 3.7A). Our working hypothesis is that the fastest ramp velocity elicits mostly I_{NaT} and slower velocities more I_{NaP} with the peak I_{NaP} at about 0.4 V/s. Triangle voltage commands with 0.4 mV/s ramp velocity showed slow inactivation of I_{NaP}. I_{NaP} turned on during the initial depolarizing voltage command, but showed inactivation during the repolarizing voltage (Fig. 3.7B). Because

the data show that I_{NaP} is not due to a "window" current (Fig. 3.6B), it would suggest the existence of two underlying conductances or two late gating modes of a single Na^+ channel, as hypothesized previously (Alzheimer et al 1993a, Brown et al 1994).

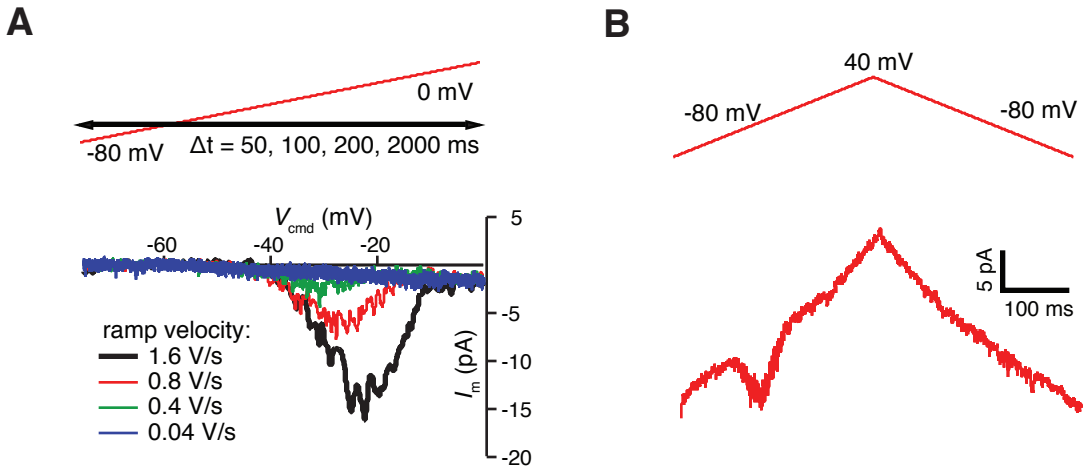

Figure 3.7: Slow inactivation of I_{NaP}
A: The ramp currents evoked by various ramp voltage commands suggested the slow inactivation of I_{NaP}. The ramp voltage command with 4 different velocities (1.6, 0.8, 0.4, and 0.04 V/s) was applied to the patch. The generated ramp currents showed decreasing peak amplitude and a leftward shift of peak location as the velocity of ramp voltage became slower (see text). **B**: The triangle voltage command with 0.4 mV/ms ramp velocity revealed clear slow inactivation of I_{NaP} around -40 to -20 mV range. I_{NaP} elicited by -80 to +40 mV rising ramp voltage command inactivated slowly and only small portion of the current remained during +40 to -80 mV falling ramp voltage command.

I_{NaT} also underwent a significant amount of slow inactivation as well. For instance, at -40 mV of prepulse potential, the currents were recorded with 5 different prepulse durations (25, 50, 100, 500, and 1000 ms). The ratio of I_{50ms} , I_{100ms} , I_{500ms}, and I_{1000ms} to I_{25ms} were 0.63, 0.37, 0.22 and 0.21 respectively (Fig. 3.8A-1). Similarly, at a prepulse of -50 mV potential, the ratios of I_{50ms} , I_{100ms} , I_{500ms}, and I_{1000ms} to I_{25ms} were 0.84,

0.71, 0.58, and 0.56 respectively (Fig. 3.8A-2). Overall, there was significant slow inactivation of I_{NaT} at -40 ~ -60 mV range (Fig. 3.8B-1) and this was shown as shift of the inactivation curve to the left by about -10mV from -43.8 mV to -54.2 mV (Fig. 3.8B-2). The observation of slow inactivation of both I_{NaP} and I_{NaT} is comparable to the previous finding of slow closed-state inactivation underlying ramp currents (Cummins et al 1998).

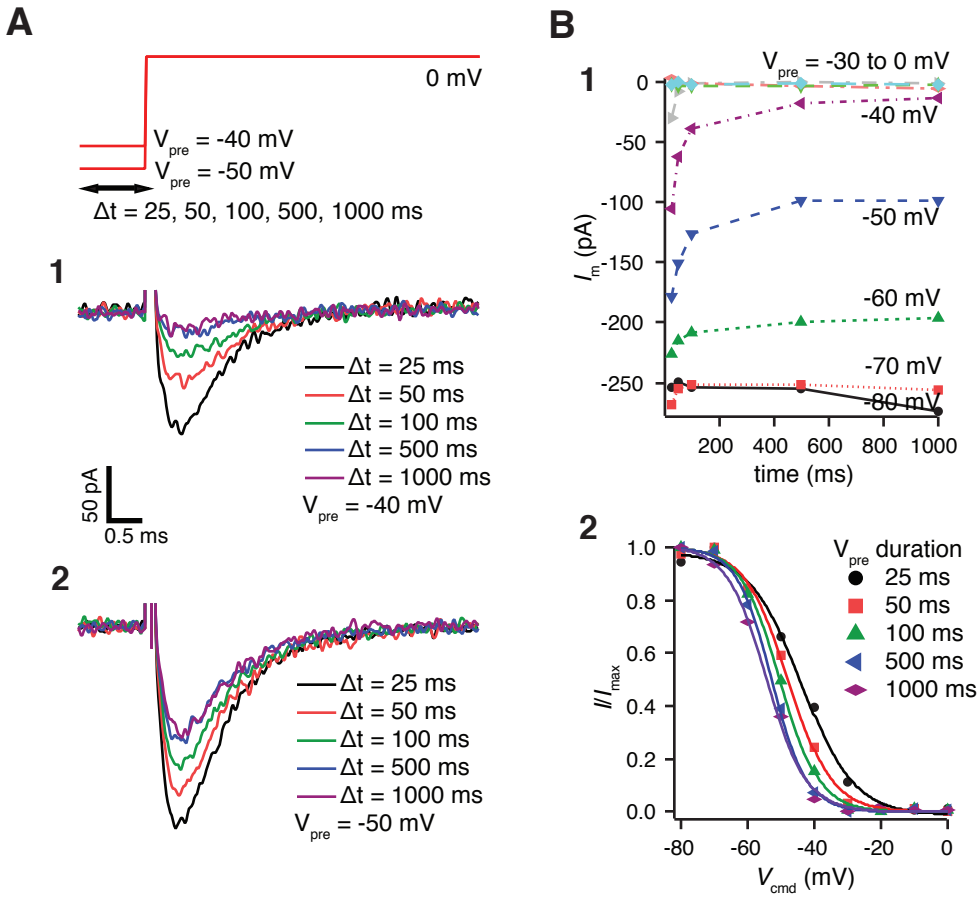

Figure 3.8: Slow closed-state inactivation of I_{NaT}
A: I_{NaT} also underwent slow closed-state inactivation. A 500 ms prepulse at -40 mV reduced the amount of available channels to ~ 20% while the prepulse at -50 mV left 42% channels available. **B**: Overall, the slow closed-state inactivation of I_{NaT} was apparent at -60 to -40 mV of prepulse condition (B-1), and this was manifested as the left shift of $V_{1/2}$ of steady state inactivation curve by -10.4 mV (B-2).

The total I_{NaP} measurements from 141 neurons gave an average I_{NaP} peak amplitude of -5.06 ± 0.23 pA and the average I_{NaP} density of 0.014 ± 0.0006 pA/μm^2 (Fig. 3.9A). I_{NaP} is known to have small amplitude compared to that of I_{NaT} (Bean 2007, Crill 1996). So, we examined the relationship between I_{NaP} and I_{NaT} recorded from the same cell (n=110). The peak amplitude of I_{NaP} was measured around -40 to -30 mV with a 0.4 mV/ms ramp command (-5.16 ± 0.22 pA), and that of I_{NaT} was measured from step commands to -10 to +10 mV (-174.6 ± 7.8 pA) (Fig. 3.9A,B). The relationship of peak amplitudes of I_{NaT} to I_{NaP} was linear and the ratio I_{NaP}/I_{NaP} was 0.0238 (n=110) indicating that the amplitude of I_{NaP} is about 2.38% of I_{NaT} (Fig. 3.9C) from these somatic patches. In order to have an estimate of I_{NaT} channel density in the patch, we calculated the number of open channels by assuming the open probability of the Na^+ channel at -10 mV is 1 and utilizing the unitary current amplitude ~ 1 pA at -10 mV and single-channel conductance of 14.8 pS as reported previously (Colbert & Johnston 1996). The average number of open channels in the nucleated patch by this estimation was 0.58 channels/μm^2 (Fig. 3.9D).

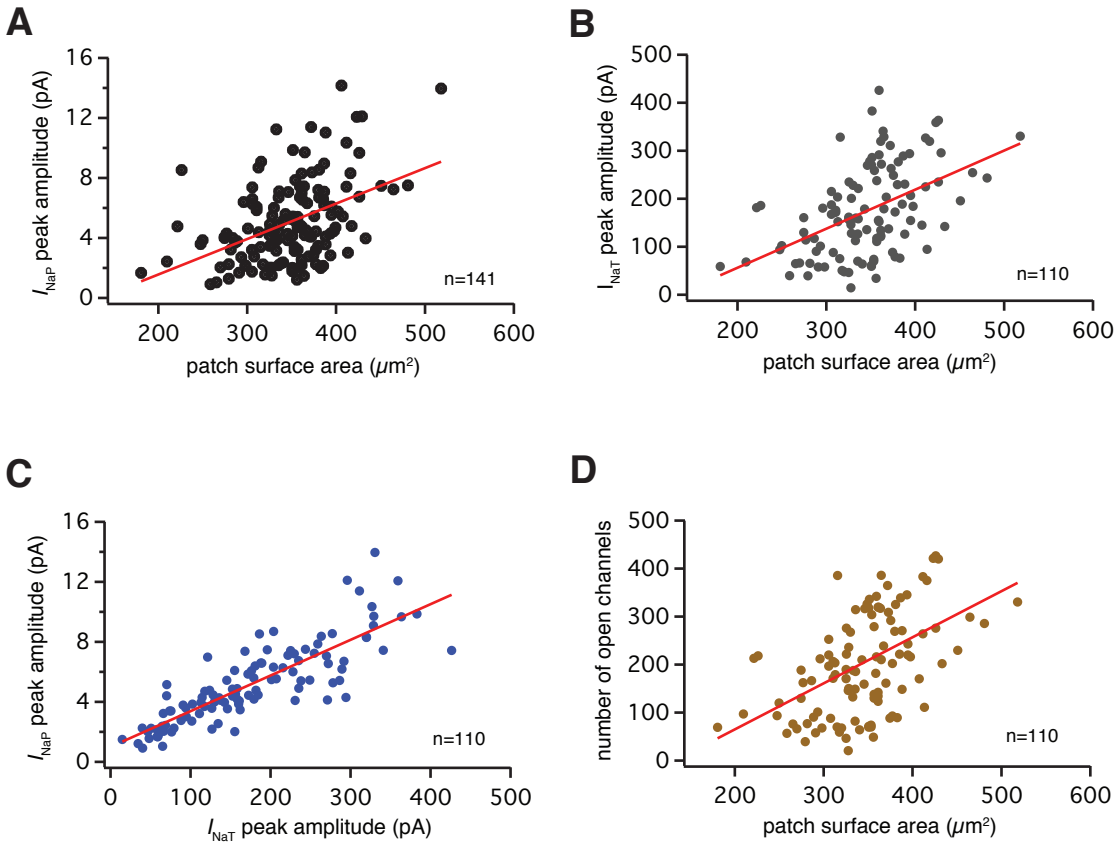

Figure 3.9: Persistent and transient Na^+ currents in the nucleated patch
A: The peak amplitudes of I_{NaP} elicited by 0.4 mV/ms V_{ramp} were plotted against the patch surface area (n=141). The average density of I_{NaP} was 0.0144 ± 0.0006 pA/μm^2 in the patch. **B**: The peak amplitudes of I_{NaT} elicited by activation protocol were plotted against the patch surface area. The peak of I_{NaT} was evoked by step voltage from -80 to -10, 0, or +10 mV (mostly to 0 mV). The average density of I_{NaT} was 0.498 ± 0.02 pA/μm^2 of current density in the patches. **C**: The relationship between the peaks of I_{NaP} and I_{NaT}: Both I_{NaP} and I_{NaT} recorded from the same patch showed linear correlation (n=110; Pearson's r = 0.839). The peak amplitude of persistent Na^+ current is 2.38% of the peak transient Na^+ current. **D**: The number of channels opened in the patch was estimated to be 0.58 ch./μm^2 (see text).

3.2 PHARMACOLOGY AND FUNCTIONAL SIGNIFICANCE OF PERSISTENT Na^+ CURRUNT IN HIPPOCAMPAL CA1 PYRAMIDAL NEURON

3.2.1 Introduction

Action potentials are used by neurons to process and communicate information. Before an action potential is triggered by a large regenerative supra-threshold Na^+ current, there is an intricate interplay between inward and outward conductances in the subthreshold voltage range. I_{NaP} and $I_{Ca(T)}$, as the sources of subthreshold inward currents, can provide a depolarizing drive to a neuron toward the spike generation while $I_{K(A)}$, I_M, and I_h may prevent the neuron from firing by supplying an opposing current. Several lines of evidence suggested that I_{NaP} could boost synaptic integration and increase the probability of neuronal firing. For example, I_{NaP} was shown to mediate self-sustained depolarization toward spike threshold (Hu & Hvalby 1992, Stafstrom et al 1985, Stafstrom et al 1982) and the amplification of somatic/dendritic depolarization (González-Burgos & Barrionuevo 2001, Schwindt & Crill 1995, Stuart & Sakmann 1995). However, becasue there is no I_{NaP} specific blocker available, the interpretation of data from the previous studies could still be limited. Thus, we first surveyed several known sodium channel blockers to find a candidate for I_{NaP} specific blocker. Then, we examined the functional role of I_{NaP} by using the identified blocker.

3.2.2 Hexanol differentially blocks persistent and transient Na^+ currents

We tested the several known Na^+ channel blockers for their ability to block I_{NaP}. Since injectable local anesthetics are known to block I_{NaP}, we hypothesized alcohols and volatile anesthetics could also affect I_{NaP}. Hexanol, one of the *n*-alcohols shown to block I_{NaT} (Horishita & Harris 2008, Shiraishi & Harris 2004) and to have anesthetic effects

(Alifimoff et al 1989), was chosen to test its effect on I_{NaP} due to its strong potency with relatively low concentration compared to other alcohols with a shorter carbon chain such as ethanol and butanol. Hexanol at 2.8 mM is four times the concentration of the minimum alveolar concentration (MAC) that can put 50% of subjects under anethesia. At first, the suppression of I_{NaP} by hexanol was tested by whole-cell voltage-clamp recording. Then, we confirmed the Hexanol effect on I_{NaP} and examined its differential blocking of I_{NaP} and I_{NaT} by nucleated patch recordings.

In whole-cell voltage clamp recording, once a giga-ohm seal was obtained, the membrane under the patch was broken to obtain the whole-cell configuration. After about 5 minutes of stability monitoring, initial baseline data were collected. Then, 1.4 mM hexnaol that is 2 MAC was applied in the bath in 10 minutes, and the hexanol was washed-out during the remaining experiment (Fig. 3.10A). The traces in Fig. 3.10B illustrate a blocking effect on I_{NaP} by 1.4 mM hexanol. The peak inward current and the amount of the charge were calculated. The blocking effects of peak I_{NaP} and charge influx (n=8) were summarized in Fig. 3.10C&D where hexanol suppressed I_{NaP} peak amplitude by 29.1 ± 8.8% and charge influx by 26.1 ± 13.3%.

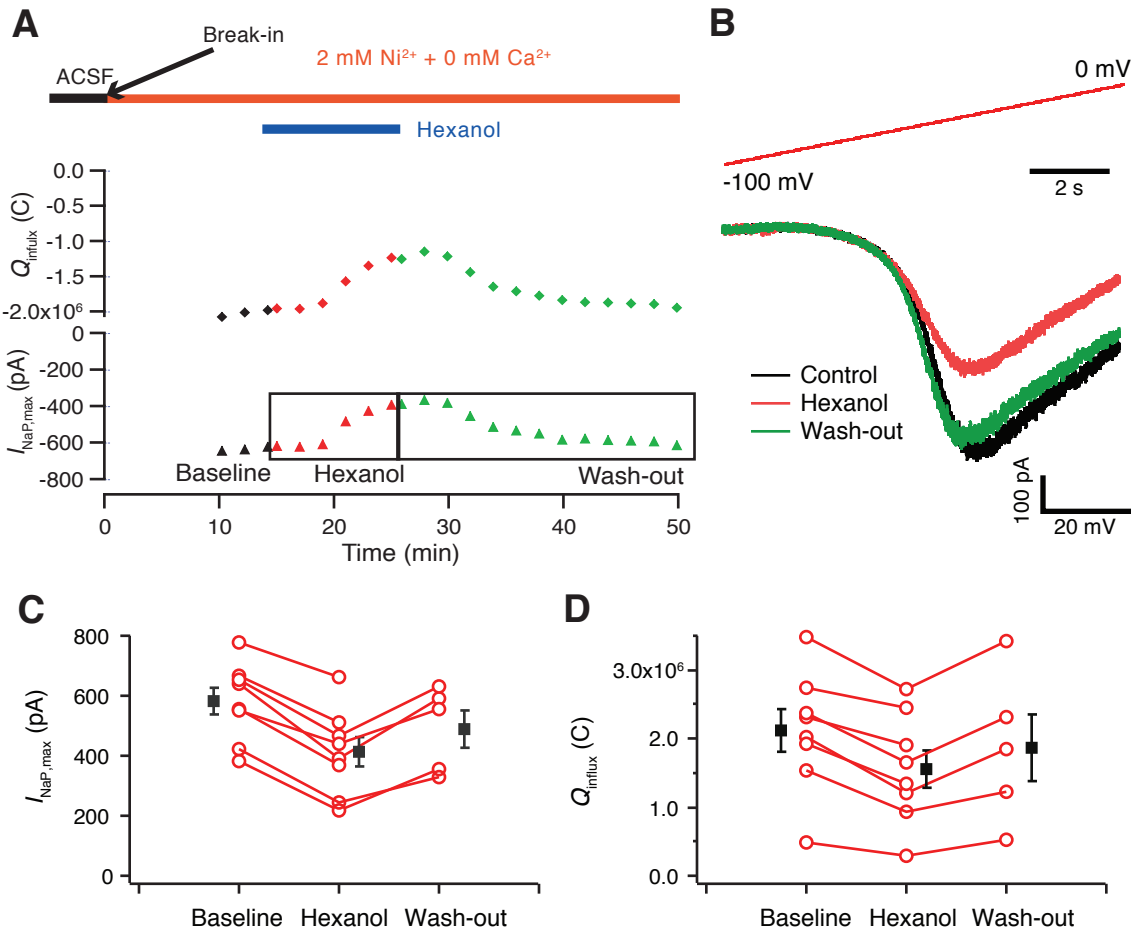

Figure 3.10: Blocking of I_{NaP} by 1.4 mM hexanol in whole-cell voltage-clamp recording **A**: Timeline and protocol of the I_{NaP} blocking experiment in whole-cell voltage-clamp experiment: Once a GΩ seal was obtained, the patch was broken to make a whole-cell recording. After about 5 minutes of stability monitoring, initial baseline data were collected. Then, 1.4 mM hexanol was applied for 10 minutes, data were collected, and the hexanol was washed-out during the remaining experiment. **B**: A ramp voltage command with -100 to 0 mV in 9 sec generated persistent sodium currents that were stably measured throughout the entire experiment. 1.4 mM hexanol caused significant reduction of the current that was completely reversible. **C**: The peak inward current amplitude was measured for all three conditions: baseline, hexanol and wash-out. The summary of peak I_{NaP} of total of 8 neurons demonstrated a significant suppression of peak I_{NaP} by hexanol (29.1 ± 8.8%). **D**: The amount of the charge was also calculated from the same traces and the similar suppression of charge influx was obtained in the summary figure (26.1 ± 13.3%).

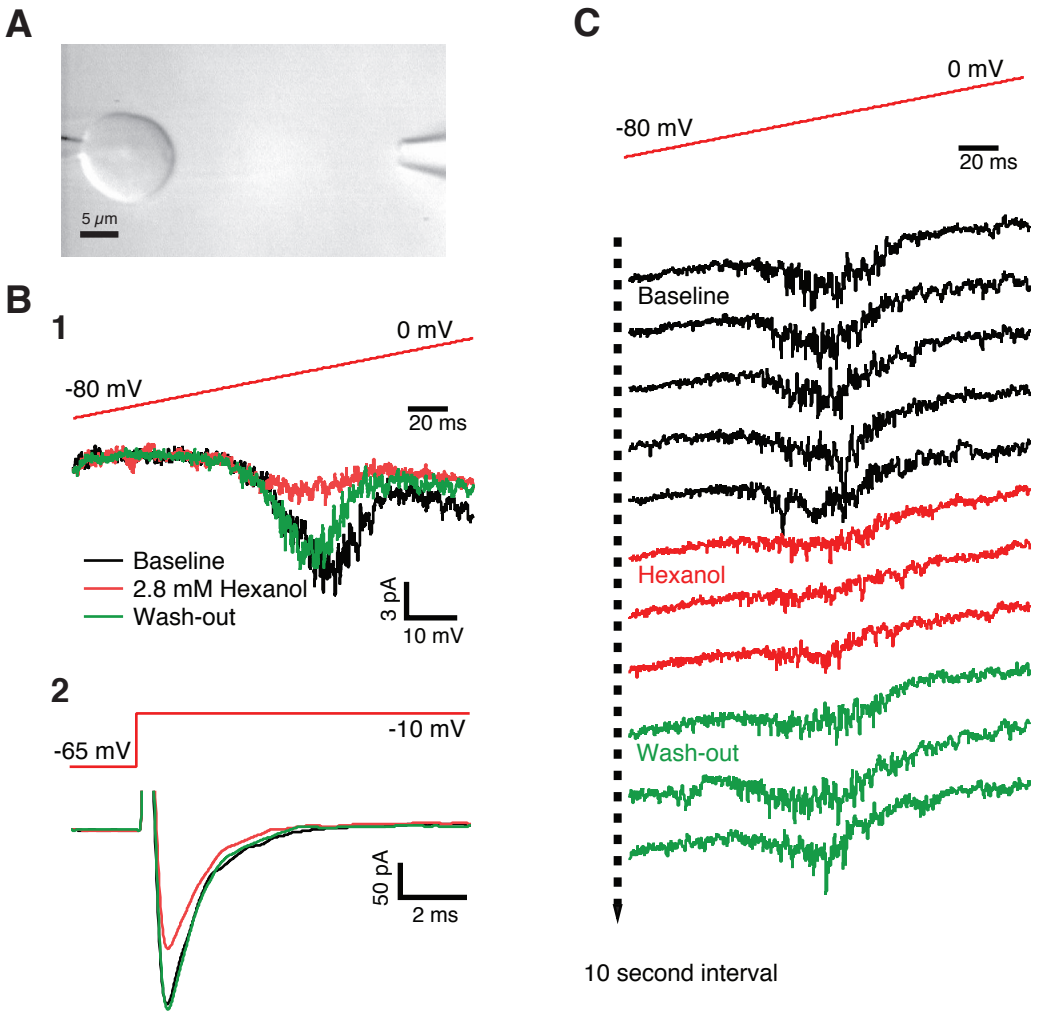

Figure 3.11: Blocking of I_{NaP} by 2.8 mM hexanol in nucleated patch recording
A: The drug was applied by a puffing pipette located nearby the patch. **B**: An exemplary trace of hexanol effects on I_{NaP} and I_{NaT} was shown. The peak amplitude of I_{NaP} evoked by 0.4 mV/ms V_{ramp} was significantly decreased under hexanol condition (A1, 64.7 % suppression). An exemplary trace of hexanol effects on I_{NaT} is shown. I_{NaT} was elicited by a voltage step from -65 to -10 mV. There was a relatively smaller decrease in peak amplitude of I_{NaT} (A2, 31.1 % blocking). Both the example of I_{NaP} and I_{NaT} were recorded from the same patch, and it gave a hint of differential block of I_{NaP} and I_{NaT} by hexanol. **C**: Series of ramp response with 10 s interval demonstrates wash-in and -out effects of hexanol on I_{NaP}.

Next, in nucleated patch recordings, we confirmed the blocking of I_{NaP} by hexanol and found the differential blocking of I_{NaP} and I_{NaT}. Puff application of 2.8 mM hexanol on the nucleated patch reduced the amplitude of I_{NaP} by 64.7% and of I_{NaT} by 31.1% (Fig. 3.11B). We further investigated this differential block of I_{NaP} and I_{NaT} using hexanol (2.8 mM) and two other drugs, riluzole (10 μM) and ranolazine (30 μM), both previously reported to block non-inactivating Na^+ channels (Benoit & Escande 1991, Rajamani et al 2009).

To test the differential block of I_{NaP} and I_{NaT}, we recorded both currents during the same experiments. We recorded I_{NaP} first in three conditions (baseline, drug, wash-out) and then recorded the activation and/or inactivation of I_{NaT} for those conditions until the integrity of the patch began to decline. Fig. 3.12 illustrates the experimental protocol used. After achieving a nucleated patch, the stabilization of the patch was monitored during 1 minute, and then baseline 0.4 mV/ms ramp responses were measured. The drug in the pipette containing HEPES or bicarbonate buffered ACSF was puffed onto the patch and the currents elicited by the same V_{ramp} were measured after 30 seconds from the initial drug puffing. The currents in wash-out condition were measured from 1 ~ 2 minutes after the completion of wash-out. The same procedure was repeated for the measurement of the currents elicited by the I_{NaT} activation or inactivation protocol (see methods) while the input resistance and baseline current were monitored.

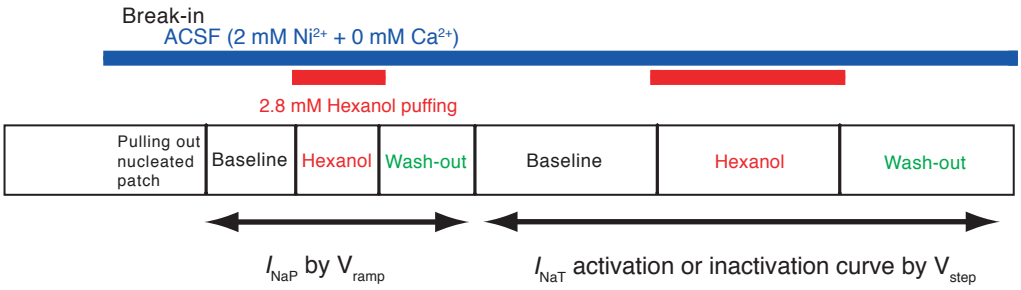

Figure 3.12: A schematic diagram explaining the experiment timeline and procedure to assess effect of the drugs on I_{NaP} and I_{NaT}

The reduction of peak I_{NaP} by hexanol is demonstrated in the exemplary traces evoked by the 0.4 mV/ms V_{ramp} in baseline, hexanol, and wash-out conditions (Fig. 3.13A-1). The conductance of I_{NaP} and curve-fitting of a Boltzmann equation to G/G_{max} were calculated in the same way as in Fig. 3.6A. The maximum conductance reduction is prominent in the presence of hexanol without change in voltage dependence of activation (Fig. 3.13A-2&3). In summary, hexanol and riluzole showed a significant reduction in $G_{NaP,max}$ (drug - saline = -49.7 ±3.3% and -52.6 ± 3.4%, respectively; $p < 0.001$) compared to the saline puffing case while ranolazine did not produce a significant suppression of $G_{NaP,max}$ ($p > 0.05$) (Fig. 3.13B-1). Neither hexanol nor riluzole produced significant changes in $V_{1/2}$ and slope factor when compared to saline puffing condition, but ranolazine caused a small increase in the slope factor (0.88 ± 0.22; n = 12) (Fig. 3.13B-2&3). Therefore, our data showed that 2.8 mM hexanol and 10 μM riluzole suppressed the conductance of I_{NaP} by about half without affecting the voltage dependence of the channel activation. For the statistical analysis of the drug effects, Kruskal-Wallis test and post hoc Dunn's test were performed

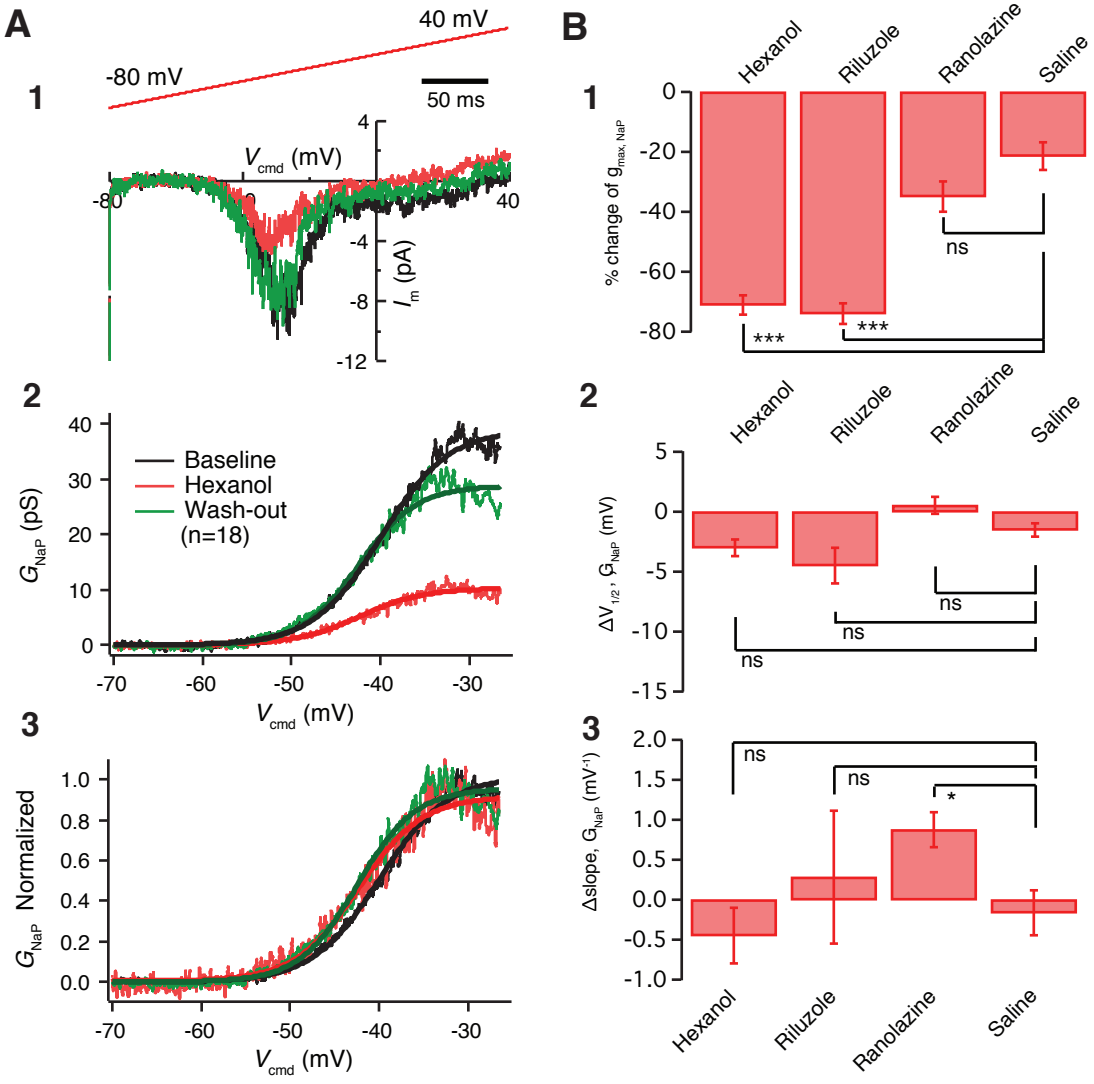

Figure 3.13: The effect of Na^+ channel blockers on I_{NaP}
A: The effect of 2.8 mM hexanol on I_{NaP} (n=18). The example trace of I_{NaP} evoked by 0.4 mV/ms V_{ramp} showed a significant suppression by hexanol (red) in reversible manner (A-1). The early part of G-V curve of I_{NaP} was fitted by a Boltzmann equation (A-2) and the normalized G-V curves in three conditions were well overlapped with each other indicating no change in voltage dependency of I_{NaP} by hexanol (A-3). **B**: Summary of the effects on I_{NaP} by 2.8 mM hexanol (n=18), 10 μM riluzole (n=7), 30 μM ranolazine (n=12), and Saline (n=11). The conductance of I_{NaP} was dramatically suppressed by hexanol and riluzole, but not ranolazine compared to saline control (B-1). There was no significant change in $V_{1/2}$ shift caused by the drugs when compared to saline control (B-2). Ranolazine caused a small change in slope factor (Δslope = 1.0; $p < 0.05$), but hexanol and riluzole did not affect the slope factor (B-3).

Fig. 3.14A shows the example recording traces of the activation of I_{NaT} in the presence and absence of hexanol. The suppression of maximum conductance was observed in the activation G-V curve (Fig. 3.14B-1) without a significant change in voltage dependence of the channel activation (Fig. 3.14B-2): $V_{1/2}$, or slope factor. In general, hexanol and riluzole decreased the maximum conductance of I_{NaT}, but to lesser degree than that of I_{NaP} (drug-saline = -24.9 ± 8.0% and -22.4 ± 6.4%, respectively; $p < 0.05$) (Fig. 3.15A). None of the three drugs caused significant changes in $V_{1/2}$ or slope factor (Fig. 3.15B&C). Fig. 3.15D illustrates the voltage dependency of drug suppression effects on the peak I_{NaT}. The peak amplitude of I_{NaT} in the presence of the drug was normalized by that of I_{NaT} in the absence of the drug, and there was slightly greater block of I_{NaT} by hexanol and ranolazine at depolarized potentials (Fig. 3.15D).

However, there was no voltage dependency on the activation kinetics, and none of the drugs affected the kinetics of channel activation. Fig. 3.16A-1 illustrates the example traces of I_{NaT} activation and those traces were fitted by $f(x) = A \cdot (1 - e^{-(x-x_0)/\tau_m})^3$ in the activation phase producing the activation time constant (τ_m). Similarly, the same traces were fitted by $f(x) = y_0 + A \cdot e^{-(x-x_0)/\tau_h}$ in the inactivation phase (Fig. 3.16A-2) to generate the inactivation time constant (τ_h). Hexanol caused no change τ_m and τ_h. (Fig. 3.16A-3&4; $p > 0.05$). In summary, neither hexaol, riluzole nor ranolazine appeared to have any effect on τ_m and τ_h (Fig. 3.16B; $p > 0.05$).

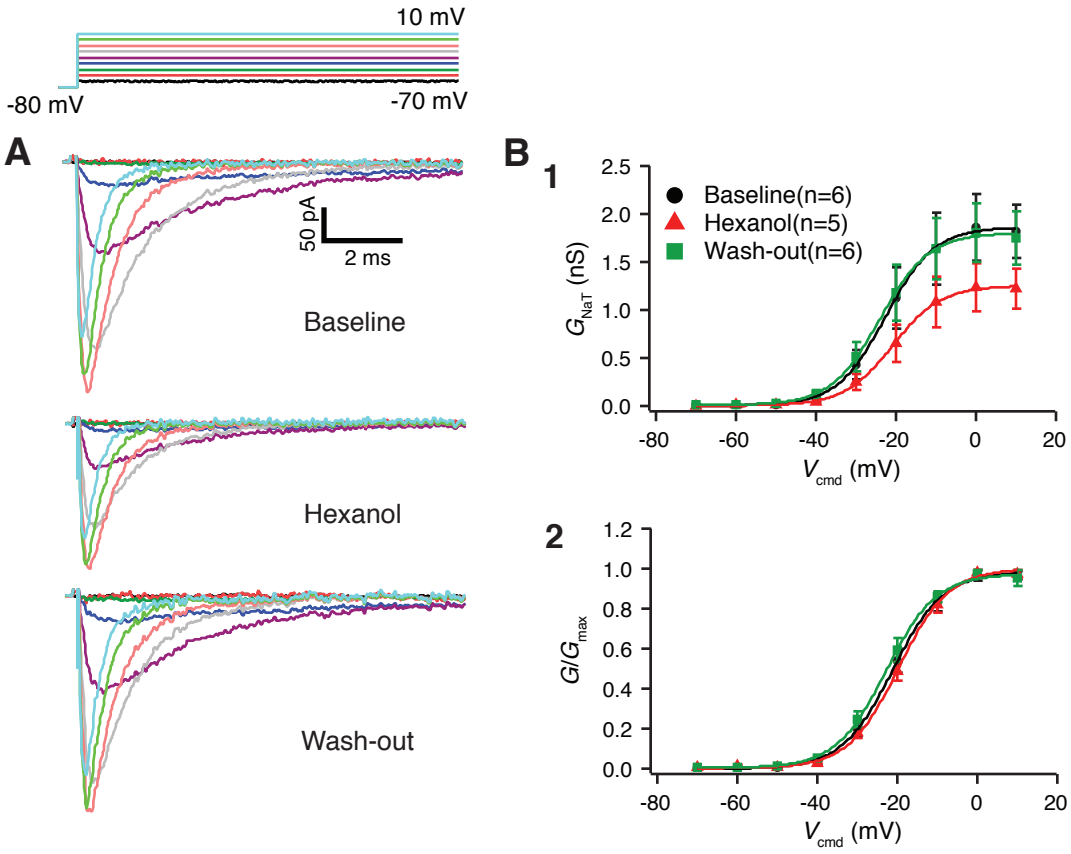

Figure 3.14: The effect of hexanol on the activation of I_{NaT}
A: The effect of 2.8 mM hexanol on the activation of I_{NaT}. Exemplary traces of activation of I_{NaT} evoked by activation protocol were shown in three different conditions: baseline, 2.8 mM hexanol puffing, and wash-out. **B**: 2.8 mM hexanol puffing caused a significant decrease in the peak amplitude of I_{NaT}, but relatively smaller amount compared to that of I_{NaP} (B-1), which was compatible with the observation in Fig. 3.11B. The activation G-V curve showed decreased maximum conductance without notable change in voltage dependency (B-2). Consequently, there was no significant change in $V_{1/2}$ and slope factor ($p > 0.05$; Kruskal-Wallis test and post hoc Dunn's test).

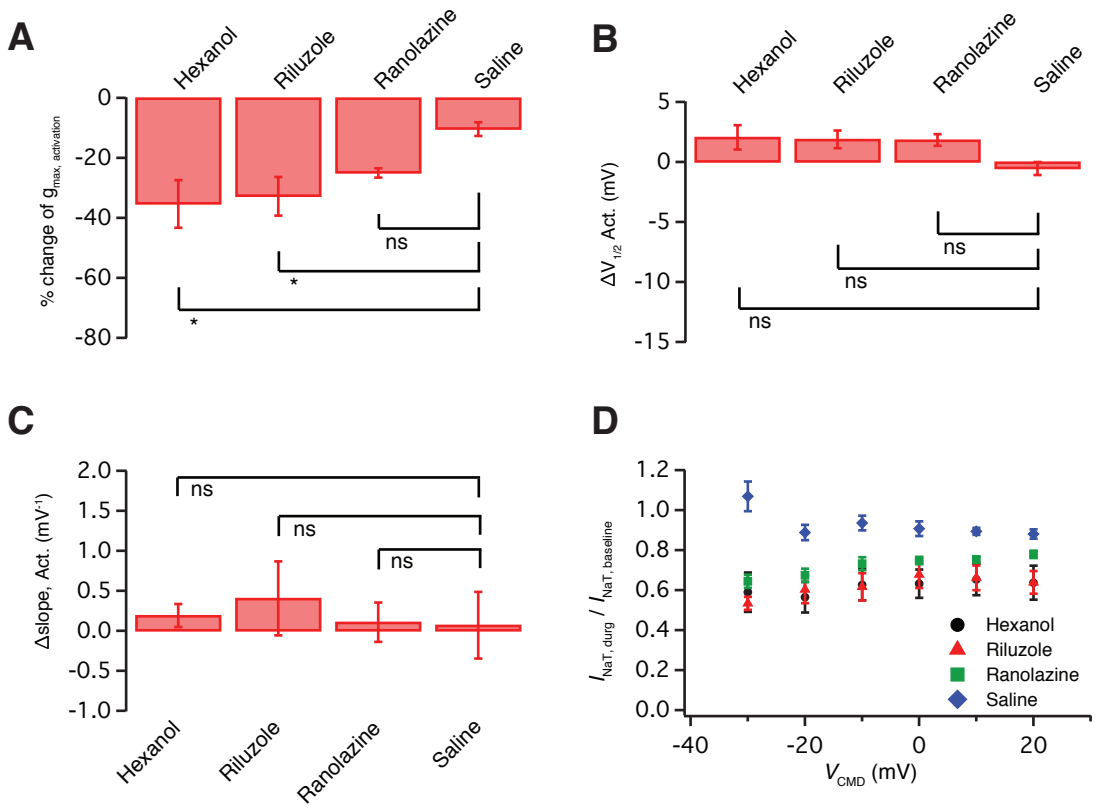

Figure 3.15: Summary of the drug effects on the activation of I_{NaT}
Summary of the effects on the activation of I_{NaT} by 2.8 mM hexanol (n=5), 10 μM riluzole (n=5), 30 μM ranolazine (n=7), and Saline (n=5). **A**: The G_{NaT} of the activation was significantly suppressed by hexanol (hexanol - saline = -24.9 ± 8.0%; $p < 0.05$) and riluzole (riluzole - saline = -22.4 ± 6.4%; $p < 0.05$), but not ranolazine when compared to saline control (Kruskal-Wallis test and post hoc Dunn's test). **B&C**: There was no significant change in $V_{1/2}$ and slope factor caused by the drugs when compared to saline control ($p > 0.05$; Kruskal-Wallis test and post hoc Dunn's test). **D**: As the command voltage increased, there was a small but statistically significant increase in the ratio of $I_{NaT,\ drug}$ to $I_{NaT,\ baseline}$ for hexanol and ranolazine when compared to saline control ($p < 0.05$; linear regression test), not riluzole indicating voltage dependency of suppression effects on the peak I_{NaT}.

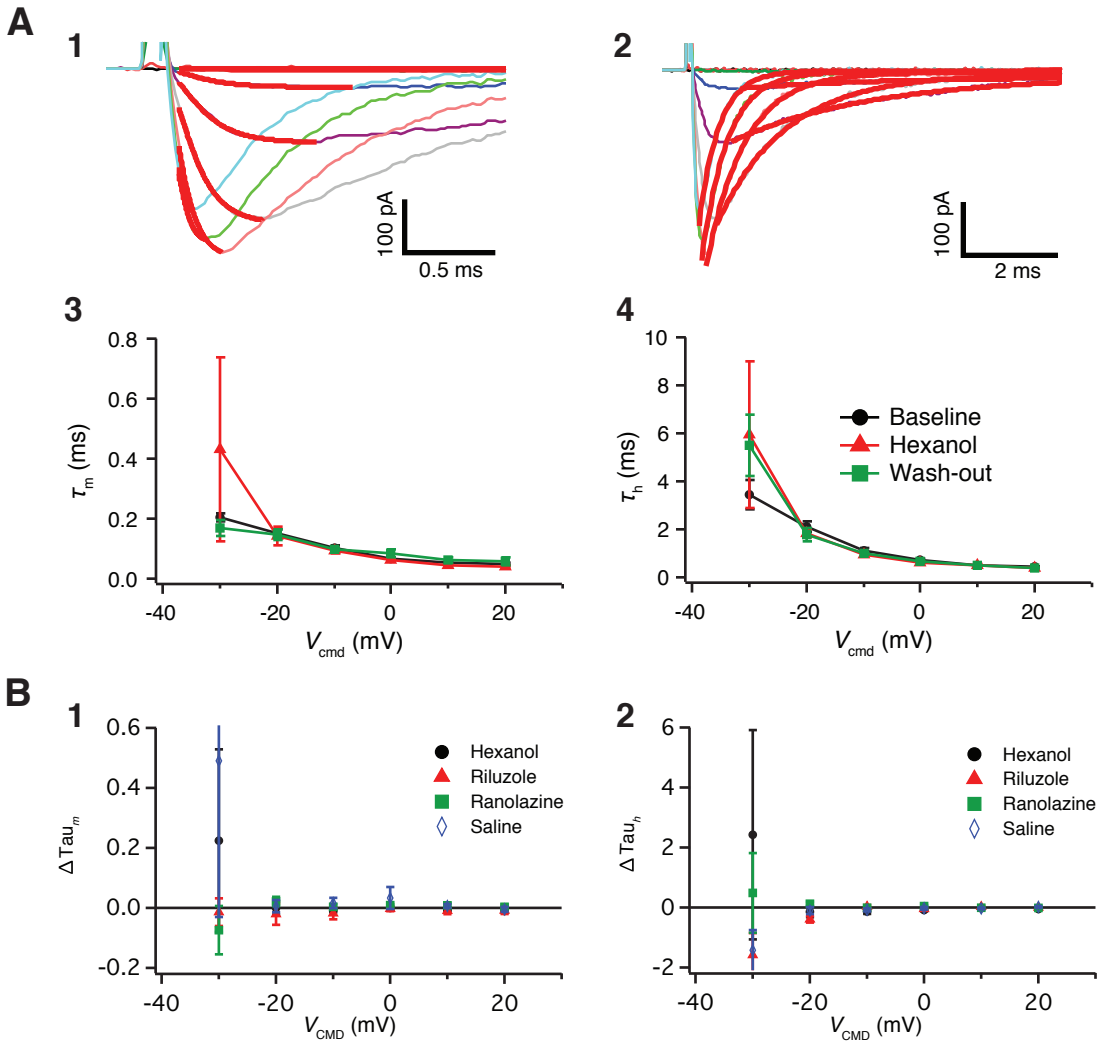

Figure 3.16: The effect of the drugs on the kinetic of I_{NaT} activation and inactivation
A: The effect of 2.8 mM hexanol on the kinetics of Na^+- channel activation and inactivation is shown as an example. The exemplary traces of I_{NaT} evoked by activation protocol were fitted by cubic exponential function, $f(x) = A(1 - e^{-(x-x_0)/\tau_m})^3$, to generate activation time constant, τ_m (A-1). Likewise, the inactivation phase of the same trace were fitted by a single exponential function, $f(x) = y_0 + Ae^{-(x-x_0)/\tau_h}$, to generate inactivation time constant, τ_h (A-2). 2.8 mM hexanol did not change the kinetics of either activation or inactivation at all command voltages (A-3&4; $p > 0.05$; Kruskal-Wallis test and post hoc Dunn's test). **B**: The effect of the drugs on the channel kinetics was summarized. None of the drugs caused any statistically significant change in the kinetics of channel activation (B-1) and inactivation (B-2) ($p > 0.05$; Kruskal-Wallis test and post hoc Dunn's test).

The effects of the drugs on steady-state inactivation were also tested. Fig. 3.17A gives exemplary traces showing the effects of hexanol on I_{NaT} elicited by the inactivation protocol. The steady state inactivation curve was constructed by displaying both the I_{NaT}s and normalized I_{NaT}s against prepulse potentials (Fig. 3.17B-2). In summary plots, hexanol and riluzole significantly decreased the maximum amplitude of I_{NaT} compared to saline puffing control (drug-saline = -21.1 ± 3.7% and -24.9 ± 3.3%, respectively; Fig. 3.18A). The left shift of $V_{1/2}$ by hexanol was insignificant when compared to the saline control ($p > 0.05$). However, riluzole produced a significant left shift of $V_{1/2}$ of steady state inactivation curve (-9.2 ± 1.4 mV; n=4; $p < 0.05$) (Fig. 3.18B). However, there was no notable change in the slope factor for any of the drugs (Fig. 3.18C). On the other hand, the voltage dependency of the drug effects on I_{NaT} was observed in the presence of hexanol and riluzole. The more depolarized the prepulse potentials, the larger the suppression of the peak amplitude of I_{NaT} by the drugs (Fig. 3.18D).

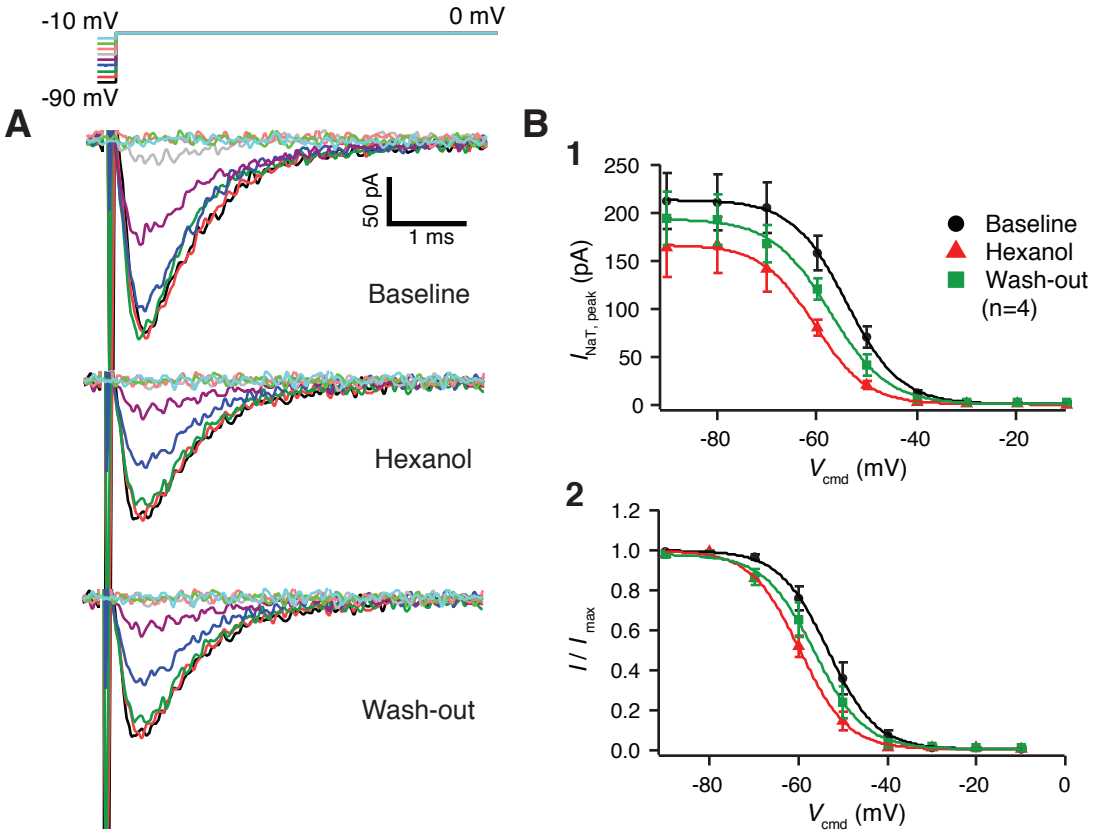

Figure 3.17: The effect of hexanol on the inactivation of I_{NaT}
A: The effect of 2.8 mM hexanol on the inactivation of I_{NaT} is shown as an example. Exemplary traces of inactivation of I_{NaT} evoked by inactivation protocol are shown in three different conditions: baseline, 2.8 mM hexanol puffing, and wash-out. **B**: 2.8 mM hexanol puffing caused a significant decrease in the peak amplitude of I_{NaT} , but relatively smaller amount compared to that of I_{NaP}, which was consistent with the observations in Fig. 3.11B and Fig. 3.14.

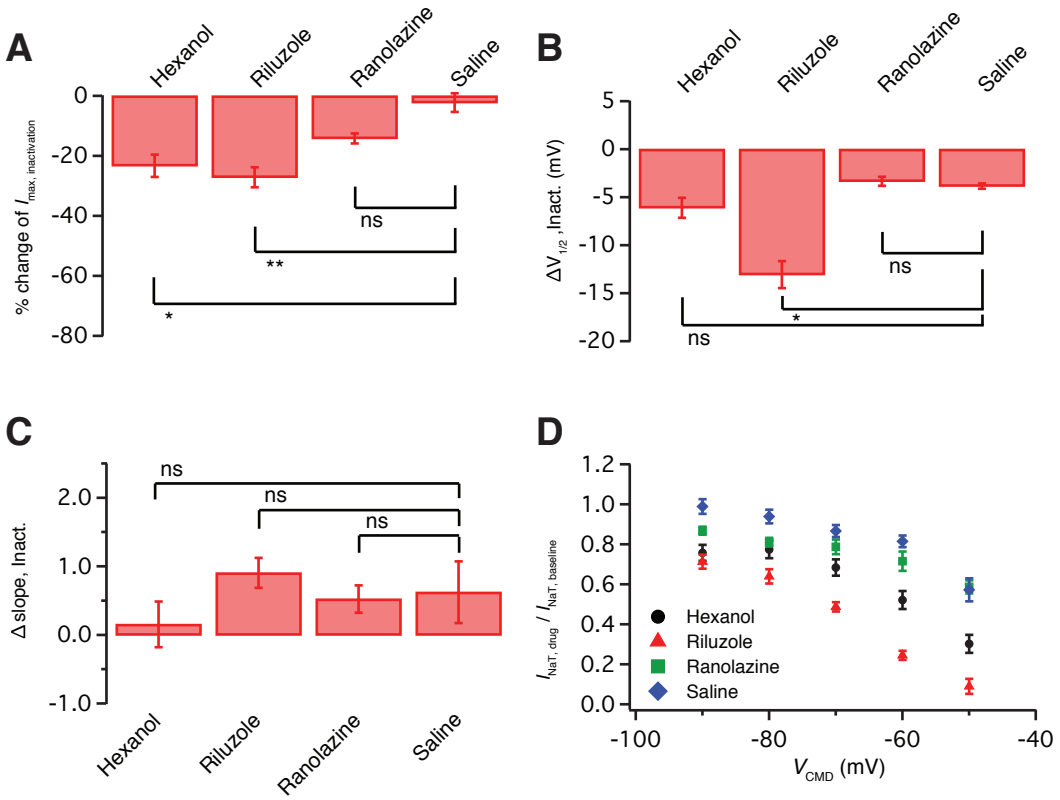

Figure 3.18: Summary of drug effect on the inactivation of I_{NaT}
Summary of the effects on the activation of I_{NaT} by 2.8 mM hexanol (n=4), 10 μM riluzole (n=4), 30 μM ranolazine (n=7), and Saline (n=5). **A**: The peak I_{NaT} of the inactivation was significantly suppressed by hexanol (hexanol - saline = -21.1 ± 3.7%; p <0.05) and riluzole (riluzole - saline = -24.8 ± 3.3%; p <0.01), but not ranolazine when compared to saline control (Kruskal-Wallis test and post hoc Dunn's test). **B**: There was a significant left shift of $V_{1/2}$ for riluzole (-9.2 ± 1.4 mV; p < 0.05) while hexanol and ranolazine did not cause statistically significant change in $V_{1/2}$ when compared to saline control (p >0.05; Kruskal-Wallis test and post hoc Dunn's test). **C**: None of the drugs caused notable changes in slope factor when compared to saline control (p > 0.05; Kruskal-Wallis test and post hoc Dunn's test). **D**: As the command voltage increased, there was a significant decrease in the ratio of $I_{NaT, drug}$ to $I_{NaT, baseline}$ for hexanol and riluzole when compared to saline control (p < 0.05; linear regression test), but ranolazine indicating voltage dependency of suppression effects on the peak I_{NaT}.

3.2.3 Persistent Na^+ currents mediate neuronal excitability by regulating action potential threshold and onset timing of spike initiation

What would be the physiological consequences of blocking I_{NaP}? In order to address this question, we used hexanol, one of the I_{NaP} blockers tested above, in current clamp recordings from *in situ* hippocampal CA1 pyramidal neurons. After neurons were isolated pharmacologically from the network (see *Methods*), we first monitored the stability of the experiment by measuring input resistance (R_N): a linear fit to the voltage responses from a series of 700 ms current injections from -50 to +20 pA by 10 pA for baseline, hexanol (bath application of 1.4 mM), and wash-out conditions (Fig. 3.19A-1). Input resistance was found unchanged during the three experimental conditions: baseline (67.6 ± 3.4 MΩ), hexanol (65.4 ± 3.2 MΩ), wash-out (66.4 ± 4.5 MΩ) (Fig. 3.19A-2). Moreover, the normalized input resistance measured at different holding potentials (R_N,hexanol/ R_N,baseline, n=5) was also unchanged across the -75 mV to -58 mV voltage ranges (Fig. 3.19A-3).

After confirming that there was no significant change in R_N, we examined the effects of hexanol on the voltage threshold (V_{th}) of an action potential evoked with moderate current injections of 700 ms duration. Current was injected to the neuron both in the absence and presence of hexanol, and the voltage thresholds (membrane voltage of dV/dt = 20 mV/ms) for both conditions were compared. The amplitude of injected current was adjusted to evoke the 1st spike at the same latency for both conditions. There was a significant increase in voltage threshold of the 1st spike in the presence of hexanol (-43.27 ± 1.54 vs. -38.68 ± 2.18 mV; n=5 ; p<0.005), which was reversible in wash-out (Fig. 3.19B-1). In the phase plane plot of the same voltage traces (Fig. 3.19B-2), the difference in voltage threshold for both baseline and hexanol conditions can be identified (Fig.

3.19B-3). There was, however, no significant change in other spike parameters such as peak dV/dt, spike amplitude, and spike half width (p>0.05).

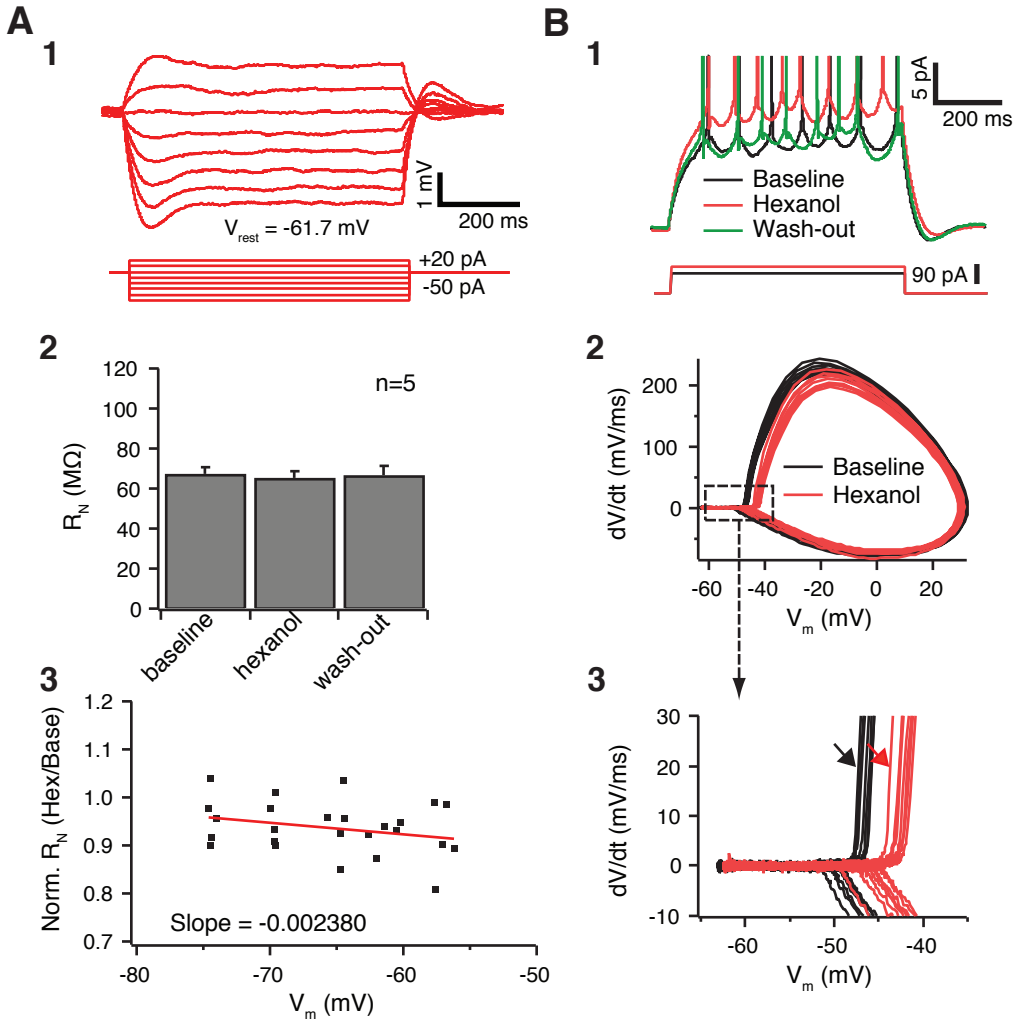

Figure 3.19: The effects of hexanol on input resistance and voltage threshold
A: Exemplary traces induced by current injection of -50 pA to +20 pA by 10 pA increment are shown (A-1). Input resistance, R_N, showed no significant change before, during and after hexanol treatment (A-2). Normalized input resistance ($R_{N,\ hexanol}$ / $R_{N,\ baseline}$; n=5) was measured at different holding potentials from -58 to -75 mV and showed no significant voltage dependency ($p > 0.05$; linear regression test) (A-3). **B**: Spikes generated by 700 ms current injection showed a significant increase in voltage threshold (4.6 mV) of the 1st spike in the presence of hexanol, which was reversible. The amplitude of the current was adjusted to elicit the 1st spikes at the same latency. There was no

significant change in other spike analysis parameters such as peak dV/dt, spike amplitude, and spike half width ($p>0.05$) (B-1). The traces are plotted in the phase plane (B-2). Each arrow in phase plane plot of the same traces (box area) indicates V_{th} for both control and hexanol conditions that is defined as the voltage at dV/dt = 20 mV/ms (B-3).

We also looked at the effect of hexanol on other physiological parameters: resting membrane potential, neuronal firing rate with given current injection, 1st spike latency, and temporal summation. In the presence of 1.4 mM hexanol, there was a hyperpolarization of the resting membrane potential of the neuron by about 2–3 mV soon after hexanol was washed into the bath (Fig. 3.20A-2; $p<0.01$; $n=5$; paired t-test). The voltage drop was compensated with 20–30 pA of current injection to maintain the same membrane potential as that of the baseline. Given the same amplitude of sustained current injection for baseline and hexanol conditions, there was also a significant delay in the latency to the 1st spike from 171.4 ± 22.6 ms to 392.1 ± 71.3 ms ($p<0.05$; n=5; paired t-test), which was reversible by wash-out (Fig. 3.20A-1&3). A series of 700 ms duration currents were injected from 30 to 180 pA by 30 pA steps and a plot of the number of spikes vs. amplitude of current injection (F-I plot) showed a significant right shift in the presence of hexanol suggesting suppression of neuronal excitability by hexanol (Fig. 3.20A-4). Wash-out of hexanol restored a slight increase in firing rate.

Physiological spike generation occurs through synaptic integration rather than sustained current injection. We mimicked synaptic integration activity by α–EPSP current injections to test the effects of hexanol. The number of spikes generated by the same amplitude of α–EPSP current injections in both conditions (supra-threshold temporal summation) was decreased in the presence of hexanol (Fig. 3.20B-2; 2.9 ± 0.1 vs. 1.1 ± 0.4 spikes; $p<0.01$; $n=5$).

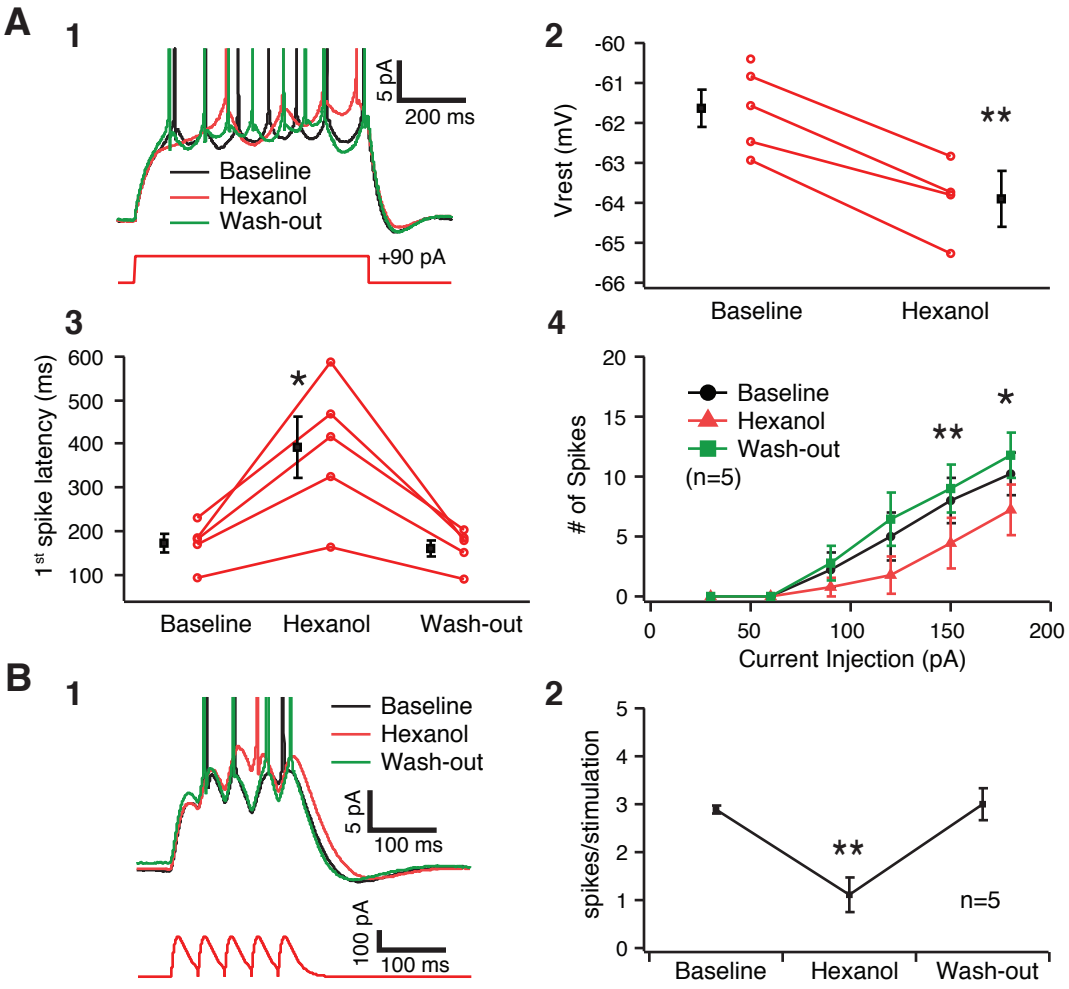

Figure 3.20: The effects of hexanol on neuronal firing and temporal summation
A: Hexanol suppressed the response of the cell to the constant current injection. Exemplary traces of neuronal firing by a sustained current input are shown. With +90 pA current injection, a neuron generated 7 spikes for control, 4 for hexanol, and 8 for wash-out, respectively (A-1). Upon wash-in of hexanol, V_{rest} was hyperpolarized by 2~3 mV ($p < 0.01$; paired t-test) and small amount of current (20~30 pA) was injected to return V_{rest} to the initial resting potential (A-2). 1st spike generated by the sustained current input showed a significant delay caused by hexanol and recovered after drug wash-out ($p < 0.05$; n=5; paired t-test) (A-3). Population data showed the right shift of F-I curve indicating diminished neuronal excitability ($p < 0.01$ at 150 pA, $p < 0.05$ at 180 pA; n=5; paired t-test) (A-4). **B**: Hexanol reduced the neuron's temporal summation capability. Supra-threshold temporal summation by 5 α–EPSP injection at 25 Hz showed reduced number of spike generation under hexanol condition in raw traces (B-1) and population data($p < 0.01$; n=5; paired t-test) where an α–EPSP = $A(t/\alpha)e(-\alpha t)$ with α=10 and A=amplitude adjusted to generate 3 spikes in baseline condition (B-2)

Chapter 4 Discussion

The main findings in the present study are the solidification of the presence of I_{NaP}, the comparison between I_{NaP} and I_{NaT}, and measurement of activation kinetics of I_{NaT} at near physiological temperature in the somatic region of hippocampal CA1 pyramidal neuron by quantitative electrophysiology. Differential blocking of I_{NaP} and I_{NaT} by hexanol and its physiological significance are also novel findings. The recorded I_{NaP} with the channel density of 1.4 ± 0.7 pA/pF showed different biophysical properties from those of I_{NaT}: lower half maximal activation, (-37.7 vs. -21.0 mV), smaller slope factor (3.7 vs. 6.3 mV^{-1}), and much smaller amplitude (2.38 % of I_{NaT}). Somatic transient Na^+ channel was activated as fast reaching 22.2 ± 2.3 μs at 40 mV. Hexanol, a known Na^+ channel blocker, has been suggested as a specific I_{NaP} blocker with the similar blocking effect, but different blocking mechanism of riluzole, another previously presumed specific I_{NaP} blocker. When hexanol blocked I_{NaP} in current-clamp recording, the voltage threshold of action potential generation was elevated by 4.6 mV. The change in other physiological parameters such as the decrease in firing rate given the same sustained input, increased 1st spike latency, and reduced temporal summation capability also suggested I_{NaP} enhanced the excitability of the hippocampal CA1 pyramidal neurons. When the presence of I_{NaP} is combined with the fast activation kinetics of Na^+ channel characterized in the presents study, it could provide a plausible explanation for the lower threshold of action potential initiation in the axon initial segment that is consistent with nearly uniform density of functional Na^+ channel along axo-soamtodendritic axis.

4.1 MEASUREMENT OF I_{NaP}

We have shown that I_{NaP} can be measured from hippocampal CA1 somata using nucleated patch recordings from adult animals. A study using nucleated patches from younger animals (P9-P16), however, did not observe I_{NaP} (Martina & Jonas 1997), suggesting age dependent differences. $Na_V1.6$ is considered to be responsible for I_{NaP} (Smith et al 1998) and is developmentally up-regulated 3-4 weeks postnatally (Osorio et al 2010). It thus may be difficult to measure I_{NaP} in the younger animals. In our recordings from 4-6 week Sprague-Dowely rats, the average peak amplitude of I_{NaP} evoked by a 0.4 mV/ms voltage ramp was 5.06 ± 0.23 pA (n=141) and the channel density was 1.44 ± 0.06 pA/pF, assuming 1 μF/cm^2 specific membrane capacitance.

Previous studies utilizing a voltage ramp protocol under whole-cell voltage clamp reported a wide range of I_{NaP} amplitude or I_{NaP} density depending on individual experimental conditions. Alzheimer and colleagues reported 8.9 ± 0.8 μA/cm^2 (= 8.9 ± 0.8 pA/pF) of I_{NaP} density measured with a 75 mV/s voltage ramp command on dissociated P17-P21 rat sensorimotor cortex neurons (Alzheimer et al 1993c). Astman and colleagues measured average 385 pA of I_{NaP} amplitude using 35 mV/s voltage ramp command and obtained median 1.9 pA/pF of I_{NaP} density on in situ layer V neocortical neurons (Astman et al 2006). Magistretti and Alonso found 17.7 ± 29.1 pA/pF (in situ neuron) or 16.5 ± 8.6 pA/pF (dissociated neuron) of I_{NaP} density by 50 mV/s voltage ramp command in layer II medial entorhinal cortex (Magistretti & Alonso 1999). Raman and colleagues reported 165 ± 13 pA of I_{NaP} amplitude that was reduced to 51 ± 6 pA in dissociated Purkinje neurons from Scn8a knock out mice using 0.1 mV/ms voltage ramp command (Raman et al 1997). Although the direct comparison between the previous findings and ours is not appropriate due to different experimental conditions, our value for density of I_{NaP} seems to be in the lower end of the range. This is not surprising,

because a recent Na^+-imaging study revealed little persistent Na^+ influx at the soma compared to the axon (Fleidervish et al 2010). Whole-cell voltage clamp can provide a reasonable clamp of the perisomatic region, including the proximal axon that is known to express $Na_V1.6$ (Lorincz & Nusser 2010), but the nucleated patch mostly contains the membrane excised from the soma only. Thus, I_{NaP} density from the nucleated patch might be expected to be lower than that from the whole-cell voltage clamp recordings.

The I_{NaT} current amplitude and density from our nucleated patch recordings were 174.6 ± 7.8 pA (n=110) and 0.498 ± 0.02 pA/μm^2 (49.8 ± 2.0 pA/pF) or 5.29 ± 0.22 pS/μm^2. Previous cell-attached recordings, however, reported 56 ± 15 pS/μm^2 (Magee & Johnston 1995a) or 3.2 ± 0.47 pA/μm^2 (Colbert & Johnston 1996), so our I_{NaT} density from nucleated patches is around 6 to 10 times lower than those values. Excising a macro patch very slowly from the soma in nucleated configuration might result in this decrease in current density. Martina and Jonas reported similar absolute I_{NaT} amplitude of 179 ± 12 pA, but about 5 ~ 10 times higher current density considering their smaller nucleated patch area (38.5 ~ 78.5 μm^2 vs 345.02 ± 4.65 μm^2) (Martina & Jonas 1997). Hu and colleagues also reported about 3 times larger I_{NaT} density (1.5 ± 0.1 pA/μm^2) in their nucleated patch recordings (Hu et al 2009). The explanation for our lower estimate for I_{NaT} density is unclear, but irrespective of the smaller amplitude, the voltage-dependent properties of I_{NaT} were similar to the previous studies.

4.2 MECHANISM OF I_{NAP} IN HIPPOCAMPAL PYRAMIDAL NEURONS

The origin of the persistent Na^+ currents was initially explained by a "window current" that was predicted by the overlap of steady-state activation and inactivation curves in the Hodgkin-Huxley gating model (Hodgkin & Huxley 1952). However, the

window current is generally confined to a narrow voltage range and does not explain sustained current at depolarized voltage range (French et al 1990). In our recordings, we obtained I_{NaT} activation and inactivation curves from the same patch (n=18) and compared I_{NaP} with the calculated window current. We found that window current failed to describe the sustained current at a depolarized potential and contributed only 16.1% of I_{NaP} with its peak at more hyperpolarized voltage than the peak of I_{NaP} (-42.3 vs. -31.2 mV). Thus, the window current hypothesis is not sufficient to account for the existence of I_{NaP}. The qualitatively similar conclusions were obtained in previous work done in whole-cell recording in different preparation such as dissociated hippocampal neurons (French et al 1990), Purkinje neurons (Kay et al 1998), and neocortical neurons (Magistretti & Alonso 1999, Maurice et al 2001, Urbani & Belluzzi 2000).

An alternative view is that I_{NaP} comes from the same population of Na^+ channels in a different gating mode (modal gating hypothesis). The gating mode switch of the channel from normal fast inactivating to late opening or sustained bursting can generate a persistent Na^+ current (Alzheimer et al 1993b, Patlak & Ortiz 1985, Patlak et al 1986). This view is supported by our data based on two observations.

First, we found a linear relationship between peak I_{NaP} amplitude evoked by 0.4 mV/ms voltage ramp command and peak I_{NaT} amplitude elicited by step voltage command (Fig. 3.9C). The peak I_{NaP} amplitude was 2.38% of the peak I_{NaT} amplitude. This is comparable to values recorded in whole-cell recordings from dissociated hippocampal CA1, tuberomammillary, or neocortical neurons (Cummins et al 1994, French et al 1990, Taddese & Bean 2002). Thus, I_{NaP} can arise in a small but constant proportion of I_{NaT}, suggesting it comes from the same channel. We also found that I_{NaP} measured by ramp voltage command underwent slow inactivation similarly to I_{NaT} (Fig. 3.4B-2, 3.7). Slow inactivation is distinct from fast inactivation in time scale, and the Na^+

channel is known to undergo this type of inactivation, although the molecular substrate of slow inactivation is not fully understood (Ulbricht 2005). I_{NaP} can come from burst and late opening Na^+ channels, which have been shown to experience a similar slow inactivation (Patlak et al 1986). Previous whole-cell studies with voltage ramp protocols showed the slow inactivation of I_{NaP} suggesting I_{NaP} and I_{NaT} have the same origin (Fleidervish et al 1996, Fleidervish & Gutnick 1996, Magistretti & Alonso 1999, Taddese & Bean 2002). Moreover, it was found that there is a positive correlation between the magnitude of I_{NaP} and the degree to which the channel undergoes slow closed state inactivation (Cummins et al 1998). Thus, it is possible that the ratio of Na^+ channels in conformation for the closed state inactivation to those not in this state could determine the amplitude of I_{NaP} based on the modal gating hypothesis.

Furthermore, this modal gating could occur preferentially in the subthreshold or near threshold voltage range where slow closed state inactivation was prominent in our data (Fig. 3.7, 3.8). Taddese and Bean reasoned that the conformational changes of Na^+ channel protein in the subthreshold voltage range would cause weak binding of an inactivation particle in the gating pathway and could generate a significant amount of background brief late opening and sustained burst activity due to incomplete or failure of inactivation of the same conventional Na^+ channel (Taddese & Bean 2002). Taking both aspects of closed state inactivation and open state inactivation into account, it could be hypothesized that the incomplete or failure of inactivation caused by weak binding of the inactivation particle would be correlated with the prior closed-state inactivation state of the same channel before opening.

On the other hand, the reversal potential of I_{NaP} (+29.5 mV) was different than that of I_{NaT} (+70.8 mV), and this could argue against the modal gating hypothesis. If, however, there was outward current contaminating inward Na^+ current at depolarized voltage range

(Astman et al 2006, Fleidervish & Gutnick 1996, Martina & Jonas 1997) and the outward current contamination was more prominent in the small I_{NaP} peak amplitude compared to the large I_{NaT} peak amplitude, then this might explain the discrepancy. The ionic basis of the outward current could be a nonspecific outward cation current, I_{cat} (Alzheimer 1994) that survived our cocktail of blockers to isolate Na^+ current. In addition, the current evoked by ramp voltage command is subject to slow inactivation during the dynamic change of membrane potential, which also could cause a shift of the reversal toward the hyperpolarized direction.

Finally, although our data support the modal gating hypothesis, we do not exclude the possibility that there also exists a separate type of non-inactivating Na^+ channel (Magistretti et al 1999b, Masukawa et al 1991).

4.3 PHARMACOLOGY OF I_{NAP}

Hexanol, riluzole, and ranolazine were used to investigate the pharmacology of I_{NaP}. The n-alcohols are well known I_{NaT} blockers (Horishita & Harris 2008, Shiraishi & Harris 2004), but their effect on I_{NaP} is still unclear. Hexanol, an n-alcohol with 6 carbon chains, was used here at concentrations similar to those where it has been reported to have anesthetic effects. In the hippocampal brain slice, G_{NaP} was suppressed about 2 times more than that of maximum G_{NaT} by 2.4 mM hexanol (49.7 ± 3.3% vs. -24.9 ± 8.0% reduction) when compared to a saline control. Hexanol did not cause any significant shift of the $V_{1/2}$ or slope factor for either activation or inactivation curves when compared to the saline control. These hexanol effects on I_{NaT} are comparable in several respects to those observed in a previous study done on oocytes. I_{NaT} of 4 α-subunit isoforms ($Na_V1.2$, $Na_V1.4$, $Na_V1.6$, and $Na_V1.8$) expressed in Xenopus oocytes showed the suppression by n-

alcohols about 30 to 40% at $V_{1/2}$ and 13 to 30% at -90 mV (Horishita & Harris 2008). It also showed voltage insensitive suppression suggesting an open channel blocking mechanism and small $V_{1/2}$ shifts without noticeable changes in slope factor (Horishita & Harris 2008). Thus, our data suggest that there would be about two times stronger suppression effects of hexanol on I_{NaP} than I_{NaT} via an open pore blocking mechanism while maintaining the availability of the channels. We also tested halothane, a volatile anesthetic agent, on I_{NaP} to test whether the effects of hexanol would be common to this anesthetic. The effects of halothane seemed comparable to those of hexanol: more blocking of I_{NaP} than I_{NaT} and no significant change in $V_{1/2}$ and slope of activation and inactivation (Fig. 4.1&2). Both I_{NaP} and I_{NaT} traces were recorded from a same patch. Halothane suppressed G_{NaP} more than G_{NaT} or I_{NaT} without a significant change in $V_{1/2}$ and slope of activation and inactivation curve (-56.6 ± 5.8%, -34.0%, and -22.0 ± 2.8%, respectively). The concentrations of halothane in the pipette were estimated to be in the 1–3 mM range by reverse phase high-performance liquid chromatography (HPLC) of the protein and metabolite analysis facility on the campus. However, the quantification of halothane was a rough estimation and its exact concentration could never be determined because the range of halothane concentration for quantification was close to the signal to noise ratio (SNR) of the HPLC system (LC-10AD VP, Shimadzu system) and the extremely high volatility of the molecule made the reasonable quantification of halothane unfeasible. Regardless of the uncertainty in the actual concentration of halothane delivered to the patch, the blocking effect on I_{NaP} by halothane was robust and reliably reproducible.

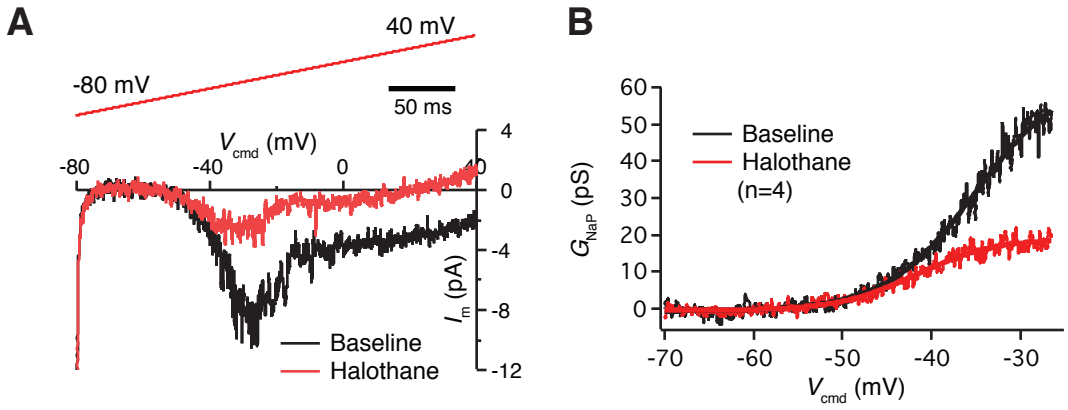

Figure 4.1: The effect of halothane on I_{NaP}
A: The example trace of I_{NaP} evoked by 0.4 mV/ms V_{ramp} showed a significant suppression by halothane (red). **B**: The early part of G-V curve of I_{NaP} was fitted by a Boltzmann equation and the normalized G-V curves in both conditions shows a significant blocking of I_{NaP} by halothane.

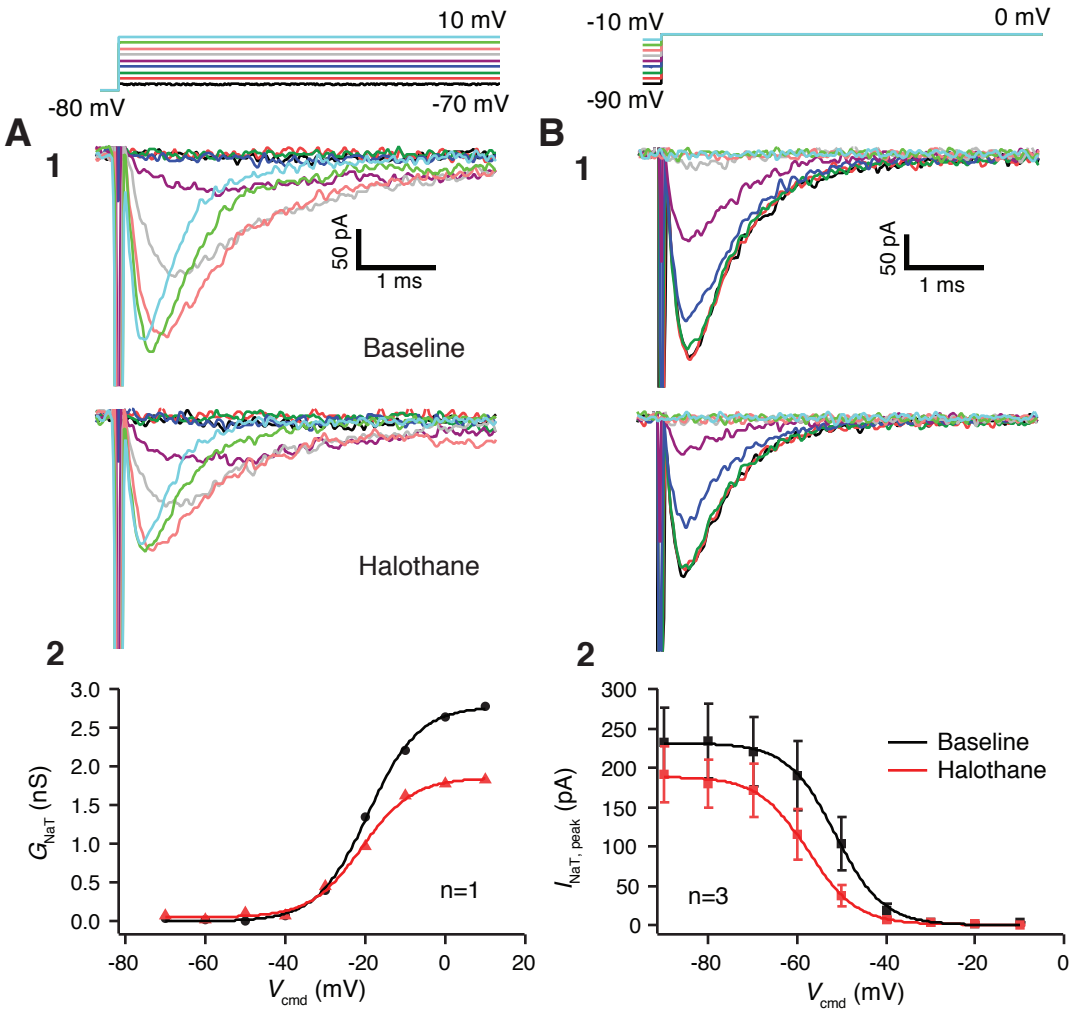

Figure 4.2: The effect of halothane on I_{NaT}
A: Exemplary traces of activation of I_{NaT} evoked by activation protocol were shown in two different conditions: baseline and halothane (A-1&2). Halothane puffing caused a significant decrease in the peak amplitude of I_{NaT}s, but relatively smaller amount compared to that of I_{NaP}. **B**: The inactivation curve showed decreased maximum conductance without notable change in voltage dependency.

Riluzole is reported to be a specific blocker for inactivated Na^+ channels (Benoit & Escande 1991, Urbani & Belluzzi 2000). We tested this drug to confirm its effects on I_{NaP} using nucleated patch recordings and compared them to those of hexanol. Similar to

hexanol, 10 μM riluzole produced about a 2-fold greater reduction in peak I_{NaP} compared to I_{NaT} (-52.6 ± 3.4% vs. -22.4 ± 6.4%). There was no notable change in the $V_{1/2}$ or slope factor of activation G-V curve compared to saline control. However, there was a significant leftward shift of $V_{1/2}$ (-9.2 ± 1.4 mV) without notable slope factor change in the inactivation curve. The time course of activation and inactivation of Na^+ current did not change significantly. These observations are also consistent with the previous findings. Benoit and Escande reported that riluzole caused no noticeable changes in I_{NaT} channel kinetics and activation G-V curve, but large left shift (~ -27 mV) of $V_{1/2}$ of steady-state inactivation curve on nodes of Ranvier of isolated nerve fibers of the frog (Benoit & Escande 1991). Urbani and Belluzzi showed -8.9 mV shift of steady state inactivation curve of I_{NaT} by 10 μM riluzole in the frontal agranular cortex neurons under whole-cell voltage clamp recordings (Urbani & Belluzzi 2000). Urbani and Belluzzi also measured I_{NaP} either by averaging Na^+ currents at 60 – 90 ms after activation that step voltage command evoked or by applying the slow voltage ramp command of 14 mV/s speed. Their I_{NaP} peaked around -10 mV in the I-V curve, and it looked more comparable to the non-(or ultraslow-) inactivating component of I_{NaP} than slowly inactivating I_{NaP} in this study (Fig. 3.4B-2). However, they found the much lower riluzole EC_{50} (~2 μM) concentration for their I_{NaP} than that of I_{NaT} (~20 μM), which indicates the differential block of I_{NaP} and I_{NaT} we found in this study (Urbani & Belluzzi 2000). On the other hand, although hexanol and riluzole block I_{NaP} to a similar degree, the blocking mechanism of both drugs would not be the same because riluzole showed much larger $V_{1/2}$ shift of inactivation curve. Thus, the larger suppression of I_{NaP} than I_{NaT} could be better explained by the preferential binding of riluzole to the inactivated state of the Na^+ channel as previously suggested considering the decrease in channel availability (Benoit & Escande 1991).

Ranolazine was shown to block the cardiac 'late' Na^+ current, which is resistant to inactivation in cardiac action potentials (Rajamani et al 2009). In our experiments we found 30 μM ranolazine had no effect on I_{NaP} and I_{NaT} compared to saline unlike both hexanol and riluzole cases. Ranolazine did not cause any significant change in slope factors, $V_{1/2}$ of inactivation curve, and channel kinetics. In the previous study done on $Na_V1.5$ isoform expressed in HEK293 cells, there was a large left shift of $V_{1/2}$ of inactivation curve of about 11 mV (Rajamani et al 2009). The main difference would be subunit composition of Na^+ channel isoforms. $Na_V1.5$ comprise cardiac Na^+ channel while the hippocampal neuron has mainly $Na_V1.1$, $Na_V1.2$, $Na_V1.3$, and $Na_V1.6$. Thus, ranolazine seems to be mainly effective on cardiac 'late' Na^+ current underlain by $Na_V1.5$ isoform and there may be few $Na_V1.5$ isoform channel density distribution in hippocampal CA1 pyramidal neurons although it is possible that there exists a certain amount of $Na_V1.5$ isoform in the limbic system (Hartmann et al 1999).

4.4 PHYSIOLOGICAL SIGNIFICANCE OF I_{NaP}

In our nucleated patch recordings, I_{NaP} evoked by a 0.4 mV/ms voltage ramp protocol showed 16.7 mV more negative $V_{1/2}$ (-37.7 vs. -21.0 mV) of activation and smaller slope factor (3.7 vs. 6.3 mV^{-1}) compared to those of I_{NaT} (Fig. 3.6). Slowly- or non- inactivating Na^+-channel activity at such a hyperpolarized voltage range and steep voltage sensitivity could affect the excitability of the neuron, although the magnitude of I_{NaP} is only 2–3% that of I_{NaT} (Crill 1996). Thus, we tested the effects of the blocking of I_{NaP} on action potential threshold under current-clamp in the presence of hexanol and found hexanol raised the voltage threshold. The 1st spike generated by 700 ms current injection showed a significant voltage threshold change in the presence of hexanol: 4.6

mV increase in V_{th}. Similar depolarization shift of V_{th} mediated by the reduction of I_{NaP} was observed in some, not all, brain areas of the $Na_V1.6$ (Scn8a) transgenic mouse. Royeck et al. observed up to 9 mV depolarization shift of V_{th} and reduced I_{NaP} in the hippcampal CA1 pyramidal neuron of $Scn8a^{med}$ mice (Royeck et al 2008). Gutnick and colleagues recently reported both a significant rise in V_{th} and decrease in Na^+ influx during prolonged somatic depolarization in Layer 5 neocortical neurons of conditional (Cre/loxP) Scn8a knock-out mouse (Gutnick et al 2010.5). However, Osorio et al. observed no alteration in V_{th} of cerebellar granular neurons of (Scn8a) mutant mouse even though I_{NaP} was reduced significantly (Osorio et al 2010). Merces et al. reported 4–5 mV rise of V_{th} without change in I_{NaP} in globus pallidus (GP) neurons of $Scn8a^{med}$ mice (Mercer et al 2007). The results suggest that, depending on the cell type and its surrounding environment, there might be other factors except I_{NaP} for setting spike threshold at the axon initial segment (AIS) such as the role of GABA-ergic inhibition onto the AIS and the other voltage-gated ionic conductances like A-type or D-type K^+ currents in AIS. Our data are consistent with the previous observation of V_{th} upswing concurrent with the reduction of I_{NaP} in hippocampal CA1 pyramidal neurons of $Scn8a^{med}$ mutant mice (Royeck et al 2008).

The blocking of I_{NaP} by hexanol also indicated the decreased excitability through the change of other physiological parameters such as the reduced number of spikes generated in response to sustained current injections or α–EPSP injections. So, I_{NaP} can affect the rate of the neuronal firing by which a neuron encodes the incoming information. Moreover, the 1^{st} spike generated by a 700 ms current injection showed a significant delay of 1^{st} spike generation in the presence of hexanol (171.4 ± 22.6 vs. 392.1 ± 71.3 ms), which suggests that blocking of I_{NaP} can cause less precise axonal spike initiation given the same input. This increased variability of an action potential

generation, in turn, means that a neuron becomes less capable to process information contained in the precise timing of the spikes. As such, the change in neuronal properties introduced by the blocking of I_{NaP} not only reduces the intrinsic excitability of the neuron, but also constrains the rate and temporal coding capability of the information processing by the neuron.

Based on the effect of I_{NaP} on temporal coding of the neuron, an interesting conjecture can be made related to the role of I_{NaP} in dendritic computation and information storage. Since it has been known that dendritic Na^+ channels undergo more prominent slow inactivation (or slow recovery from inactivation) than those at the soma and there is different phosphorylation state at distal dendrites compared to the counterpart at proximal dendrites (Colbert et al 1997, Gasparini & Magee 2002), distal dendrites could have a high density of I_{NaP}. When the dendritic spike is generated by the clustered synaptic inputs restricted in a narrow spatio-temporal window, I_{NaP} could facilitate the dendritic integration of the synaptic inputs generating more precisely timed dendritic spikes, which would affect axonal spike generation and/or synaptic plasticity. The more I_{NaP} is up-regulated on the distal dendrite, the smaller the size of dendritic branch segment recruiting the coincident synaptic inputs become for the generation of the dendritic spike. This means the amount of I_{NaP} regulated in the dendrite can contribute to the degree of compartmentalization of the dendrite and, consequently, the increased computation power and memory storage of the neuron (Ariav et al 2003, Poirazi & Mel 2001). The expression and interaction of other voltage gated ionic conductances on the dendrite such as A- or D-type K^+ current and I_h could be a limiting factor for the role of I_{NaP} in this mechanism

4.5 SUBCELLULAR DISTRIBUTION OF PERSISTENT Na^+ CONDUCTANCE

The knowledge of the distribution of the voltage gated ion channels in a neuron can provide a hint of the mechanism of information processing performed by the neuron. For instance, the increasing density of I_{KA} along the dendrite decreases the probability of action potential generation in the distal dendrite where the ratio of I_{KA} to I_{Na} becomes higher, and dampens the amplitude of bAPs for the regulation of synaptic plasticity and local dendritic excitability (Hoffman et al 1997). Likewise, if there were non-uniform distribution of I_{NaP}, it would be interesting because of its possible impact on the neuronal computation. When this question was initially addressed, the same cell-attached patch recording of persistent Na^+ channel might not be a preferred choice because of the very low probability of isolating the persistent Na^+ channel activity in the small size of the patch. Instead, whole-cell voltage-clamp or current-clamp combined with focal drug application technique was utilized to provide a rough estimate of the distribution of this elusive conductance in the neuronal compartments.

The perisomatic locus of I_{NaP} was suggested by the experiment showing that the amplification of somatic EPSPs was mediated by Na^+ channels located in the axon and soma, not dendrite (González-Burgos & Barrionuevo 2001, Stuart & Sakmann 1995). Astman and colleagues further narrowed down the origin of I_{NaP} to the proximal axon (Astman et al 2006). In the cell-attached recording on the neocortical neuron, Astman et al. failed to observe the persistent Na^+ channel activity (brief late opening or non-inactivating) or modal gating in the soma in the subthreshold voltage range at which whole-cell I_{NaP} operates. Rather, they noticed that local TTX application to the proximal axon (20 ~ 50 μm from the soma) not the soma or apical dendrite blocked whole-cell I_{NaP} (Astman et al 2006). Since Martina and Jonas failed to detect I_{NaP} in nucleated patches that were excised from the somatic membrane (Martina & Jonas 1997), these results

raised a possibility that I_{NaP} might not exist in the soma. However, our current study reports the presence of somatic I_{NaP} that was evoked by a 0.4 mV/ms voltage and has the channel density of 1.4 ± 0.7 pA/pF supporting modal gating hypothesis of I_{NaP} mechanism (as in section 3.1). Recording the small somatic I_{NaP} is consistent with the small persistent Na^+ conductance activated in the soma at more depolarized potentials in the Na^+ imaging study where I_{NaP} was activated predominantly in the axon in the subthreshold voltage range (Fleidervish et al 2010). The discrepancy between the previous studies and ours could result from the different experimental conditions such as animal age and voltage command protocol. For example, Astman et al. used a voltage ramp with 0.14 mV/ms velocity in their cell-attached recording to detect persistent Na^+ channel activity. The velocity of their voltage ramp is more than 2 times slower than ours (0.4 vs. 0.14 mV/ms), and slow inactivation of I_{NaP} would be more prominent in their experiment making it difficult to detect the persistent Na^+ channel activity (see Fig. 3.7 for the slow inactivation of I_{NaP} depending on the ramp velocity). On the contrary to their observation, the Na^+ channel activity underlying our I_{NaP} could be measured in the cell-attached recording using the same voltage protocol as shown in Fig. 4.3 below. Thus, the I_{NaP} can be generated in both the soma and axon.

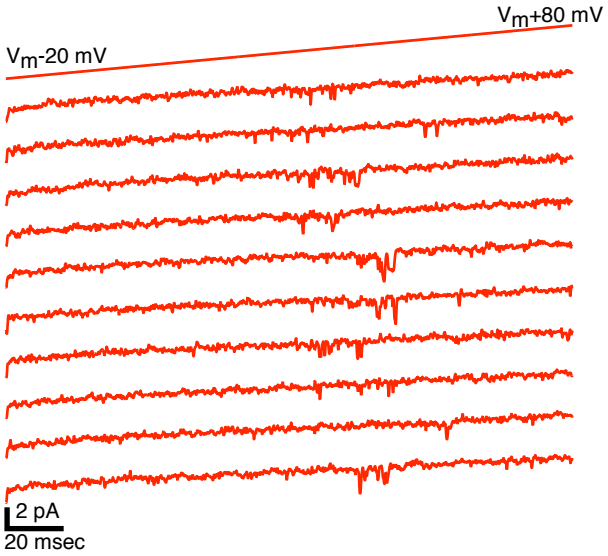

Figure 4.3: Persistent Na^+ channel activity underlying I_{NaP}
Cell-attached recording on the hippocampal CA1 neuron soma revealed persistent Na^+ channel activities with a 0.4 mV/ms ramp voltage command. The above graph shows several sample current traces in response to a voltage ramp from V_m-20 mV to V_m+80 mV with duration of 200 msec. Cells were bathed in standard ACSF and the patch pipette contained HEPES-buffered ACSF, pH adjusted with TEA-OH, with the addition of 100 μM 3,4-diaminopyridine and 200 μM $CdCl_2$. Single Na^+ channels open over the same voltage range as that seen in nucleated patches. (Collaboration with Dr. R. Gray and data figure courtesy of Dr. R Gray)

On the other hand, the studies with similar experimental conditons indicate that substantial mount of I_{NaP} would exist in the dendrite. Dendritic Na^+ channel was shown to be activated by subthreshold EPSPs (Magee & Johnston 1995b) and presumed to underlie the dendritic I_{NaP}. Local application of TTX to the apical dendrite blocked the presumed I_{NaP} and abolished the amplification of EPSPs in hippocampal CA1 pyramidal neurons (Lipowsky et al 1996) and neocortical pyramidal neurons (Schwindt & Crill 1995). The persistent activity of the dendritic Na^+ channel was also demonstrated on the residual dendrite of the dissociated entorhinal cortex layer II pyramidal neuron (Magistretti et al

1999a). Na^+ imaging studies further provided the evidence of the presence of I_{NaP} in the dendrite (Fleidervish et al 2010, Gutnick et al 2010, Mittmann et al 1997).

Taken together, all compartments of the neuron (the axon, soma, and dendrite) are expected to generate I_{NaP}. However, the density of I_{NaP} generated in the individual compartments may vary. The current study presents quantitative data about the somatic I_{NaP} measured in nucleated patch recording (in Chapter 3), but the direct recording of the axonal and dendritic I_{NaP} remains technically difficult. Outside-out patch from *in situ* neurons might be possible for estimating the I_{NaP} density gradient in axo-somatic region due to the expected high density of I_{NaP} in the axon, but ultamately the cell-attached single channel recording in brain slice will be the decisive quantitative measure to characterize the detail distribution of I_{NaP} in the entire axo-somatodendritic axis and shed some light on the mechanism of I_{NaP}.

4.6 MOLECULAR IDENTITY AND MECHANISM OF PERSISTENT NA^+ CURRENT

The subcellular expression of I_{NaP} should be supported by underlying molecular substrates. As noted previously, $Na_V1.1$, $Na_V1.2$, and $Na_V1.6$ are the main α-subunit isoforms of Na^+ channel found in neuron in the central nervous system (Vacher et al 2008). The functional Na^+ imaging indicated the presence of I_{NaP} in the entire neuron, but in different degree: predominant axonal I_{NaP} at subthreshold voltages and relatively small somatic and dendritic of I_{NaP} at more depolarized potentials (Fleidervish et al 2010). The immunohistochemistry data pointed out that such a non-uniform subcellular distribution of I_{NaP} is matched with the distribution of $Na_V1.6$ in the axo-somatodendritic axis compared to that of $Na_V1.1$ and $Na_V1.2$, which are mostly localized at the proximal AIS

and unmyelinated axon (Boiko et al 2001, Boiko et al 2003, Kaplan et al 2001, Lorincz & Nusser 2008, Lorincz & Nusser 2010, Van Wart et al 2007).

In agreement with this idea, there was the significant decrease in the amplitude of I_{NaP} measured in the neurons from several brain regions of $Na_V1.6$ knock-out transgenic mouse such as Purkinje neuron (Raman et al 1997), cerebellar granule cell (Osorio et al 2010), hippcampal CA1 pyramdial neuron (Royeck et al 2008), pyramidal prefrontal cortex neuron (Maurice et al 2001), subthalamic nucleus neuron (Do & Bean 2004), and mesencephalic trigeminal neuron (Enomoto et al 2007). Also, Royeck et al. and Enomoto et al. observed 2–5 mV depolarization shift of voltage dependence of activation in $Na_V1.6$ mutant mice (Enomoto et al 2007, Royeck et al 2008), which can be explained by the hypothesis that presence of $Na_V1.6$ could cause the more hyperpolarized voltage dependence of activation. Indeed, the ~15 mV more hyperpolarized voltage dependence of activation was observed when $Na_V1.6$ isoform was expressed in mammalian neuronal cell background compared to $Na_V1.2$ isofrom (Rush et al 2005) and this is also consistent with the result of the present study that the $V_{1/2}$ of I_{NaP} is more hyperpolarized than that of I_{NaT} by -16.7 mV. Thus, the nucleated patch recording of the hippocampal CA1 pyramidal neurons from $Na_V1.6$ knock out mouse might be a way to test whether the I_{NaP} we recorded would come from $Na_V1.6$ as it is normally assumed to be the molecular identity of persistent Na^+ current.

To make a more realistic and accurate mapping between the distribution of I_{NaP} density and $Na_V1.6$, both the neuron specific regional difference in the distribution of β-subunits associated with α-subunit and neuromodulation of Na^+ channel would also need to be taken into account because of their effects on the expression, amplitude, and kinetics of Na^+ current (Cantrell & Catterall 2001, Isom 2001).

On the other hand, we hypothesized that I_{NaP} could come from the different gating mode of the same population of Na^+ channel (modal gating) generating I_{NaT}, and it was mainly based on our two observations: slow inactivation and proportionality of I_{NaP} to I_{NaT}. A Na^+ channel model that includes slow inactivation (Migliore et al 1999, Migliore et al 2004) can qualitatively describe some of the results in section 3.1. In the model, one more gating variable is incorporated into the conventional Hodgkin-Huxley (HH) formulation for Na^+ channel gating to explain slow inactivation of Na^+ channel. When simulated in NEURON (see *methods*), the voltage dependence of kinetics of the model gave more hyperpolarized G-V curve of I_{NaP} than that of I_{NaT} (Fig. 4.4D). The slow inactivation of I_{NaP} under the ramp and triangular voltage commands could be qualitatively replicated (Fig. 4.5). The ratio of I_{NaP} to I_{NaT} was 2.98 %.

The model with the addition of one more gating variable to conventional HH scheme rather than including an additional ionic conductance made it possible to explain some aspects of our I_{NaP} and further supported the modal gating hypothesis as the mechanism of I_{NaP}. However, the Na^+ channel gating kinetics is too complex to be realistically described by this model. Unlike the HH scheme, Na^+ channel in CNS neurons has the gating particles that are not independent to each other and the inactivation process is tightly coupled to the activation process (Aldrich et al 1983, Aldrich & Stevens 1987). Although a more realistic multistate Na^+ channel model was recently proposed by Milescu and colleagues (Milescu et al 2010), their inaccurate I_{Na} measurements plagued by space clamp problem still undermined the effectiveness of the model. Thus, the multistate kinetic modeling of Na^+ channel based on our quantitative I_{Na} measurements would be necessary in the future to describe Na^+ channel kinetics more realistically, and provide some insights about the origin of I_{NaP}.

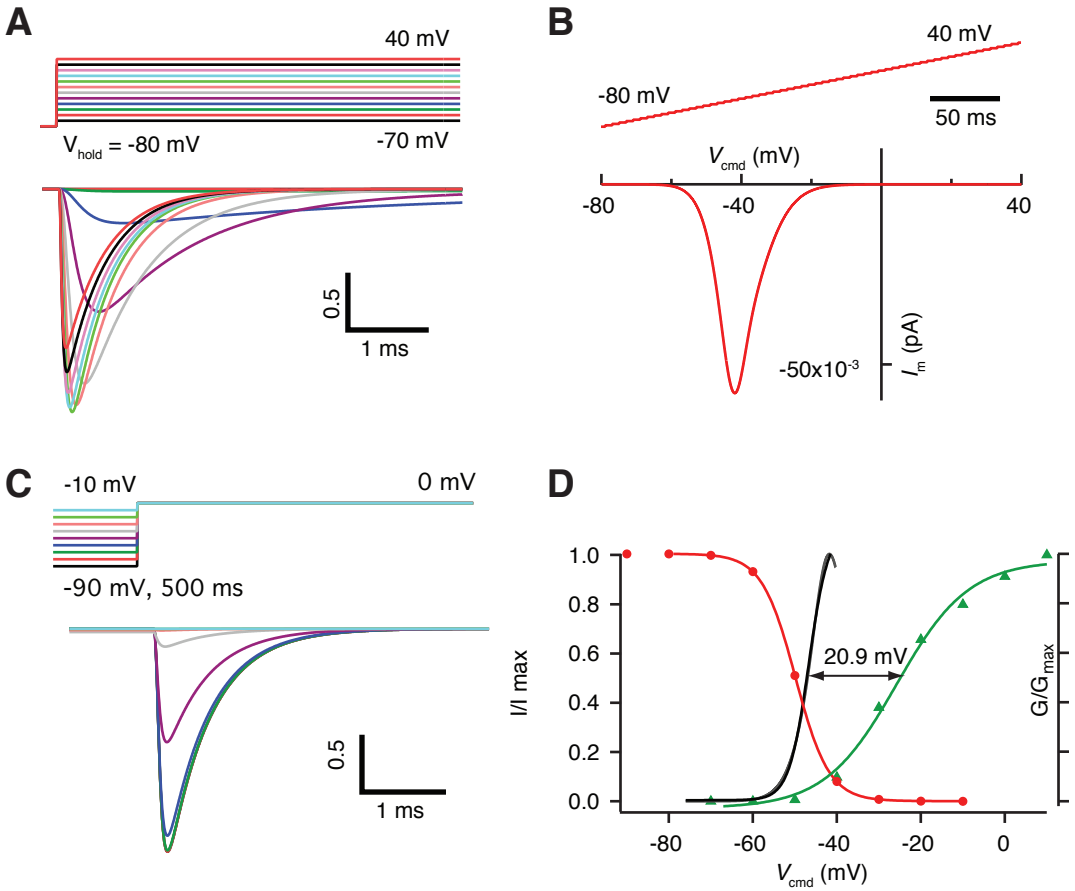

Figure 4.4: Simulation of I_{NaT} and I_{NaP} and voltage dependence of channel gating of the model

A, C: Simulated I_{NaT} traces for activation and inactivation curves were generated with the same voltage command protocol used in the experiment. **B**: Simulated I_{NaP} trace was evoked with the same 0.4 mV/ms ramp voltage command used in the experiment. **D**: The activation G-V curve of the simulated I_{NaP} and I_{NaT} shows more hyperpolarized (-20.9mV) and steeper slope (2.34 vs. 8.54 mV^{-1}).

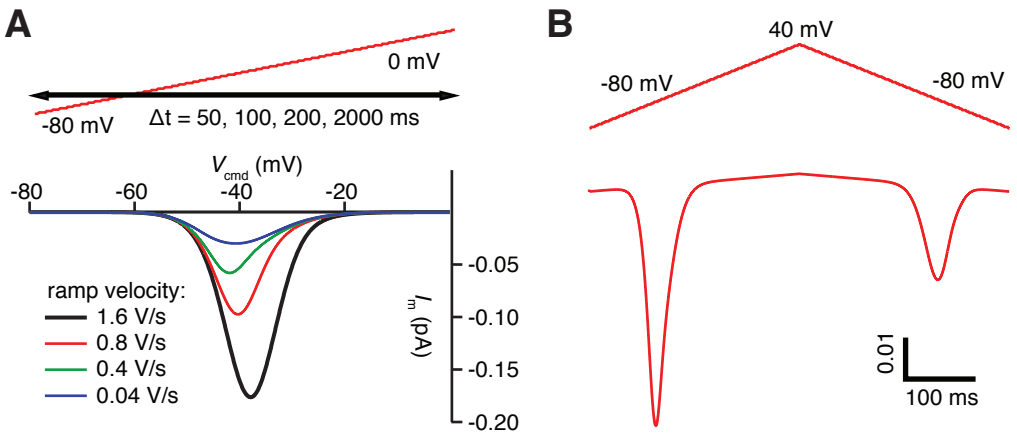

Figure 4.5: Slow inactivation of simulated I_{NaP} of the model
A: As the slope of ramp voltage decreased, the simulated I_{NaP} generated a gradual decrease in amplitude and left shift of the peak that were observed in the experimental results (Fig. 3.7A). **B:** the simulated I_{NaP} evoked by a triangular voltage command also showed slow inactivation (Fig. 3.7B).

4.7 Action potential initiation and persistent Na^+ current in the axon initial segment

With the assumption that I_{NaP} would be predominantly generated from the axon and expressed by $Na_V1.6$ isoform, the role of I_{NaP} in action potential generation is one of the most interesting questions. Action potentials are used by neurons to process and communicate information and the site of their initiation can determine a way that the neuron integrates synaptic inputs into neuronal output. There is a consensus that action potential is initiated in the axon initial segment (AIS) and propagates down the axon as well as backwards into the soma and dendrites (Colbert & Johnston 1996, Kole & Stuart 2008, Stuart et al 1997, Stuart & Sakmann 1994). Under some conditions local spikes can also be initiated in dendritic branches (Gasparini et al 2004, Losonczy et al 2008, Schiller et al 2000). The reason why the AIS shows a low threshold for action potential generation, however, is still not well understood. A higher density of Na^+ channels (about

40x – 1000x) of the AIS than that of the soma was proposed and supported by theoretical modeling studies and with immunohistochemistry (Boiko et al 2003, Hu et al 2009, Kole et al 2008, Lorincz & Nusser 2010, Mainen et al 1995, Van Wart et al 2007). However, the functional Na^+ current density measured on the plasma membrane of the axon was not consistent with a high density of Na^+ channels (Colbert & Johnston 1996, Fleidervish et al 2010, Kole et al 2008).

An alternative hypothesis is that a class of Na^+ channels with different biophysical properties is responsible for a lower threshold for action potential generation in the AIS. A negative shift of the voltage dependence of Na^+ channel kinetics in the AIS was suggested in some modeling studies (Dodge & Cooley 1973, Traub et al 1994). The cell-attached/outside-out patch clamp recordings later confirmed the more hyperpolarized voltage dependence (-6 – -14 mV) of activation of Na^+ channel in the myelinated axon of the neocortical L5 pyramidal neuron (Colbert & Pan 2002, Hu et al 2009, Kole et al 2008) and the unmyelinated hippocampal mossy fibers (Schmidt-Hieber & Bischofberger 2010). However, the model incorporated with the negative shift in voltage dependence of activation alone cannot provide a full explanation about the localization of action potential initiation in the AIS region and caused conflicting results depending on the model used. While a model with the moderately higher density (3x larger) of Na^+ channels and more negative voltage dependence of Na^+ channel activation (up to -8 mV) in the AIS succeeded to localize the action potential initiation site to the AIS (Colbert & Pan 2002), the other models could explain the spike initiation at the AIS only when high density (40x – 50x larger) of Na^+ channel was incorporated into the AIS despite the hyperpolarized voltage dependence of activation (Hu et al 2009, Kole et al 2008). This discrepancy could originate from the distorted Na^+ activation time constant (τ_m) incorporated in the models. Both models of Hu et al. and Kole et al. were based on the

Mainen and colleagues' model (Mainen et al 1995) that in turn utilized the kinetics of the Na^+ current obtained from whole-cell voltage-clamp recording on acutely isolated rat neocortical neurons at room temperature (Hamill et al 1991, Huguenard et al 1988). Colbert and Pan used the modified Na^+ model parameters that were based on data measured by cell-attached recordings in brain slice experiment at room temperature (Colbert & Johnston 1996, Magee & Johnston 1995a). Whichever data the above Na^+ models were based on, the actual onset kinetics of Na^+ current could be distorted to some degree by imperfect voltage control and/or the narrow bandwidth (<5 kHz low pass filtering) of the recording conditions. Moreover, considering the effect of temperature on channel kinetics, the onset kinetics of Na^+ current in the models would be quite deviated from true Na^+ current activation kinetics at physiological temperature. These shortcomings of the above models were addressed by Fleidervish and colleagues, and they showed that the AIS could become the preferred site of action potential initiation by correcting their model with the τ_m = 23 μs at 0 mV at 32 ºC that is one fifth of τ_m in the Colbert and Pan's model (Fleidervish et al 2010). One fifth scaling of τ_m was based on the data obtained by Engel and Jonas in outside-out patch recording on the mossy fiber bouton at room temperature (Engel & Jonas 2005), which gave as fast Na^+ current activation time constant as 45 ± 29 μs at +40 mV. When we measured the Na^+ current activation kinetics at near physiological temperature (31 – 33 ºC) with a 20 kHz low pass filtering, we obtained τ_m that was twice as fast of that measured by Engel and Jonas (Fig. 3.3; 45 ± 29 vs. 22.2 ± 2.3 μs at +40 mV) supporting Fleidervish and colleagues' argument.

Moreover, this fast τ_m can explain a very fast action potential rise and the corresponding high rate of rise up to 1130 mV/ms observed in the axonal whole-cell recording (Kole et al 2008) without assuming unnecessarily high density of Na^+

conductance in this area (Fleidervish et al 2010). Thus, the fast τ_m needs to be considered as another specialized biophysical property of axonal Na^+ channel for the low threshold in the axon, as it was implied in the previous modeling study (Traub et al 1994). Indeed, it has been recently reported that the axonal Na^+ channels have both twice-faster activation kinetics and negative shift (-5.9 – -7.6 mV) of $V_{1/2}$ than the somatic counterpart in the granule cell of the dentate gyrus (Schmidt-Hieber & Bischofberger 2010). When the authors combined them with moderately high density Na^+ channel (5x larger) in the axon, the nonmyelinated axon became a preferred spike initiation site compared to the soma-dendritic axis (Schmidt-Hieber & Bischofberger 2010). By extrapolating these data, it can be predicted that the τ_m of axonal Na^+ channels could be at least twice as fast as the τ_m recorded in the soma in the myelinated neocortical and hippocampal pyramidal neurons, but this remains to be confirmed by future experiments.

In addition to the specialized gating properties of axonal Na^+ channels, I_{NaP} can be a source for the lower threshold for spike generation in the AIS because of its perisomatic distribution and lower half maximal activation voltage than that of I_{NaT}. Our preliminary immunohistochemistry data showed perisomatic distribution of $Na_V1.6$ isoform in the neuron (Fig. 4.6) and our recording gave 16.7 mV more negative $V_{1/2}$ of I_{NaP} activation than that of I_{NaT} (-37.7 vs. -21.0 mV). When the I_{NaP} was incorporated into the axonal area with different biophysical properties of axonal Na^+ channel, the voltage threshold for action potential initiation in the AIS even became lower supporting the hypothesis that the axonal I_{NaP} is necessary to set the low voltage threshold for action potential generation in the AIS (Astman et al 2006, Fleidervish et al 2010, Gutnick et al 2010).

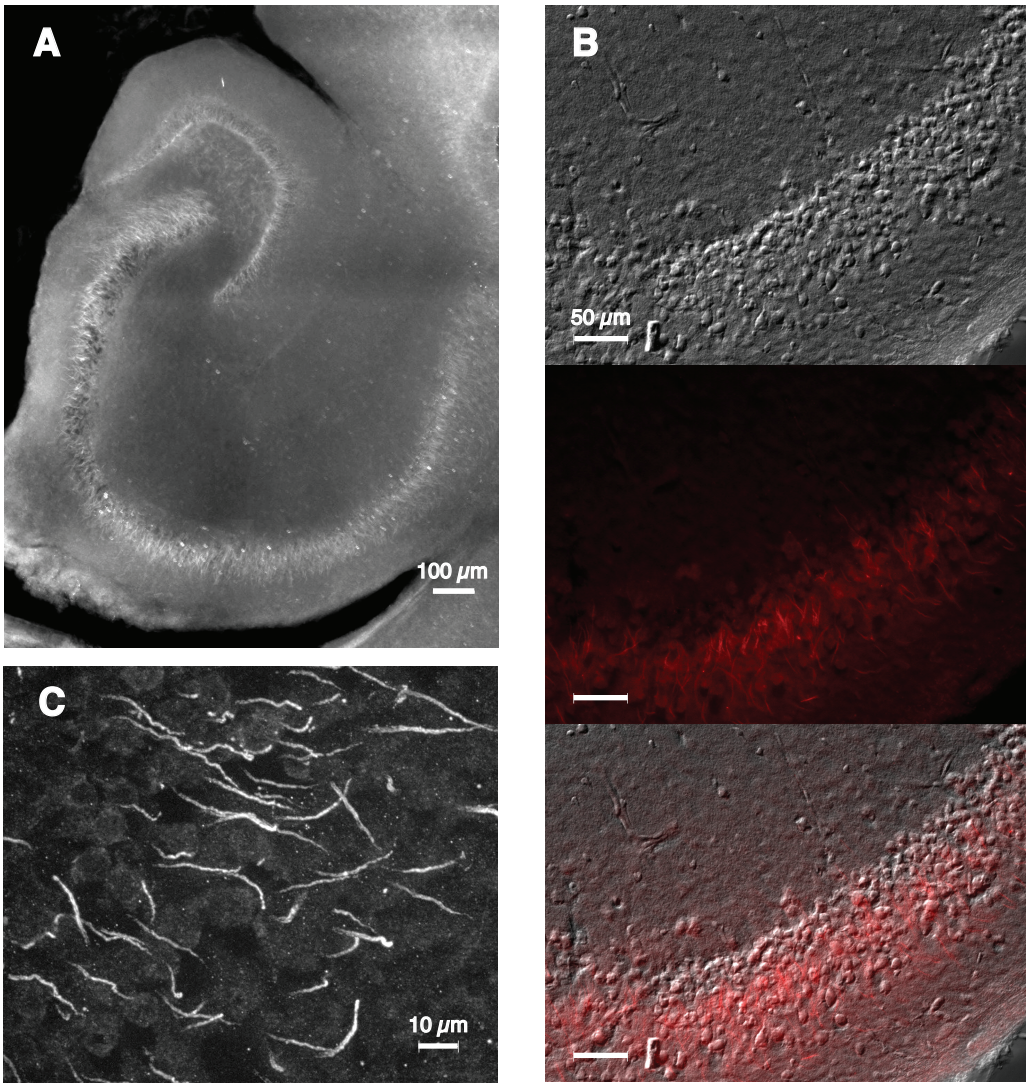

Figure 4.6: Expression of $Na_V1.6$ isoform in hippocampal neurons
The expression of $Na_V1.6$ was shown by immunofluorescence $Na_V1.6$ antibody staining. **A**: The strong perisomatic immunofluorescence signal by Alexa-594 probe was observed in all the areas of hippocampal formation in the mouse transverse hippocampal slice (50 μm thickness by cryostat resectioning). **B**: The perisomatic, but predominantly axonal, distribution of $Na_V1.6$ can be observed in the CA1 subfield: DIC image (top), $Na_V1.6$ immunofluorescence signal (middle), and overlaid image (bottom). **C**: The higher magnification image (with 63X objective) demonstrates low density of $Na_V1.6$ in perisomatic region and high density in the axonal region.

When the I_{NaP} was blocked by hexanol, a putative I_{NaP} specific blocker tested in the present study, The voltage threshold was elevated by 4.6 mV in recorded voltage traces and corresponding phase-plane plot (Fig. 3.19B). Blocking of I_{NaP} also reduced the number of spikes generated by 700 ms step current injection, prolonged the generation of 1st spike given the same input, and decreased the number of spike generated by temporal summation. These data all indicate the impairment of spike generation capability and consequent reduced neuronal excitability. Taken together, our data support the hypothesis that I_{NaP} is a crucial factor for setting the action potential threshold and low threshold in the AIS.

4.8 DENDRITIC COMPUTATION AND PERSISTENT NA^+ CURRENT IN THE DENDRITE

Dendritic distribution of I_{NaP} can have a significant impact on dendritic synaptic integration and dendritic excitability. For the incoming EPSPs, dendritic I_{NaP} can compensate for attenuation of EPSP caused by passive dendritic filtering effect and increase temporal summation occurring near the site of EPSP generation or soma by elevating EPSP amplitude and extending the EPSP duration (Mittmann et al 1997, Schwindt & Crill 1995). The enhancement of the strength and duration of EPSPs in turn means the strengthening of synaptic efficacy. Also, the regenerative I_{NaP} evoked by spatially and temporally correlated synaptic inputs could cause localized change in membrane property such as input resistance and time constant generating Na^+ and/or Ca^{2+} spikes in the dendrite, which trigger a somatic spike or make the post-synaptic depolarization for the induction of synaptic plasticity (Golding et al 1999, Golding & Spruston 1998, Golding et al 2002). Although the present study was limited to test the role of I_{NaP} in somatic spike generation and excitability, the decrease in temporal

summation capability of the neuron concurrent with the reduction of I_{NaP} was demonstrated by using hexanol, a possible I_{NaP} specific blocker (Fig. 3.17B). In the future, the synaptic transmission and LTP experiments with the same blocker might further elucidate the functional roles of dendritic I_{NaP} in dendritic computation and synaptic plasticity.

Dendritic I_{NaP} could also affect the activity dependent amplitude attenuation of a train of bAPs. bAPs have been known to be an important retrograde feedback signal for the induction of Hebbian plasticity (Magee & Johnston 1997). When they backpropagates to the distal dendrite, the amplitude of bAPs during repetitive firing undergoes progressive reduction, which is mediated by inactivation of Na^+ channels rather than alteration of K^+ channel in the dendrite (Colbert et al 1997, Jung et al 1997, Spruston et al 1995). The activation of PKC reduced the activity dependent attenuation of bAPs by enhancing the rate of rise of bAPs and resulted in increased dendritic excitability (Colbert & Johnston 1998). However, the effects of PKC modulation of Na^+ channel on the amplitude and kinetics generally seem to favor the decrease in neuronal excitability. PKC activation reduces the peak Na^+ current by the decrease in channel availability (channel number and/or open probability) without change in voltage dependence of activation or inactivation, and slows Na^+ channel inactivation (Numann et al 1991). One way to explain how the reduced Na^+ channel availability by PKC activation increases the maximum rate of rise of bAPs is to assume that PKC modulation might up-regulate dendritic I_{NaP}, which is implicated in the substantial slowing of inactivation kinetics by PKC modulation. PKC phosphorylation of Na^+ channels changed the gating mode of the channel from transient opening to sustained and frequent reopening (Numann et al 1991), and augmented I_{NaP} at more hyperpolarized voltage (Astman et al 1998). Then, as the same argument in the previous section, the up-regulated I_{NaP} with faster τ_m can contribute

to the increased rate of rise and dendritic excitability due to increase in the ratio of I_{NaP} to I_{NaT}. The application of phobol ester, PKC activator, to the nucleated patch and measuring I_{NaP} will be a simple way to test this hypothesis.

On the other hand, the attenuation of dendritic Na^+ current during bAP train resembles the slow closed state inactivation of Na^+ current observed in the present study where 63% of Na^+ channel became unavailable in 100 ms at -40 mV prepulse potential (Fig.3.7B). Considering the relationship between slow close state inactivation and I_{NaP} (Cummins et al 1998), the I_{NaP} evoked by a ramp voltage command with various velocities could be a tool to estimate the degree of activity dependent decrease in Na^+ current. Also, the role of dendritic I_{NaP} in the increased local dendritic excitability and EPSP-spike (E-S) potentiation accompanied by LTP need further exploration, which might coexist with intrinsic plasticity of I_{KA} (Frick et al 2004).

4.9 PERSISTANT NA^+ CURRENT IN NEUROLOGICAL DISEASE: FUTURE DIRECTIONS

Pathological conditions might alter the biophysical properties and/or expression level of voltage gated ion channels. Various diseases can develop following an acute or chronic change in voltage gated ion channels. For instance, theta burst pairing (TBP), which mimicks a physiological pre- and post- synaptic activity for synaptic plasticity induction, induced both a robust LTP and the -7 mV shift of the inactivation curve of A-type K^+ current in hyperpolarized direction producing an increase in dendritic excitability as an intrinsic mechanism of information processing and storage (Frick et al 2004). On the other hand, the synaptic overstimulation triggered in the pilocarpine-treated rat, an animal model of temporal lobe epilepsy (TLE), down-regulated dendritic I_{KA} through both the decrease in the channel expression and increase in ERK phosphorylation, which

could make neurons hyperexcitable and possibly generate epileptic discharges (Bernard et al 2004). In the similar way, if I_{NaP} were regulated in pathological conditions, it would be of interest because it can have a profound effect on neuronal excitability due to its role in action potential generation. Although persistent sodium current is relatively less understood in pathophysiological conditions of CNS neurons, it is reported that the up-regulation of persistent Na^+ current is involved in epilepsy and corresponding change in the expression of $Na_V1.6$ (Agrawal et al 2003, Blumenfeld et al 2009). Following the lead of others, we tested this hypothesis by examining the change of expression of $Na_V1.6$ protein and alteration of I_{NaP} in hippocampal CA1 pyramidal neurons from 5 weeks after induction of status epilepticus (SE) in kainate epilepsy model rat, but failed to observe any significant difference in $Na_V1.6$ expression level and peak I_{NaP} from control and epileptic animal (data not shown). There exist several possibilities for these observations. Because nucleated patch recording can only test somatic I_{NaP}, a change of I_{NaP} in the axon or dendrite might still be responsible for the seizure activity of the epileptic animal. Also, the alteration of Na^+ channel would be dominant in earlier or later period of post SE. Another possibility is the other voltage- or ligand-gated ion channels contributing to epileptogenesis. For example, the altered expression and function of dendritic, not somatic I_h was observed in the hippocampal neuron, and it was significant at earlier times after induction of SE (Jung et al 2007, Shin et al 2008). Therefore, the different location of the neuron and earlier time point post SE need to be considered in future experiments.

Another interesting pathological condition that might regulate I_{NaP} in the neuorn is the hyperexcitability observed in Alzheimer's disease (AD). Alzheimer disease (AD) is one of the devastating forms of dementia that has the hallmark of amyloid-beta protein (Aβ) plaque and tau protein tangle formation in the brain. Along with the cognitive deficit, the incidence of unprovoked seizures is a common clinical symptom of early

onset and progression of AD (Amatniek et al 2006, Cabrejo et al 2006). Although the impairment of LTP and the suppression of synaptic transmission were well documented in animal models of AD (Kamenetz et al 2003, Shankar et al 2008, Walsh et al 2002), they cannot provide an adequate explanation for the epileptiform activity in the same animal. This hyperexcitability of the neurons can be generated by coordinated network activity mediated by enhancement of inhibitory circuits in AD model mouse (Amatniek et al 2006, Cabrejo et al 2006, Palop et al 2007, Palop & Mucke 2009, Palop & Mucke 2010).

However, the hyperexcitable state of the neurons initially caused and maintained by the high level Aβ deposition before the homeostatic inhibitory circuit remodeling still needs to be explained. This is a particularly important question to be answered in order to identify the upstream of the pathogenesis of AD and find an appropriate therapeutic intervention. In this context, several studies have reported that high level of Aβ peptides itself could affect calcium and potassium currents: Increased L- and N- type calcium current influx, reduction in P/Q- type calcium current, and inhibition or up-regulation of A- type potassium current depending on the Aβ exposure time (Good et al 1996, Kerrigan et al 2008, MacManus et al 2000, Nimmrich et al 2008, Plant et al 2006, Ramsden et al 2002, Ueda et al 1997, Ye et al 2003). However, the causal link between those observations and the seizure activity of AD disease is still elusive, so the neuronal hyperexcitability triggered by Aβ peptides through the alteration of I_{NaP} is a promising possibility. Because the up-regulation of $Na_V1.6$ was observed in the animal model of epilepsy (Blumenfeld et al 2008, Blumenfeld et al 2009), it could be an interesting target to explain the hyper-excitability observed in the AD animal model (Busche et al 2008). If I_{NaP} participates in the seizure activity of AD animal model and there is effect of Aβ

peptides on its regulation, it could imply a possible ionic mechanism of AD pathogenesis and suggest a potential therapeutic target of AD treatment.

Chapter 5 Conclusion

This dissertation reports for the first time a reasonable separation of I_{NaP} and I_{NaT} from the somatic region of hippocampal neurons that enables us to compare biophysical properties of I_{NaP} and I_{NaT}. The direct comparison of them showed that the activation of a proportionally small amount of I_{NaP} always preceded the much larger I_{NaP} in respond to voltage change. I_{NaP} was not non-inactivating, but slowly inactivating. Such a temporal dynamics of I_{NaP} also provides a temporal window within which the information processing ability of the neuron could be affected by this conductance. In addition, the quantitative measurement of activation time constant of somatic transient Na^+ current at near physiological temperature gave a value 2 times faster than that reported previously. When considered in the context of the action potential intiation in the axon initial segment, these results suggest that different biophysical properties of Na^+ channel are largely reponsible for the biased locus of spike generation.

We also discovered that the preferrential blocking of I_{NaP} by hexanol caused the elevation of voltage threshold and delayed onset of 1st spike, which are landmarks of reduced neuronal excitability. As a consequence, a significant suppression of spike generation was observed in α-EPSP integration in presence of hexanol. Considering the anaesthetic effect of hexanol, these results suggest I_{NaP} as a intrinsic mechanism that underlies the anesthetic state mediated by the administration of alcohol and volatile anesthetics. Moreover, due to the remarkable alteration of input-output function of the neuron by the modification of I_{NaP}, this study raises the possibility that I_{NaP} could be an interesting target of intrinsic plasticity.

Appendix: frequency response of data acquisition system

The frequency response of Axopatch 200B patch clamp amplifier with various low pass filter cutoff frequencies (f_c) was measured. Either a 4-pole low pass Bessel filter built-in amplifier with 1, 5, 10, 100 kHz cutoff frequencies or an external 8-pole low pass Bessel filter (model-902, Frequency devices) with 20 kHz cutoff frequency was used to generate a Bode plot of the DAQ system (Fig. A.1A). Seven simulated Na^+ currents with different activation kinetics (τ_m) ranging from 16 – 116 μs were given to the system. Among 3 LPF cutoff frequencies, f_c = 20 kHz gave output I_{Na} without the distortion of τ_m (Fig. A.1B). All traces were sample at 200 kHz.

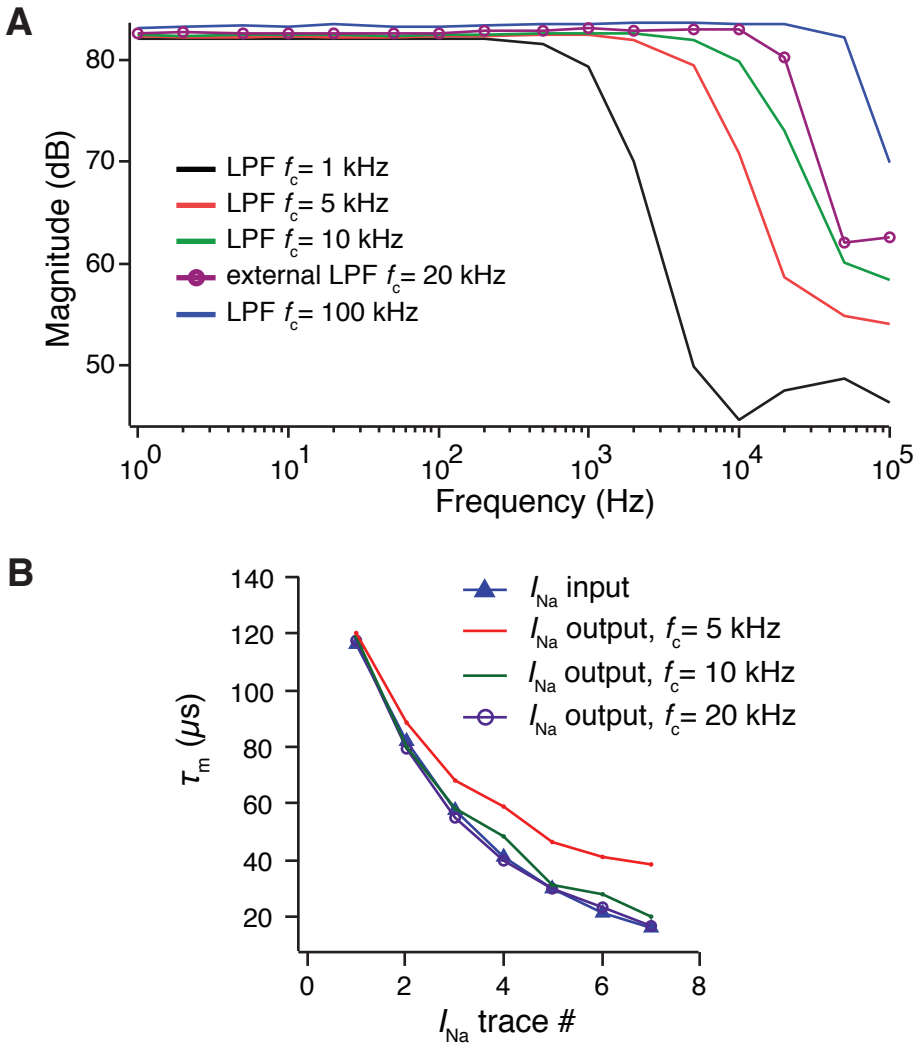

Figure A.1: Frequency response of data acquisition system
A: Bode plot of the data acquisition system with various LPF cutoff frequencies. **B:** the measurement of activation kinetics of Na^+ current at different LPF filter settings.

Bibliography

Agrawal N, Alonso A, Ragsdale DS. 2003. Increased persistent sodium currents in rat entorhinal cortex layer V neurons in a post-status epilepticus model of temporal lobe epilepsy. *Epilepsia* 44: 1601-4

Aizenman CD, Muñoz-Elías G, Cline HT. 2002. Visually driven modulation of glutamatergic synaptic transmission is mediated by the regulation of intracellular polyamines. *Neuron* 34: 623-34

Aldrich RW, Corey DP, Stevens CF. 1983. A reinterpretation of mammalian sodium channel gating based on single channel recording. *Nature* 306: 436-41

Aldrich RW, Stevens CF. 1987. Voltage-dependent gating of single sodium channels from mammalian neuroblastoma cells. *J Neurosci* 7: 418-31

Alifimoff JK, Firestone LL, Miller KW. 1989. Anaesthetic potencies of primary alkanols: implications for the molecular dimensions of the anaesthetic site. *British journal of pharmacology* 96: 9-16

Alonso A, Llinás RR. 1989. Subthreshold Na+-dependent theta-like rhythmicity in stellate cells of entorhinal cortex layer II. *Nature* 342: 175-7

Alzheimer C. 1994. A novel voltage-dependent cation current in rat neocortical neurones. *J Physiol (Lond)* 479 (Pt 2): 199-205

Alzheimer C, Schwindt PC, Crill WE. 1993a. Composite nature of a persistent sodium current in rat neocortical neurones. *Eur J Neurosci* Suppl. 1: R24

Alzheimer C, Schwindt PC, Crill WE. 1993b. Modal gating of Na+ channels as a mechanism of persistent Na+ current in pyramidal neurons from rat and cat sensorimotor cortex. *J Neurosci* 13: 660-73

Alzheimer C, Schwindt PC, Crill WE. 1993c. Postnatal development of a persistent Na+ current in pyramidal neurons from rat sensorimotor cortex. *J Neurophysiol* 69: 290-2

Amatniek JC, Hauser WA, DelCastillo-Castaneda C, Jacobs DM, Marder K, et al. 2006. Incidence and predictors of seizures in patients with Alzheimer's disease. *Epilepsia* 47: 867-72

Anderson P, Bliss TV, Skrede KK. 1971. Lamellar organization of hippocampal pathways. *Exp Brain Res* 13: 222-38

Andrasfalvy BK, Magee JC. 2001. Distance-dependent increase in AMPA receptor number in the dendrites of adult hippocampal CA1 pyramidal neurons. *J Neurosci* 21: 9151-9

Ariav G, Polsky A, Schiller J. 2003. Submillisecond precision of the input-output transformation function mediated by fast sodium dendritic spikes in basal dendrites of CA1 pyramidal neurons. *J Neurosci* 23: 7750-8

Astman N, Gutnick MJ, Fleidervish IA. 1998. Activation of protein kinase C increases neuronal excitability by regulating persistent Na+ current in mouse neocortical slices. *J Neurophysiol* 80: 1547-51

Astman N, Gutnick MJ, Fleidervish IA. 2006. Persistent sodium current in layer 5 neocortical neurons is primarily generated in the proximal axon. *J Neurosci* 26: 3465-73

Attwell D, Cohen I, Eisner D, Ohba M, Ojeda C. 1979. The steady state TTX-sensitive ("window") sodium current in cardiac Purkinje fibres. *Pflugers Arch* 379: 137-42

Bean BP. 2007. The action potential in mammalian central neurons. *Nat Rev Neurosci* 8: 451-65

Bear MF. 2003. Bidirectional synaptic plasticity: from theory to reality. *Philos Trans R Soc Lond, B, Biol Sci* 358: 649-55

Benoit E, Escande D. 1991. Riluzole specifically blocks inactivated Na channels in myelinated nerve fibre. *Pflugers Arch* 419: 603-9

Bernard C, Anderson A, Becker A, Poolos NP, Beck H, Johnston D. 2004. Acquired dendritic channelopathy in temporal lobe epilepsy. *Science* 305: 532-5

Beurrier C, Bioulac B, Hammond C. 2000. Slowly inactivating sodium current (I(NaP)) underlies single-spike activity in rat subthalamic neurons. *J Neurophysiol* 83: 1951-7

Bevan MD, Wilson CJ. 1999. Mechanisms underlying spontaneous oscillation and rhythmic firing in rat subthalamic neurons. *J Neurosci* 19: 7617-28

Bliss TV, Collingridge GL. 1993. A synaptic model of memory: long-term potentiation in the hippocampus. *Nature* 361: 31-9

Bliss TV, Lomo T. 1973. Long-lasting potentiation of synaptic transmission in the dentate area of the anaesthetized rabbit following stimulation of the perforant path. *J Physiol (Lond)* 232: 331-56

Blumenfeld H, Klein JP, Schridde U, Vestal M, Rice T, et al. 2008. Early treatment suppresses the development of spike-wave epilepsy in a rat model. *Epilepsia* 49: 400-9

Blumenfeld H, Lampert A, Klein JP, Mission J, Chen MC, et al. 2009. Role of hippocampal sodium channel Nav1.6 in kindling epileptogenesis. *Epilepsia* 50: 44-55

Boiko T, Rasband MN, Levinson SR, Caldwell JH, Mandel G, et al. 2001. Compact myelin dictates the differential targeting of two sodium channel isoforms in the same axon. *Neuron* 30: 91-104

Boiko T, Van Wart A, Caldwell JH, Levinson SR, Trimmer JS, Matthews G. 2003. Functional specialization of the axon initial segment by isoform-specific sodium channel targeting. *J Neurosci* 23: 2306-13

Brager DH, Johnston D. 2007. Plasticity of intrinsic excitability during long-term depression is mediated through mGluR-dependent changes in I(h) in hippocampal CA1 pyramidal neurons. *J Neurosci* 27: 13926-37

Brown AM, Schwindt PC, Crill WE. 1994. Different voltage dependence of transient and persistent Na+ currents is compatible with modal-gating hypothesis for sodium channels. *J Neurophysiol* 71: 2562-5

Busche MA, Eichhoff G, Adelsberger H, Abramowski D, Wiederhold K-H, et al. 2008. Clusters of hyperactive neurons near amyloid plaques in a mouse model of Alzheimer's disease. *Science* 321: 1686-9

Cabrejo L, Guyant-Maréchal L, Laquerrière A, Vercelletto M, De la Fournière F, et al. 2006. Phenotype associated with APP duplication in five families. *Brain* 129: 2966-76

Cantrell AR, Catterall WA. 2001. Neuromodulation of Na+ channels: an unexpected form of cellular plasticity. *Nat Rev Neurosci* 2: 397-407

Cantrell AR, Tibbs VC, Yu FH, Murphy BJ, Sharp EM, et al. 2002. Molecular mechanism of convergent regulation of brain Na(+) channels by protein kinase C and protein kinase A anchored to AKAP-15. *Mol Cell Neurosci* 21: 63-80

Catterall WA, Goldin AL, Waxman SG. 2005. International Union of Pharmacology. XLVII. Nomenclature and structure-function relationships of voltage-gated sodium channels. *Pharmacol Rev* 57: 397-409

Chen X, Johnston D. 2004. Properties of single voltage-dependent K+ channels in dendrites of CA1 pyramidal neurones of rat hippocampus. *J Physiol (Lond)* 559: 187-203

Chen X, Johnston D. 2005. Constitutively active G-protein-gated inwardly rectifying K+ channels in dendrites of hippocampal CA1 pyramidal neurons. *J Neurosci* 25: 3787-92

Chen X, Johnston D. 2006. Voltage-gated ion channels in dendrites of hippocampal pyramidal neurons. *Pflugers Arch* 453: 397-401

Chen X, Yuan L-L, Zhao C, Birnbaum SG, Frick A, et al. 2006. Deletion of Kv4.2 gene eliminates dendritic A-type K+ current and enhances induction of long-term potentiation in hippocampal CA1 pyramidal neurons. *J Neurosci* 26: 12143-51

Christie BR, Eliot LS, Ito K, Miyakawa H, Johnston D. 1995. Different Ca2+ channels in soma and dendrites of hippocampal pyramidal neurons mediate spike-induced Ca2+ influx. *J Neurophysiol* 73: 2553-7

Colbert CM, Johnston D. 1996. Axonal action-potential initiation and Na+ channel densities in the soma and axon initial segment of subicular pyramidal neurons. *J Neurosci* 16: 6676-86

Colbert CM, Johnston D. 1998. Protein kinase C activation decreases activity-dependent attenuation of dendritic Na+ current in hippocampal CA1 pyramidal neurons. *J Neurophysiol* 79: 491-5

Colbert CM, Magee JC, Hoffman DA, Johnston D. 1997. Slow recovery from inactivation of Na+ channels underlies the activity-dependent attenuation of dendritic action potentials in hippocampal CA1 pyramidal neurons. *J Neurosci* 17: 6512-21

Colbert CM, Pan E. 1999. Arachidonic acid reciprocally alters the availability of transient and sustained dendritic K(+) channels in hippocampal CA1 pyramidal neurons. *J Neurosci* 19: 8163-71

Colbert CM, Pan E. 2002. Ion channel properties underlying axonal action potential initiation in pyramidal neurons. *Nat Neurosci* 5: 533-8

Connors BW, Gutnick MJ, Prince DA. 1982. Electrophysiological properties of neocortical neurons in vitro. *J Neurophysiol* 48: 1302-20
Crill WE. 1996. Persistent sodium current in mammalian central neurons. *Annu Rev Physiol* 58: 349-62
Cummins TR, Howe JR, Waxman SG. 1998. Slow closed-state inactivation: a novel mechanism underlying ramp currents in cells expressing the hNE/PN1 sodium channel. *J Neurosci* 18: 9607-19
Cummins TR, Xia Y, Haddad GG. 1994. Functional properties of rat and human neocortical voltage-sensitive sodium currents. *J Neurophysiol* 71: 1052-64
Do MTH, Bean BP. 2003. Subthreshold sodium currents and pacemaking of subthalamic neurons: modulation by slow inactivation. *Neuron* 39: 109-20
Do MTH, Bean BP. 2004. Sodium currents in subthalamic nucleus neurons from Nav1.6-null mice. *J Neurophysiol* 92: 726-33
Dodge FA, Cooley JW. 1973. Action Potential of the Motorneuron. *IBM Journal of Research and Development* 17: 219 - 29
Dudel J, Peper K, Rüdel R, Trautwein W. 1967. Effect of tetrodotoxin on membrane currents in mammalian cardiac fibres. *Nature* 213: 296-7
Engel D, Jonas P. 2005. Presynaptic action potential amplification by voltage-gated Na+ channels in hippocampal mossy fiber boutons. *Neuron* 45: 405-17
Enomoto A, Han JM, Hsiao C-F, Chandler SH. 2007. Sodium currents in mesencephalic trigeminal neurons from Nav1.6 null mice. *J Neurophysiol* 98: 710-9
Fan Y, Fricker D, Brager DH, Chen X, Lu H-C, et al. 2005. Activity-dependent decrease of excitability in rat hippocampal neurons through increases in I(h). *Nat Neurosci* 8: 1542-51
Fleidervish IA, Friedman A, Gutnick MJ. 1996. Slow inactivation of Na+ current and slow cumulative spike adaptation in mouse and guinea-pig neocortical neurones in slices. *J Physiol (Lond)* 493 (Pt 1): 83-97
Fleidervish IA, Gutnick MJ. 1996. Kinetics of slow inactivation of persistent sodium current in layer V neurons of mouse neocortical slices. *J Neurophysiol* 76: 2125-30
Fleidervish IA, Lasser-Ross N, Gutnick MJ, Ross WN. 2010. Na(+) imaging reveals little difference in action potential-evoked Na(+) influx between axon and soma. *Nat Neurosci*
French CR, Sah P, Buckett KJ, Gage PW. 1990. A voltage-dependent persistent sodium current in mammalian hippocampal neurons. *J Gen Physiol* 95: 1139-57
Frick A, Magee J, Johnston D. 2004. LTP is accompanied by an enhanced local excitability of pyramidal neuron dendrites. *Nat Neurosci* 7: 126-35
Gasparini S, Magee JC. 2002. Phosphorylation-dependent differences in the activation properties of distal and proximal dendritic Na+ channels in rat CA1 hippocampal neurons. *J Physiol (Lond)* 541: 665-72
Gasparini S, Migliore M, Magee JC. 2004. On the initiation and propagation of dendritic spikes in CA1 pyramidal neurons. *J Neurosci* 24: 11046-56

Golding NL, Jung HY, Mickus T, Spruston N. 1999. Dendritic calcium spike initiation and repolarization are controlled by distinct potassium channel subtypes in CA1 pyramidal neurons. *J Neurosci* 19: 8789-98
Golding NL, Spruston N. 1998. Dendritic sodium spikes are variable triggers of axonal action potentials in hippocampal CA1 pyramidal neurons. *Neuron* 21: 1189-200
Golding NL, Staff NP, Spruston N. 2002. Dendritic spikes as a mechanism for cooperative long-term potentiation. *Nature* 418: 326-31
González-Burgos G, Barrionuevo G. 2001. Voltage-gated sodium channels shape subthreshold EPSPs in layer 5 pyramidal neurons from rat prefrontal cortex. *J Neurophysiol* 86: 1671-84
Good TA, Smith DO, Murphy RM. 1996. Beta-amyloid peptide blocks the fast-inactivating K+ current in rat hippocampal neurons. *Biophys J* 70: 296-304
Gorelova NA, Yang CR. 2000. Dopamine D1/D5 receptor activation modulates a persistent sodium current in rat prefrontal cortical neurons in vitro. *J Neurophysiol* 84: 75-87
Grieco TM, Malhotra JD, Chen C, Isom LL, Raman IM. 2005. Open-channel block by the cytoplasmic tail of sodium channel beta4 as a mechanism for resurgent sodium current. *Neuron* 45: 233-44
Gutnick MJ, Fleidervish IA, Katz E, Scheller A, Goebbels S, et al. 2010. Role of axonal NaV1.6 sodium channels in action potential generation in Layer 5 neocortical neurons. *Soc Neurosci Abstr 339.5*
Hamill OP, Huguenard JR, Prince DA. 1991. Patch-clamp studies of voltage-gated currents in identified neurons of the rat cerebral cortex. *Cereb Cortex* 1: 48-61
Hammarström AK, Gage PW. 1999. Nitric oxide increases persistent sodium current in rat hippocampal neurons. *J Physiol (Lond)* 520 Pt 2: 451-61
Hartmann HA, Colom LV, Sutherland ML, Noebels JL. 1999. Selective localization of cardiac SCN5A sodium channels in limbic regions of rat brain. *Nat Neurosci* 2: 593-5
Hebb D. 1949. The Organization of Behavior. New York: Wiley
Hines ML, Carnevale NT. 1997. The NEURON simulation environment. *Neural Comput* 9: 1179-209
Hodgkin AL, Huxley AF. 1952. A quantitative description of membrane current and its application to conduction and excitation in nerve. *J Physiol (Lond)* 117: 500-44
Hoehn K, Watson TW, Macvicar BA. 1993. A novel tetrodotoxin-insensitive, slow sodium current in striatal and hippocampal neurons. *Neuron* 10: 543-52
Hoffman DA, Johnston D. 1998. Downregulation of transient K+ channels in dendrites of hippocampal CA1 pyramidal neurons by activation of PKA and PKC. *J Neurosci* 18: 3521-8
Hoffman DA, Magee JC, Colbert CM, Johnston D. 1997. K+ channel regulation of signal propagation in dendrites of hippocampal pyramidal neurons. *Nature* 387: 869-75
Horishita T, Harris RA. 2008. n-Alcohols inhibit voltage-gated Na+ channels expressed in Xenopus oocytes. *J Pharmacol Exp Ther* 326: 270-7

Hotson JR, Prince DA, Schwartzkroin PA. 1979. Anomalous inward rectification in hippocampal neurons. *J Neurophysiol* 42: 889-95

Hu GY, Hvalby O. 1992. Glutamate-induced action potentials are preceded by regenerative prepotentials in rat hippocampal pyramidal cells in vitro. *Exp Brain Res* 88: 485-94

Hu H, Vervaeke K, Storm JF. 2002. Two forms of electrical resonance at theta frequencies, generated by M-current, h-current and persistent Na+ current in rat hippocampal pyramidal cells. *J Physiol (Lond)* 545: 783-805

Hu W, Tian C, Li T, Yang M, Hou H, Shu Y. 2009. Distinct contributions of Na(v)1.6 and Na(v)1.2 in action potential initiation and backpropagation. *Nat Neurosci* 12: 996-1002

Huguenard JR, Hamill OP, Prince DA. 1988. Developmental changes in Na+ conductances in rat neocortical neurons: appearance of a slowly inactivating component. *J Neurophysiol* 59: 778-95

Hyman BT, Van Hoesen GW, Damasio AR, Barnes CL. 1984. Alzheimer's disease: cell-specific pathology isolates the hippocampal formation. *Science* 225: 1168-70

Hyman BT, Van Hoesen GW, Kromer LJ, Damasio AR. 1986. Perforant pathway changes and the memory impairment of Alzheimer's disease. *Ann Neurol* 20: 472-81

Isom LL. 2001. Sodium channel beta subunits: anything but auxiliary. *Neuroscientist* 7: 42-54

Jaffe DB, Johnston D, Lasser-Ross N, Lisman JE, Miyakawa H, Ross WN. 1992. The spread of Na+ spikes determines the pattern of dendritic Ca2+ entry into hippocampal neurons. *Nature* 357: 244-6

Johnston D. 2010. The Na+ channel conundrum: axon structure versus function. *Nat Neurosci* 13: 784-5

Johnston D, Christie BR, Frick A, Gray R, Hoffman DA, et al. 2003. Active dendrites, potassium channels and synaptic plasticity. *Philos Trans R Soc Lond, B, Biol Sci* 358: 667-74

Johnston D, Wu SM. 1995. Foundations of Cellular neurophysiology. Cambridge: The MIT Press

Jung HY, Mickus T, Spruston N. 1997. Prolonged sodium channel inactivation contributes to dendritic action potential attenuation in hippocampal pyramidal neurons. *J Neurosci* 17: 6639-46

Jung S, Jones TD, Lugo JN, Sheerin AH, Miller JW, et al. 2007. Progressive dendritic HCN channelopathy during epileptogenesis in the rat pilocarpine model of epilepsy. *J Neurosci* 27: 13012-21

Kamenetz F, Tomita T, Hsieh H, Seabrook G, Borchelt D, et al. 2003. APP processing and synaptic function. *Neuron* 37: 925-37

Kaplan MR, Cho MH, Ullian EM, Isom LL, Levinson SR, Barres BA. 2001. Differential control of clustering of the sodium channels Na(v)1.2 and Na(v)1.6 at developing CNS nodes of Ranvier. *Neuron* 30: 105-19

Kay AR, Sugimori M, Llinás R. 1998. Kinetic and stochastic properties of a persistent sodium current in mature guinea pig cerebellar Purkinje cells. *J Neurophysiol* 80: 1167-79
Kerrigan TL, Atkinson L, Peers C, Pearson HA. 2008. Modulation of 'A'-type K+ current by rodent and human forms of amyloid beta protein. *Neuroreport* 19: 839-43
Kole MHP, Ilschner SU, Kampa BM, Williams SR, Ruben PC, Stuart GJ. 2008. Action potential generation requires a high sodium channel density in the axon initial segment. *Nat Neurosci* 11: 178-86
Kole MHP, Stuart GJ. 2008. Is action potential threshold lowest in the axon? *Nat Neurosci* 11: 1253-5
Lipowsky R, Gillessen T, Alzheimer C. 1996. Dendritic Na+ channels amplify EPSPs in hippocampal CA1 pyramidal cells. *J Neurophysiol* 76: 2181-91
Llinás R, Sugimori M. 1980. Electrophysiological properties of in vitro Purkinje cell somata in mammalian cerebellar slices. *J Physiol (Lond)* 305: 171-95
Lorincz A, Nusser Z. 2008. Cell-type-dependent molecular composition of the axon initial segment. *J Neurosci* 28: 14329-40
Lorincz A, Nusser Z. 2010. Molecular identity of dendritic voltage-gated sodium channels. *Science* 328: 906-9
Losonczy A, Makara JK, Magee JC. 2008. Compartmentalized dendritic plasticity and input feature storage in neurons. *Nature* 452: 436-41
Ma JY, Catterall WA, Scheuer T. 1997. Persistent sodium currents through brain sodium channels induced by G protein betagamma subunits. *Neuron* 19: 443-52
MacManus A, Ramsden M, Murray M, Henderson Z, Pearson HA, Campbell VA. 2000. Enhancement of (45)Ca(2+) influx and voltage-dependent Ca(2+) channel activity by beta-amyloid-(1-40) in rat cortical synaptosomes and cultured cortical neurons. Modulation by the proinflammatory cytokine interleukin-1beta. *J Biol Chem* 275: 4713-8
Macvicar BA. 1985. Depolarizing prepotentials are Na+ dependent in CA1 pyramidal neurons. *Brain Res* 333: 378-81
Magee JC. 1998. Dendritic hyperpolarization-activated currents modify the integrative properties of hippocampal CA1 pyramidal neurons. *J Neurosci* 18: 7613-24
Magee JC. 1999. Dendritic lh normalizes temporal summation in hippocampal CA1 neurons. *Nat Neurosci* 2: 508-14
Magee JC. 2000. Dendritic integration of excitatory synaptic input. *Nat Rev Neurosci* 1: 181-90
Magee JC, Christofi G, Miyakawa H, Christie B, Lasser-Ross N, Johnston D. 1995. Subthreshold synaptic activation of voltage-gated Ca2+ channels mediates a localized Ca2+ influx into the dendrites of hippocampal pyramidal neurons. *J Neurophysiol* 74: 1335-42
Magee JC, Cook EP. 2000. Somatic EPSP amplitude is independent of synapse location in hippocampal pyramidal neurons. *Nat Neurosci* 3: 895-903

Magee JC, Johnston D. 1995a. Characterization of single voltage-gated Na+ and Ca2+ channels in apical dendrites of rat CA1 pyramidal neurons. *J Physiol (Lond)* 487 (Pt 1): 67-90
Magee JC, Johnston D. 1995b. Synaptic activation of voltage-gated channels in the dendrites of hippocampal pyramidal neurons. *Science* 268: 301-4
Magee JC, Johnston D. 1997. A synaptically controlled, associative signal for Hebbian plasticity in hippocampal neurons. *Science* 275: 209-13
Magistretti J, Alonso A. 1999. Biophysical properties and slow voltage-dependent inactivation of a sustained sodium current in entorhinal cortex layer-II principal neurons: a whole-cell and single-channel study. *J Gen Physiol* 114: 491-509
Magistretti J, Ragsdale DS, Alonso A. 1999a. Direct demonstration of persistent Na+ channel activity in dendritic processes of mammalian cortical neurones. *J Physiol (Lond)* 521 Pt 3: 629-36
Magistretti J, Ragsdale DS, Alonso A. 1999b. High conductance sustained single-channel activity responsible for the low-threshold persistent Na(+) current in entorhinal cortex neurons. *J Neurosci* 19: 7334-41
Mainen ZF, Joerges J, Huguenard JR, Sejnowski TJ. 1995. A model of spike initiation in neocortical pyramidal neurons. *Neuron* 15: 1427-39
Martina M, Jonas P. 1997. Functional differences in Na+ channel gating between fast-spiking interneurones and principal neurones of rat hippocampus. *J Physiol (Lond)* 505 (Pt 3): 593-603
Masukawa LM, Hansen AJ, Shepherd G. 1991. Distribution of single-channel conductances in cultured rat hippocampal neurons. *Cell Mol Neurobiol* 11: 231-43
Maurice N, Tkatch T, Meisler M, Sprunger LK, Surmeier DJ. 2001. D1/D5 dopamine receptor activation differentially modulates rapidly inactivating and persistent sodium currents in prefrontal cortex pyramidal neurons. *J Neurosci* 21: 2268-77
Megías M, Emri Z, Freund TF, Gulyás AI. 2001. Total number and distribution of inhibitory and excitatory synapses on hippocampal CA1 pyramidal cells. *Neuroscience* 102: 527-40
Mercer JN, Chan CS, Tkatch T, Held J, Surmeier DJ. 2007. Nav1.6 sodium channels are critical to pacemaking and fast spiking in globus pallidus neurons. *J Neurosci* 27: 13552-66
Migliore M, Hoffman DA, Magee JC, Johnston D. 1999. Role of an A-type K+ conductance in the back-propagation of action potentials in the dendrites of hippocampal pyramidal neurons. *Journal of computational neuroscience* 7: 5-15
Migliore M, Messineo L, Ferrante M. 2004. Dendritic Ih selectively blocks temporal summation of unsynchronized distal inputs in CA1 pyramidal neurons. *Journal of computational neuroscience* 16: 5-13
Milescu LS, Yamanishi T, Ptak K, Smith JC. 2010. Kinetic properties and functional dynamics of sodium channels during repetitive spiking in a slow pacemaker neuron. *J Neurosci* 30: 12113-27

Mittmann T, Alzheimer C. 1998. Muscarinic inhibition of persistent Na+ current in rat neocortical pyramidal neurons. *J Neurophysiol* 79: 1579-82
Mittmann T, Linton SM, Schwindt P, Crill W. 1997. Evidence for persistent Na+ current in apical dendrites of rat neocortical neurons from imaging of Na+-sensitive dye. *J Neurophysiol* 78: 1188-92
Narayanan R, Johnston D. 2007. Long-term potentiation in rat hippocampal neurons is accompanied by spatially widespread changes in intrinsic oscillatory dynamics and excitability. *Neuron* 56: 1061-75
Narayanan R, Johnston D. 2008. The h channel mediates location dependence and plasticity of intrinsic phase response in rat hippocampal neurons. *J Neurosci* 28: 5846-60
Nimmrich V, Grimm C, Draguhn A, Barghorn S, Lehmann A, et al. 2008. Amyloid beta oligomers (A beta(1-42) globulomer) suppress spontaneous synaptic activity by inhibition of P/Q-type calcium currents. *J Neurosci* 28: 788-97
Nolan MF, Malleret G, Dudman JT, Buhl DL, Santoro B, et al. 2004. A behavioral role for dendritic integration: HCN1 channels constrain spatial memory and plasticity at inputs to distal dendrites of CA1 pyramidal neurons. *Cell* 119: 719-32
Numann R, Catterall WA, Scheuer T. 1991. Functional modulation of brain sodium channels by protein kinase C phosphorylation. *Science* 254: 115-8
Osorio N, Cathala L, Meisler MH, Crest M, Magistretti J, Delmas P. 2010. Persistent Nav1.6 current at axon initial segments tunes spike timing of cerebellar granule cells. *J Physiol (Lond)* 588: 651-70
Palop JJ, Chin J, Roberson ED, Wang J, Thwin MT, et al. 2007. Aberrant excitatory neuronal activity and compensatory remodeling of inhibitory hippocampal circuits in mouse models of Alzheimer's disease. *Neuron* 55: 697-711
Palop JJ, Mucke L. 2009. Epilepsy and cognitive impairments in Alzheimer disease. *Arch Neurol* 66: 435-40
Palop JJ, Mucke L. 2010. Amyloid-beta-induced neuronal dysfunction in Alzheimer's disease: from synapses toward neural networks. *Nat Neurosci* 13: 812-8
Patlak JB, Ortiz M. 1985. Slow currents through single sodium channels of the adult rat heart. *J Gen Physiol* 86: 89-104
Patlak JB, Ortiz M, Horn R. 1986. Opentime heterogeneity during bursting of sodium channels in frog skeletal muscle. *Biophys J* 49: 773-7
Patton DE, West JW, Catterall WA, Goldin AL. 1992. Amino acid residues required for fast Na(+)-channel inactivation: charge neutralizations and deletions in the III-IV linker. *Proc Natl Acad Sci USA* 89: 10905-9
Plant LD, Webster NJ, Boyle JP, Ramsden M, Freir DB, et al. 2006. Amyloid beta peptide as a physiological modulator of neuronal 'A'-type K+ current. *Neurobiol Aging* 27: 1673-83
Poirazi P, Mel BW. 2001. Impact of active dendrites and structural plasticity on the memory capacity of neural tissue. *Neuron* 29: 779-96
Rajamani S, El-Bizri N, Shryock JC, Makielski JC, Belardinelli L. 2009. Use-dependent block of cardiac late Na(+) current by ranolazine. *Heart Rhythm* 6: 1625-31

Raman IM, Bean BP. 1997. Resurgent sodium current and action potential formation in dissociated cerebellar Purkinje neurons. *J Neurosci* 17: 4517-26
Raman IM, Sprunger LK, Meisler MH, Bean BP. 1997. Altered subthreshold sodium currents and disrupted firing patterns in Purkinje neurons of Scn8a mutant mice. *Neuron* 19: 881-91
Ramsden M, Henderson Z, Pearson HA. 2002. Modulation of Ca2+ channel currents in primary cultures of rat cortical neurones by amyloid beta protein (1-40) is dependent on solubility status. *Brain Res* 956: 254-61
Rosenkranz JA, Johnston D. 2007. State-dependent modulation of amygdala inputs by dopamine-induced enhancement of sodium currents in layer V entorhinal cortex. *J Neurosci* 27: 7054-69
Royeck M, Horstmann M-T, Remy S, Reitze M, Yaari Y, Beck H. 2008. Role of axonal NaV1.6 sodium channels in action potential initiation of CA1 pyramidal neurons. *J Neurophysiol* 100: 2361-80
Rush AM, Dib-Hajj SD, Waxman SG. 2005. Electrophysiological properties of two axonal sodium channels, Nav1.2 and Nav1.6, expressed in mouse spinal sensory neurones. *J Physiol (Lond)* 564: 803-15
Sather W, Dieudonné S, MacDonald JF, Ascher P. 1992. Activation and desensitization of N-methyl-D-aspartate receptors in nucleated outside-out patches from mouse neurones. *J Physiol (Lond)* 450: 643-72
Schiller J, Major G, Koester HJ, Schiller Y. 2000. NMDA spikes in basal dendrites of cortical pyramidal neurons. *Nature* 404: 285-9
Schmidt-Hieber C, Bischofberger J. 2010. Fast sodium channel gating supports localized and efficient axonal action potential initiation. *J Neurosci* 30: 10233-42
Schwindt PC, Crill WE. 1995. Amplification of synaptic current by persistent sodium conductance in apical dendrite of neocortical neurons. *J Neurophysiol* 74: 2220-4
Scoville WB, Milner B. 1957. Loss of recent memory after bilateral hippocampal lesions. *J Neurol Neurosurg Psychiatr* 20: 11-21
Shankar GM, Li S, Mehta TH, Garcia-Munoz A, Shepardson NE, et al. 2008. Amyloid-beta protein dimers isolated directly from Alzheimer's brains impair synaptic plasticity and memory. *Nat Med* 14: 837-42
Shin M, Brager D, Jaramillo TC, Johnston D, Chetkovich DM. 2008. Mislocalization of h channel subunits underlies h channelopathy in temporal lobe epilepsy. *Neurobiol Dis* 32: 26-36
Shiraishi M, Harris RA. 2004. Effects of alcohols and anesthetics on recombinant voltage-gated Na+ channels. *J Pharmacol Exp Ther* 309: 987-94
Smith MR, Smith RD, Plummer NW, Meisler MH, Goldin AL. 1998. Functional analysis of the mouse Scn8a sodium channel. *J Neurosci* 18: 6093-102
Smith RD, Goldin AL. 1997. Phosphorylation at a single site in the rat brain sodium channel is necessary and sufficient for current reduction by protein kinase A. *J Neurosci* 17: 6086-93

Spruston N, Schiller Y, Stuart G, Sakmann B. 1995. Activity-Dependent Action Potential Invasion and Calcium Influx into Hippocampal CA1 Dendrites. *Science* 268: 297-300

Squire LR, Zola-Morgan S. 1991. The medial temporal lobe memory system. *Science* 253: 1380-6

Stafstrom CE, Schwindt PC, Chubb MC, Crill WE. 1985. Properties of persistent sodium conductance and calcium conductance of layer V neurons from cat sensorimotor cortex in vitro. *J Neurophysiol* 53: 153-70

Stafstrom CE, Schwindt PC, Crill WE. 1982. Negative slope conductance due to a persistent subthreshold sodium current in cat neocortical neurons in vitro. *Brain Res* 236: 221-6

Stafstrom CE, Schwindt PC, Flatman JA, Crill WE. 1984. Properties of subthreshold response and action potential recorded in layer V neurons from cat sensorimotor cortex in vitro. *J Neurophysiol* 52: 244-63

Stuart G, Sakmann B. 1995. Amplification of EPSPs by axosomatic sodium channels in neocortical pyramidal neurons. *Neuron* 15: 1065-76

Stuart G, Schiller J, Sakmann B. 1997. Action potential initiation and propagation in rat neocortical pyramidal neurons. *J Physiol (Lond)* 505 (Pt 3): 617-32

Stuart GJ, Häusser M. 2001. Dendritic coincidence detection of EPSPs and action potentials. *Nat Neurosci* 4: 63-71

Stuart GJ, Sakmann B. 1994. Active propagation of somatic action potentials into neocortical pyramidal cell dendrites. *Nature* 367: 69-72

Stühmer W, Conti F, Suzuki H, Wang XD, Noda M, et al. 1989. Structural parts involved in activation and inactivation of the sodium channel. *Nature* 339: 597-603

Taddese A, Bean BP. 2002. Subthreshold sodium current from rapidly inactivating sodium channels drives spontaneous firing of tuberomammillary neurons. *Neuron* 33: 587-600

Tanaka M, Cummins TR, Ishikawa K, Black JA, Ibata Y, Waxman SG. 1999. Molecular and functional remodeling of electrogenic membrane of hypothalamic neurons in response to changes in their input. *Proc Natl Acad Sci USA* 96: 1088-93

Taylor CP. 1993. Na+ currents that fail to inactivate. *Trends Neurosci* 16: 455-60

Traub RD, Jefferys JG, Miles R, Whittington MA, Tóth K. 1994. A branching dendritic model of a rodent CA3 pyramidal neurone. *J Physiol (Lond)* 481 (Pt 1): 79-95

Turrigiano GG. 2008. The self-tuning neuron: synaptic scaling of excitatory synapses. *Cell* 135: 422-35

Turrigiano GG, Leslie KR, Desai NS, Rutherford LC, Nelson SB. 1998. Activity-dependent scaling of quantal amplitude in neocortical neurons. *Nature* 391: 892-6

Turrigiano GG, Nelson SB. 2000. Hebb and homeostasis in neuronal plasticity. *Curr Opin Neurobiol* 10: 358-64

Ueda K, Shinohara S, Yagami T, Asakura K, Kawasaki K. 1997. Amyloid beta protein potentiates Ca2+ influx through L-type voltage-sensitive Ca2+ channels: a possible involvement of free radicals. *J Neurochem* 68: 265-71

Ulbricht W. 2005. Sodium channel inactivation: molecular determinants and modulation. *Physiol Rev* 85: 1271-301
Urbani A, Belluzzi O. 2000. Riluzole inhibits the persistent sodium current in mammalian CNS neurons. *Eur J Neurosci* 12: 3567-74
Vacher H, Mohapatra DP, Trimmer JS. 2008. Localization and targeting of voltage-dependent ion channels in mammalian central neurons. *Physiol Rev* 88: 1407-47
Van Wart A, Trimmer JS, Matthews G. 2007. Polarized distribution of ion channels within microdomains of the axon initial segment. *J Comp Neurol* 500: 339-52
Vassilev P, Scheuer T, Catterall WA. 1989. Inhibition of inactivation of single sodium channels by a site-directed antibody. *Proc Natl Acad Sci USA* 86: 8147-51
Vervaeke K, Hu H, Graham LJ, Storm JF. 2006. Contrasting effects of the persistent Na+ current on neuronal excitability and spike timing. *Neuron* 49: 257-70
Walsh DM, Klyubin I, Fadeeva JV, Cullen WK, Anwyl R, et al. 2002. Naturally secreted oligomers of amyloid beta protein potently inhibit hippocampal long-term potentiation in vivo. *Nature* 416: 535-9
Watanabe S, Hoffman DA, Migliore M, Johnston D. 2002. Dendritic K+ channels contribute to spike-timing dependent long-term potentiation in hippocampal pyramidal neurons. *Proc Natl Acad Sci USA* 99: 8366-71
Waxman SG. 2000. The neuron as a dynamic electrogenic machine: modulation of sodium-channel expression as a basis for functional plasticity in neurons. *Philos Trans R Soc Lond, B, Biol Sci* 355: 199-213
Waxman SG. 2006. Axonal conduction and injury in multiple sclerosis: the role of sodium channels. *Nat Rev Neurosci* 7: 932-41
West JW, Numann R, Murphy BJ, Scheuer T, Catterall WA. 1991. A phosphorylation site in the Na+ channel required for modulation by protein kinase C. *Science* 254: 866-8
Williams SR, Mitchell SJ. 2008. Direct measurement of somatic voltage clamp errors in central neurons. *Nat Neurosci* 11: 790-8
Witter MP, Groenewegen HJ, Lopes da Silva FH, Lohman AH. 1989. Functional organization of the extrinsic and intrinsic circuitry of the parahippocampal region. *Prog Neurobiol* 33: 161-253
Wittmack EK, Rush AM, Hudmon A, Waxman SG, Dib-Hajj SD. 2005. Voltage-gated sodium channel Nav1.6 is modulated by p38 mitogen-activated protein kinase. *J Neurosci* 25: 6621-30
Xu J, Kang N, Jiang L, Nedergaard M, Kang J. 2005. Activity-dependent long-term potentiation of intrinsic excitability in hippocampal CA1 pyramidal neurons. *J Neurosci* 25: 1750-60
Ye CP, Selkoe DJ, Hartley DM. 2003. Protofibrils of amyloid beta-protein inhibit specific K+ currents in neocortical cultures. *Neurobiol Dis* 13: 177-90
Yuan L-L, Adams JP, Swank M, Sweatt JD, Johnston D. 2002. Protein kinase modulation of dendritic K+ channels in hippocampus involves a mitogen-activated protein kinase pathway. *J Neurosci* 22: 4860-8

Yue C, Remy S, Su H, Beck H, Yaari Y. 2005. Proximal persistent Na+ channels drive spike afterdepolarizations and associated bursting in adult CA1 pyramidal cells. *J Neurosci* 25: 9704-20

Zhang W, Linden DJ. 2003. The other side of the engram: experience-driven changes in neuronal intrinsic excitability. *Nat Rev Neurosci* 4: 885-900

Zola-Morgan S, Squire LR, Amaral DG. 1986. Human amnesia and the medial temporal region: enduring memory impairment following a bilateral lesion limited to field CA1 of the hippocampus. *J Neurosci* 6: 2950-67

Zola-Morgan S, Squire LR, Mishkin M. 1982. The neuroanatomy of amnesia: amygdala-hippocampus versus temporal stem. *Science* 218: 1337-9

Vita

Yul Young Park attended Jang-hoon High School, Seoul, Kyounggi, South Korea. In 1992 he entered Sogang Univertsity in Seoul, Kyounggi, South Korea. From January 1993 to March 1995, he served in the Korean Army for the military duty. He received the degree of Bachelor of Science in Electrical Engineering from Sogang University in February 1999. During the following years he was employed as a staff engineer for Hansol wireless telecommunication service company and later worked for 4Csoft software development company as an associate engineer. In September 2001, he entered the Graduate School at The University of Texas at Austin and earned the degree of Master of Science in Biomedical Engineering (Hearing Science) in August 2004. He continued to pursue his Doctoral degree in Biomedical Engineering (Neuroscience) at The University of Texas at Austin.

Permanent e-mail Address: yypark@gmail.com

This manuscript was typed by the author.